การเสริมโลหะออกไซด์ของโคบอลต์/ซิลิกาสำหรับการสังเคราะห์ฟิสเชอร์โทรป

นางสาว สุกมล หิญชีระนันทน์

METAL OXIDE PROMOTION OF Co/SiO$_2$ FOR FISCHER-TROPSCH SYNTHESIS

Miss Sukamon Hinchiranan

A Dissertation Submitted in Partial Fulfillment of the Requirements

for the Degree of Doctor of Philosophy Program in Chemical Technology

Department of Chemical Technology
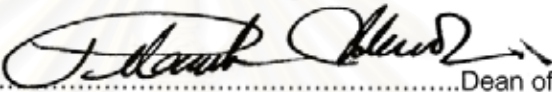
Faculty of Science

Chulalongkorn University

Academic year 2005

Thesis Title   METAL OXIDE PROMOTION OF Co/SiO_2 FOR FISCHER-TROPSCH SYNTHESIS

By   Miss Sukamon Hinchiranan

Filed of study   Chemical Technology

Thesis Advisor   Associate Professor Tharapong Vitidsant, Ph.D.

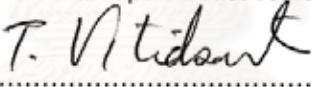Thesis Co-advisor   Professor Noritatsu Tsubaki, Ph.D.

         Accepted by the Faculty of Science, Chulalongkorn University in Partial Fulfillment of the Requirements for the Doctor's Degree

                                       ....Dean of the Faculty of Science

                                       (Professor Piamsak Menasveta, Ph.D.)

THESIS COMMITTEE

                                       ....Chairman

                                       (Professor Pattarapan Prasassarakich, Ph.D.)

                                       ....Thesis Advisor

                                       (Associate Professor Tharapong Vitidsant, Ph.D.)

                                       ....Thesis Co-advisor

                                       (Professor Noritatsu Tsubaki, Ph.D.)

                                       .... Member

                                       (Associate Professor Somkiat Ngamprasertsith, Ph.D.)

                                       .... Member

                                       (Assistant Professor Apinya Duangchan, Ph.D.)

                                       .... Member

                                       (Chawalit Ngamjarussrivichai, Ph.D.)

สุกมล หิญชีระนันทน์ : การเสริมโลหะออกไซด์ของโคบอลต์/ซิลิกาสำหรับการสังเคราะห์ฟิสเชอร์
โทรป (METAL OXIDE PROMOTION OF Co/SiO2 FOR FISCHER-TROPSCH SYNTHESIS)
อ. ที่ปรึกษา : รศ.ดร.ธราพงษ์ วิทิตศานต์, อ. ที่ปรึกษาร่วม : Prof. Noritatsu Tsubaki, 98 หน้า.
ISBN 974-53-2418-3

        การสังเคราะห์ฟิสเชอร์โทรปเป็นกระบวนการเชิงเร่งปฏิกิริยาซึ่งเปลี่ยนแก๊สสังเคราะห์ที่
ผลิตจากถ่านหินและแก๊สธรรมชาติไปเป็นเชื้อเพลิงสะอาด ในปัจจุบันตัวเร่งปฏิกิริยาโคบอลต์ถูกอ้างว่ามี
ข้อได้เปรียบเหนือกว่าตัวเร่งปฏิกิริยาชนิดอื่นเนื่องจากมีความสามารถในการเกิดปฏิกิริยาสูง มีอายุการใช้
เร่งปฏิกิริยานาน มีความว่องไวต่อการเกิดปฏิกิริยาวอเตอร์แก๊สชิฟต์ต่ำ และ มีความสามารถต่อการเลือก
เกิดผลิตภัณฑ์จำพวกพาราฟินสายยาวสูง จุดประสงค์ของงานวิจัยนี้เพื่อพัฒนาความสามารถในการ
เกิดปฏิกิริยาของตัวเร่งปฏิกิริยาโคบอลต์บนตัวรองรับซิลิกาโดยการเติม Al_2O_3, TiO_2 และ ZrO_2 เป็นตัว
ส่งเสริม   ศึกษาผลของการเตรียมตัวเร่งปฏิกิริยาโดยวิธีซีเควนเชียลอิมเพรกเนชันและโคอิมเพร็กเนชัน
ความสามารถในการเร่งปฏิกิริยาทดสอบด้วยเครื่องปฏิกรณ์แบบกึ่งต่อเนื่องในภาวะของผสมแขวนลอย
XRD, TPR, SEM, H_2 chemisorption และ DRIFT ใช้สำหรับวิเคราะห์สมบัติของตัวเร่งปฏิกิริยาที่พัฒนา
แล้ว ผลของการเติมโลหะออกไซด์บนตัวเร่งปฏิกิริยาโคบอลต์แสดงถึงการปรับปรุงความสามารถในการเร่ง
ปฏิกิริยาของโคบอลต์ในปฏิกิริยาฟิสเชอร์โทรปโดยเพิ่มการกระจายตัวบนตัวรองรับ ที่ไม่ขัดขวาง
ความสามารถในการถูกรีดิวส์ของโคบอลต์ วิธีการเตรียม Al_2O_3 และ ZrO_2 ลงบนตัวเร่งปฏิกิริยาโคบอลต์/ซิ
ลิกา ไม่มีผลต่อความสามารถในการเร่งปฏิกิริยา ต่างจากผลที่ได้จากปฏิกิริยาที่มี TiO_2 เป็นตัวส่งเสริม
การเกิดขึ้นของ $CoTiO_3$ ซึ่งถูกรีดิวส์ได้ยากเกิดขึ้นจากการเตรียมโดยวิธีโคอิมเพรกเนชันได้ง่ายกว่าการ
เตรียมโดยวิธีซีเควนเชียลอิมเพรกเนชัน ไฮโดรเจนสปิวโอเวอร์อาจเป็นสาเหตุของการเพิ่มความว่องไวใน
การเกิดปฏิกิริยาของตัวเร่งปฏิกิริยาที่ถูกส่งเสริมด้วย ZrO_2

ภาควิชา .... เคมีเทคนิค	ลายมือชื่อนิสิต.....สุกมล..หิญชีระนันทน์..................
สาขาวิชา .... เคมีเทคนิค	ลายมือชื่ออาจารย์ที่ปรึกษา.........................
ปีการศึกษา 2548	ลายมือชื่ออาจารย์ที่ปรึกษาร่วม...................

4573844023   : MAJOR   CHEMICAL TECHNOLOGY

KEY WORD: FISCHER-TPROSCH SYNTHESIS / COBALT CATALYST / SYNGAS / ALUMINA / TITANIA / ZIRCONIA

SUKAMON HINCHIRANAN : METAL OXIDE PROMOTION OF Co/SiO$_2$ FOR FISCHER-TROPSCH SYNTHESIS. THESIS ADVISOR : ASSOC. PROF. THARAPONG VITIDSANT, THESIS COADVISOR : PROF. NORITATSU TSUBAKI , 98 pp. ISBN 974-53-2418-3.

Fischer-Tropsch synthesis (FTS) is a catalytic process which converts coal and natural gas to chemicals and clean fuels via syngas. Currently, cobalt-based catalyst is claimed to have certain advantages over other catalysts because of their high activity, long catalytic life time, low water-gas shift activity and high selectivity for long chain paraffin. The purpose of the present work was to improve the activity of cobalt-based catalyst on the silica support by the addition of aluminium oxide, titanium oxide and zirconium oxide as promoters. The effect of catalyst preparation by the sequential-impregnation and the co-impregnation methods was also investigated. The catalytic activity was examined in a semi-batch slurry-phase reactor. XRD, TPR, SEM, H$_2$ chemisorption and DRIFT were used to characterize the modified catalysts. The results of metal oxide addition onto the cobalt catalyst indicated the improvement on the catalytic activity of cobalt in FTS reaction by increasing the cobalt dispersion without obstruction of the cobalt reducibility. The method of preparation of Al$_2$O$_3$ and ZrO$_2$ loaded onto Co/SiO$_2$ catalyst did not affect the catalytic activity, unlike the results from the preparation of TiO$_2$-promoted catalyst. The formation of hardly reducible CoTiO$_3$ from the co-impregnation method was easier than that from the sequential-impregnation method. Hydrogen spillover might be the reason for the enhancement of activity in ZrO$_2$-promoted catalyst.

Department ..... Chemical Technology .... Student's signature...Sukamon Hinchiranan

Field of study... Chemical Technology ... Advisor's signature....T. Vitidsant

Academic year.. 2005 .... Co-advisor' signature...Noritatsu Tsubaki

ACKNOWLEDGEMENTS

CONTENTS

LIST OF TABLES

TABLE   PAGE

LIST OF FIGURES

FIGURE   PAGE

FIGURE   PAGE

FIGURE   PAGE

NOMENCLATURES

ASF	:	Anderson-Schulz-Flory equation
BET	:	Brunauer-Emmett-Teller
Co	:	Cobalt
Co/SiO$_2$	:	Cobalt on silica support
DRIFTS	:	Diffuse Reflectance Infrared Fourier Transform Spectroscopy
EDX	:	Energy Dispersive X-ray analysis
Fe	:	Iron
FID	:	Flame ionization detector
FTS	:	Fischer-Tropsch synthesis
LTFT	:	Low temperature Fischer-Tropsch synthesis
n	:	Carbon number
Ni	:	Nickel
Q-10	:	Silica support with mean pore diameter: 10 nm
SEM	:	Scanning electron microdcope
SPR	:	Slurry phase reactor
TCD	:	Thermal conductivity detector
TEM	:	Transmission electron microscope
TFBR	:	Tubular fixed bed reactor
TOF	:	Turn over frequency
TPR	:	Temperature-programmed reduction
W/F	:	Ratio of weight of catalyst (g) to flow rate of reactant (mol/h)
WGS	:	Water-gas shift reaction
W$_n$	:	Mass fraction of a product consisting of n carbon atoms
XRD	:	X-ray Diffraction
$\propto$	:	Chain growth probability factor

CHAPTER I

INTRODUCTION

Environmental demands for clean fuels lead to an obvious trend in energy consumption from oil and coal to clean resources. Uses of natural gas have been attracted because of their clean burn and abundant supply. Natural gas is well known as a clean and efficient hydrocarbon source. There is about 4000 trillion (4000×10^{12}) cubic feet of natural gas in the world, but about half is found in remote area that it is not economic to transport as a gas for long distance. Therefore, the conversion of remote natural gas to clean liquids is a desirable goal. An example of possible use of this remote resource was given by Velocci, 1991 (cited in Wender, 1996) that from only six trillion cubic of gas reserves, gas conversion technology could furnish about 100,000 barrel per day of premium transportation fuels for some 20 years.

Fischer-Tropsch synthesis (FTS) is a promising way to convert coal and natural gas to clean, environmentally-sound fuels and chemicals via synthesis gas (syngas). Although Fe, Co, Ni and Ru are the excellent catalysts for the FTS, only Fe and Co are the practical catalysts. When the coal gasification is the source of syngas containing a high ratio of CO/H_2, the iron based catalyst with high water-gas shift reaction (WGS) activity is preferable due to less hydrogen need. Nevertheless, CO_2 produced together with -CH_2- by using iron catalysts can lead to the greenhouse effect. On the other hand, cobalt is not a good WGS catalyst and oxygen mostly exits as water (Wender, 1996). Since FTS is a group of highly exothermic reactions, the slurry-phase reactors, which have high heat removal capabilities, are suitable for this reaction (Zhang et al., 2002). Co-based catalyst prepared with supports can provide the good attrition in slurry-phase reactor.

According to the high activity and selectivity to straight-chain hydrocarbon and the low activity for WGS, Co-based catalysts are chosen as preferable catalysts for FTS. However, the specific activities of these catalysts still need to be improved. To reach this purpose, the variation of promoters is being considered. Although the noble metals can provide the promotional effects for FTS,

their applications are limited because of their high cost. As a result, the addition of metal oxides as promoters is a preferable way to improve the performance of FTS catalyst because of their cheap price and availability.

The objective of this work is to improve the Co/SiO_2 activity by metal oxide promoters. The interesting effects of promoters are investigated in three cases.

Case I: Study on the effect of metal oxides promoters consisting of Al_2O_3, TiO_2 and ZrO_2 on Co/SiO_2 catalysts on Fischer-Tropsch synthesis in a semi-batch slurry-phase reactor.

Case II: Study on the loading amount of metal oxide promoters on Co/SiO_2 catalysts on Fischer-Tropsch synthesis.

CaseIII: Investigate preparation methods of metal oxide promoted on Co/SiO_2 catalysts by co-impregnation and sequential-impregnation methods.

CHAPTER II

BACKGROUND AND LITERATURE SURVEY

2.1 Synthesis Gas

Synthesis gas or syngas, a mixture of hydrogen and carbon monoxide, can be manufactured from ubiquitous natural gas, coal, petroleum, biomass and even from organic wastes (Wender, 1996). According to the availability and flexibility of the sources, the syngas has been widely used since the last century.

A very large number of publications point the way to possible future commercial applications and to new uses of syngas. The beginning of syngas chemistry occurred in the early part of 20th century. The hydrogenation of carbon monoxide to produce methane was occurred in 1902, followed by the discovery of ammonia (NH_3) synthesis in 1910. After decade, the Fischer-Tropsch synthesis was developed and then came the manufacture of methanol and higher alcohols. Nowadays, the uses of syngas are spread in many ways as shown in Figure2.1.

The largest commercial use of syngas is the hydrogen production, more than half of which is used in the synthesis of ammonia. The methanol synthesis is the second largest commercial use of syngas. The third industrial use of syngas is in the manufacture of paraffin, olefins and oxygenates via the Fischer-Tropsch synthesis. The hydroformylation (oxo) reaction is the fourth largest industrial use of syngas.
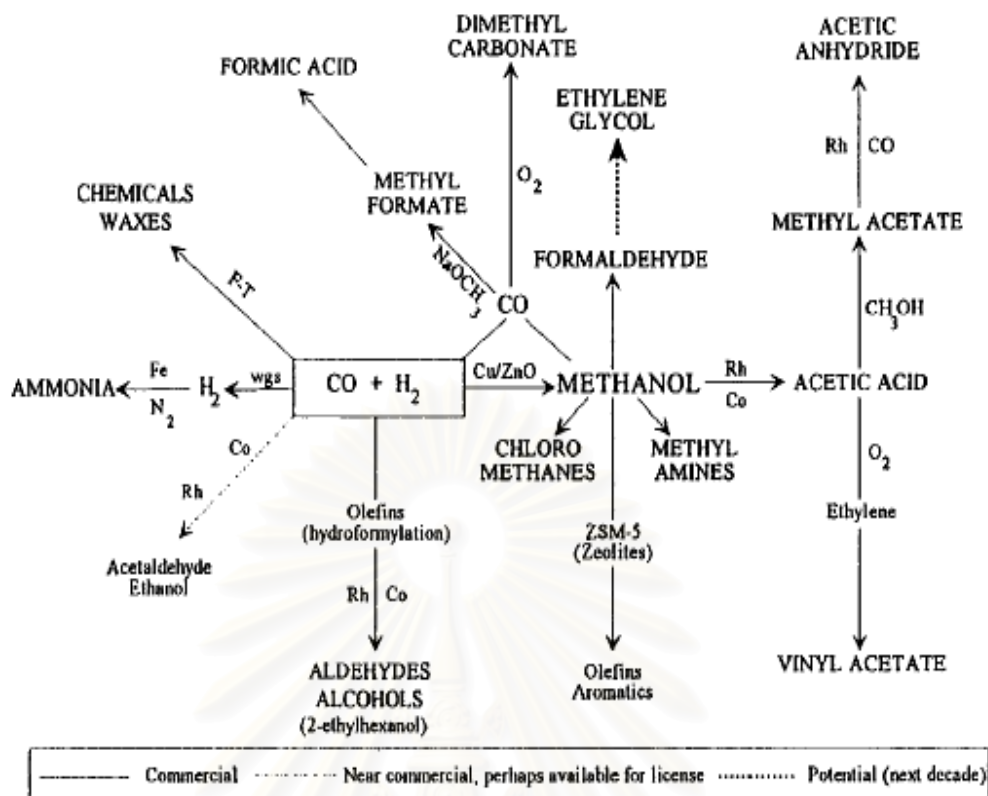
Figure 2.1 Commercial, near commercial and potential chemicals from synthesis gas (Wender, 1994).

2.1.1 Preparation of Synthesis Gas

The largest source of syngas is natural gas, which mainly constituents by methane. Petroleum fractions are the next largest syngas source and considerable quantities of syngas are made from coal. Various sources and processes for syngas production yield different ratios of H_2 to CO.

From natural gas

$$CH_4 + H_2O \Leftrightarrow 3H_2 + CO \qquad \Delta H = +49.0 \text{ kcalmol}^{-1} \qquad (2.1)$$

From oil fraction

$$-CH_2- + H_2O \Leftrightarrow 2H_2 + CO \qquad \Delta H = +36.1 \text{ kcalmol}^{-1} \qquad (2.2)$$

From coal

$$C + H_2O \Leftrightarrow H_2 + CO \qquad \Delta H = +31.1 \text{ kcalmol}^{-1} \qquad (2.3)$$

Steam/O_2 reforming of CH_4 is more efficient than steam/O_2 gasification of coal. In CH_4 reforming about 20% of the carbon ends up as CO_2, while for coal gasification the CO_2 production is about 50%. This large difference in efficiency is because of high hydrogen content of CH_4 compared to coal. Currently, natural gas is the preferable raw material for synthesis gas production because of both economic and environmental reasons. The use of CH_4 results in lower CO_2 emission than the use of coal.

2.2 Fischer-Tropsch Synthesis

Currently, the world's fuel and chemical production is based predominantly on petroleum crude oil. Table 2.1 gives an estimate of the ultimate economic recoverable sources of energy. The reserves of coal and of methane are higher than the others. Especially, the reserves of coal are about six fold higher than the sum of the others. Then, in the long term coal and methane should become the main source of liquid fuels and chemicals via, for example, the methanol and FT processes and both these processes are based on synthesis gas. The production of syngas from methane or coal and the conversion of syngas to a range of fuels and chemicals become increasingly because of the depletion and the risen price of crude oil. As a result, the Fischer-Tropsch synthesis is the promising route to produce transportation fuels in the age of energy crisis.

Table 2.1 Recoverable energy (Dry, 1996 and 2002)

Source	Reserve (10^9 barrel oil equivalent)	Life (years)[a]
Tar Sands	1500	40
Oil	2000	50
Shale Oil	2500	65
Gas (methane)	3000	75
Coal	53000	1300

[a] At an annual energy demand of about 40.10^9 barrel oil per year.

The Fischer-Tropsch Synthesis (FTS) is regarded as a surface-catalyzed polymerization process. The hydrogenation of adsorbed CO produces CH_x monomers, which react with the surface H atoms and hydrocarbon fragments to produce higher hydrocarbons as illustrated in equation 2.4 (Iglesia, 1997). The FTS has an interesting potential in the synthesis of high molecular weight products which can be cracked to yield high-grade diesel fuel in addition to gasoline.

$$CO + 2H_2 \rightarrow -CH_2- + H_2O \qquad \Delta H = -39.4 kcalmol^{-1} \qquad (2.4)$$
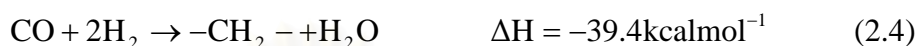
By the way, a lot of possible reactions occur during FTS reaction. The major reactions are given below.

Paraffins formation:

$$(2n+1)H_2 + nCO \rightarrow C_nH_{2n+2} + nH_2O \qquad (2.5)$$

Olefins formation:

$$2nH_2 + nCO \rightarrow C_nH_{2n} + nH_2O \qquad (2.6)$$

Alcohols formation:

$$2nH_2 + nCO \rightarrow C_nH_{2n+1}OH + (n-1)H_2O \qquad (2.7)$$

Water gas shift reaction:

$$CO + H_2O \rightarrow CO_2 + H_2 \qquad (2.8)$$

Boudouard reaction:

$$2CO \rightarrow C + CO_2 \qquad (2.9)$$

Coke deposition:

$$H_2 + CO \rightarrow C + H_2O \qquad (2.10)$$
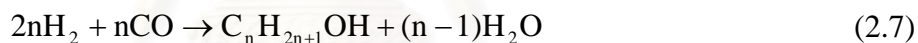
For alkalized iron, which is a good WGS catalyst, the water formed in equation (2.5), (2.6) and (2.7) reacts with CO to form H_2, so the apparent H_2/CO usage become smaller. For cobalt catalyst, which is not a good WGS catalyst, water is the main reaction by-product.

2.2.1 Products of Fischer- Tropsch Synthesis

The subsequent FT chain-growth process is comparable with a polymerization process resulting in a distribution of chain lengths of the products. In general, the reaction yields compose of hydrocarbons and oxygenated compounds. The major constituents of hydrocarbons are n-paraffins and olefins. Primary alcohols are the chief of oxygenated products. The distribution of the products depends on the catalyst and the process operation conditions such as temperature, pressure and residence time. The chain length distribution can be described by mean of the Anderson-Schulz-Flory (ASF) equation, which is represented as:

$$\log \frac{W_n}{n} = (n-1)\log\alpha + 2\log(1-\alpha) \qquad (2.11)$$

W_n is the mass fraction of a product consisting of n carbon atoms and α is the chain growth probability factor, which is the ratio of the chain propagation rate constant (r_p) to the chain propagation plus the termination rate constants (r_t) (Bond, 1987).

$$\alpha = \frac{r_p}{r_p + r_t} \qquad (2.12)$$

Anderson et al. (1984) analyzed the FT product distribution in fixed bed reactor and proposed that plots of $\log W_n/n$ against the carbon number n yielded straight line over a fairly large range of products. This showed the probability of chain growth α was constant. The assumption was that the monomer unit in most FT mechanisms is the same weight. A plot of the relative mass fraction of products formed as function of the ASF chain growth factor is illustrated in Figure 2.2. From this plot, higher values of α give higher molecular weight products.
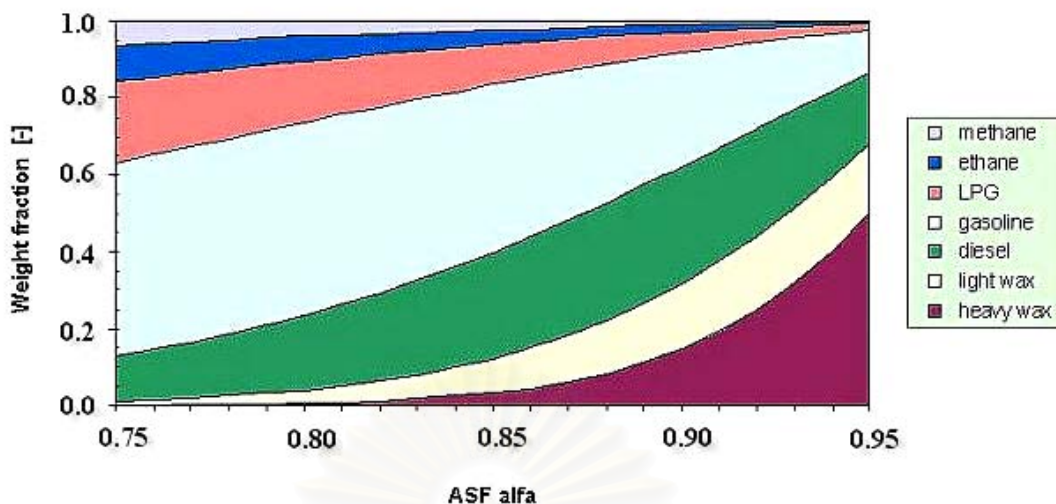
Figure 2.2 A plot of the relative mass fraction of products formed as function of the probability of chain growth (Energy research centre of the Netherlands, 2005).

2.2.2 Mechanism of Fischer-Tropsch Synthesis

Schulz (1999) proposed the main reaction pathway which composes of dissociation and the formation of $-CH_2-$ as the monomers of FT chain growth as shown in Figure 2.3. The FTS process has many kinds of hydrocarbon products including alcohols and other oxygenates. Therefore, Dry (1996) proposed a possible mechanisms which could account for the formation of these products. As can be seen in Figure 2.4, the first step is the dissociation of CO followed by the chemisorption of hydrogen. The insertion of CO into the chain causes the formation of aldehydes and alcohols while methylene insertion causes the formation of alkanes. The final step is a chain growth termination.
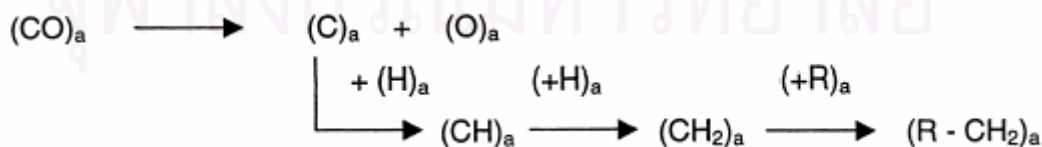
Figure 2.3 Reaction pathway of surface-carbon formation via CO dissociation.
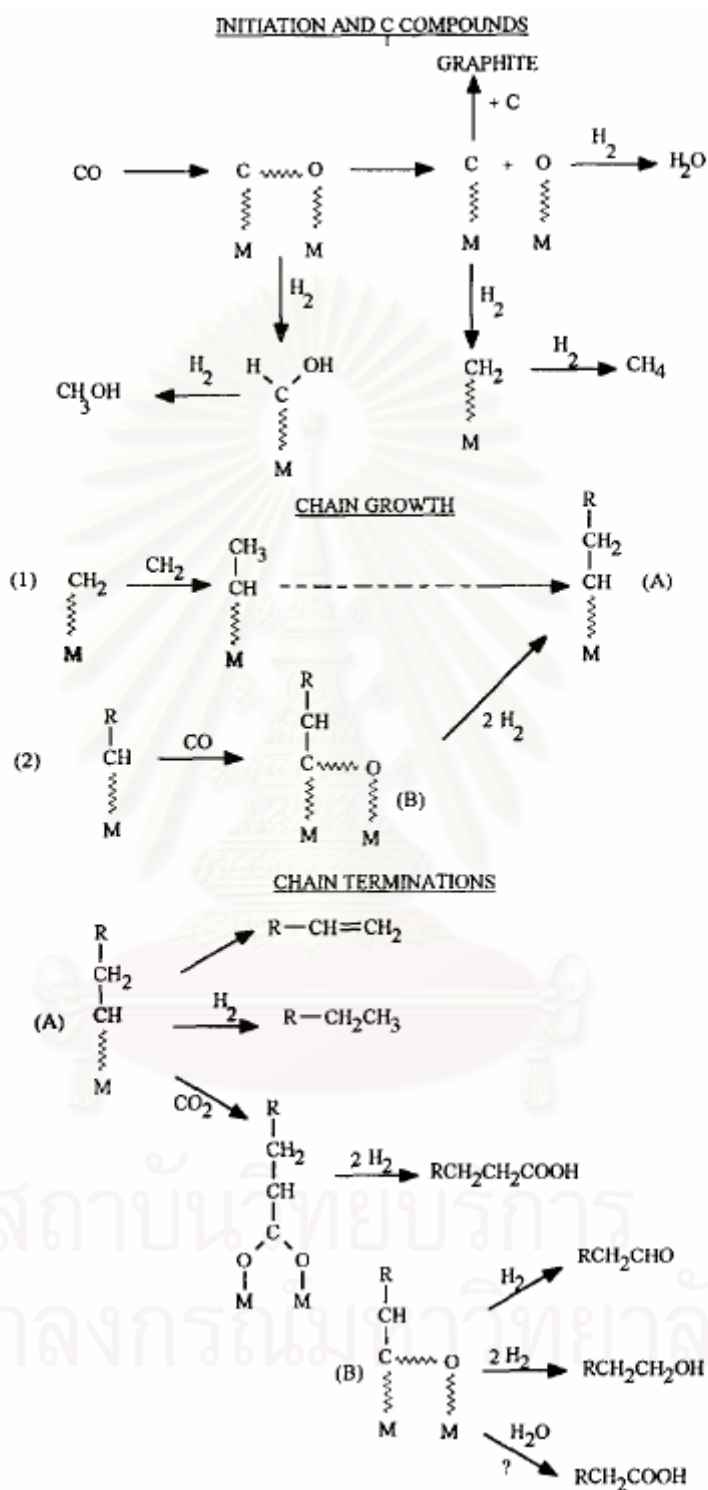
Figure 2.4 Mechanism of the FT reaction (Dry, 1996).

2.3 Fischer-Tropsch Reactors and Developments

Currently, there are two FT operating modes, high- and low-temperature processes. The high-temperature (300-350°C) process (HTFT) is operated with iron-based catalysts to produce low molecular weight olefins for petrochemical production. The low-temperature (200-240°C) process (LTFT) uses either iron or cobalt catalysts to produce high molecular weight paraffins for diesel and gasoline productions (Dry, 2002). There are two kinds of reactors which are practically used at present.

2.3.1 Arge Tubular Fixed Bed Reactor (TFBR)

From 1955 up to 1993, Sasol used only Arge tubular fixed bed reactors (TFBR's) for LTFT synthesis. The catalyst used for this reactor is an extruded precipitated and promoted iron based catalyst. The general arrangement of the reactor is shown in Figure 2.5.

An advantage of the TFBR is that it is easy to separate the wax product from the catalyst but there are several disadvantages of TFBR. The reactor has a high capital cost and scale up of reactor is difficult due to mechanical problems. Because of low heat removal capabilities of this reactor, the maximum temperature, which is required for maximum reaction rate, is limited in order to prevent catalyst deactivation due to carbon formation on the catalyst. Carbon formation brings about the blockage of reactor tubes, a loss in catalytic efficiency and a need of catalyst replacement. Pressure drops across the TFBR are high and this causes the high compression cost.

In a fixed bed commercial reactor, the extent of deactivation and the potential deactivation mechanisms can be separated into three regions related to the reactor axial position. In the case that the synthesis gas enters from the top of the reactor, these three regions can be normally characterized as shown below (Espinoza et al., 1999).

Top region   acts as a sulphur trap, low partial pressure of water

Middle region less sulphur, higher partial pressure of water

Bottom region almost no sulphur, the highest partial pressure of water
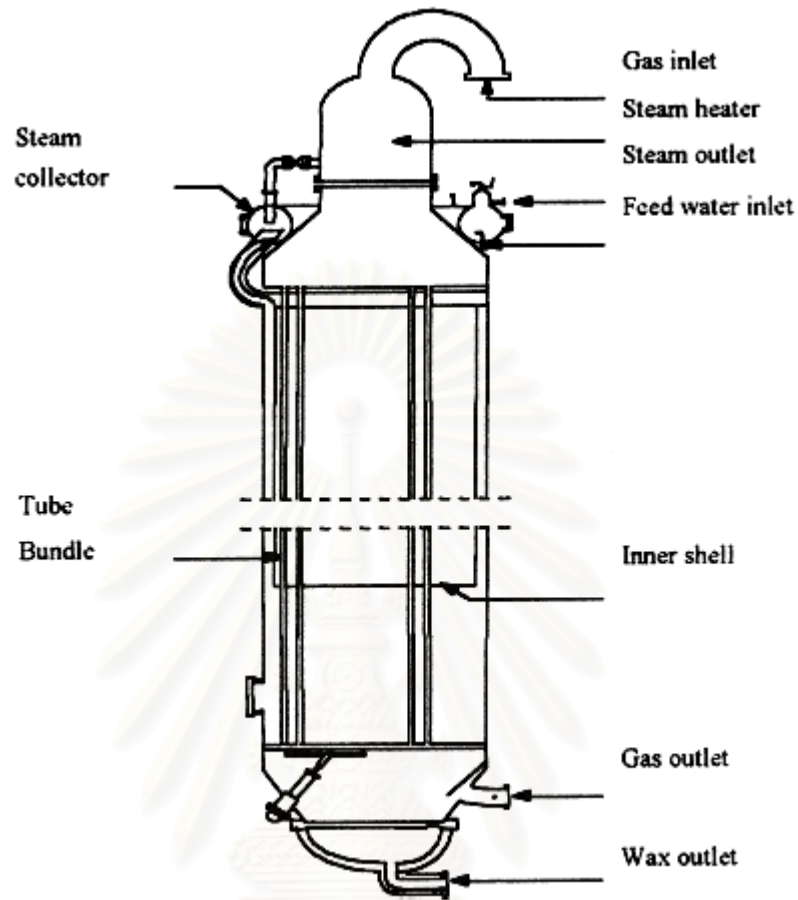
Figure 2.5 Tubular fixed bed (ARGE) reactor.

The deactivation of FT catalysts in fixed bed reactor is due to sulphur, a well know irreversible poison for either Fe or Co based FT catalyst, and water. Sulphur is preferentially located from the top of the catalyst bed and its concentrations in the bed decreased rapidly at the position far from the top section. The middle section of reactor is a mild catalyst deactivation region, where the reoxidising effect of water causes the deactivation of catalysts. At the bottom of the reactor, the water partial pressure is high that it increases the reoxidation and loss of active surface area resulting in low FTS activity. Carbon formation or coke is present in very small amount and it does not have a significant effect on the catalyst deactivation.

2.3.2 Sasol Slurry Phase Reactor (SPR)

The slurry phase reactor (SPR, also known as slurry bed reactor or slurry bubble column reactor) was developed by Sasol to convert natural gas to liquid fuels. The SPR is simpler than a TFBR as depicted in Figure 2.6.
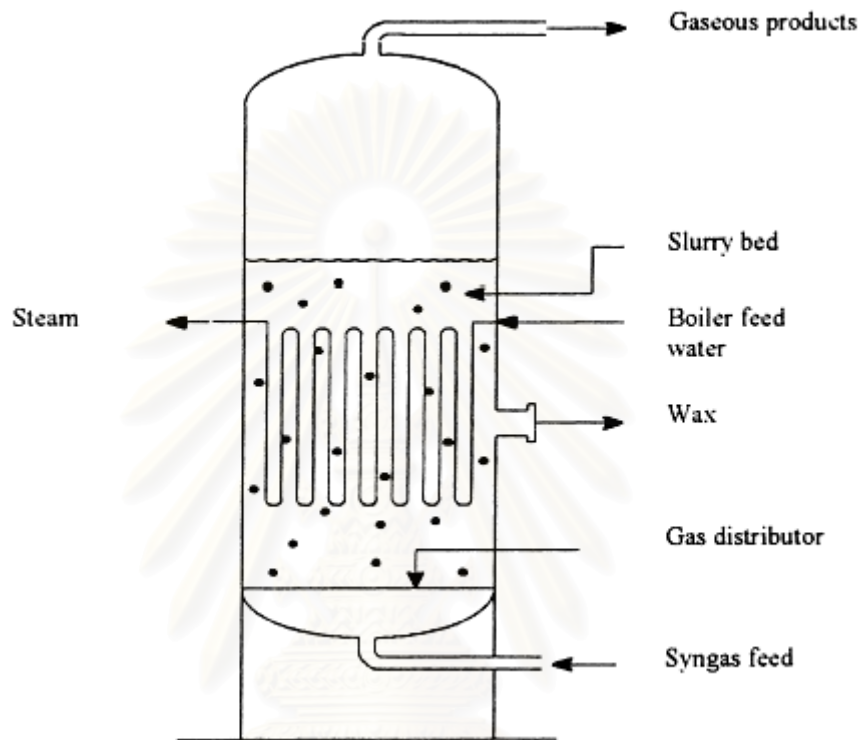
Figure 2.6 Slurry bed reactor.

The SPR consists of a shell fitted with cooling coils in which steam is generated. Syngas is distributed at the bottom and it rises through the slurry, which consists of liquid reaction products and suspended catalyst particles, to produce hydrocarbon. The reagent gas diffuses from the gas bubbles through the liquid phase to the suspended catalyst. Hydrocarbon and water were generated during FTS. The heavier hydrocarbon products are still in the slurry phase, while the lighter gaseous products, unreacted syngas and water pass through the slurry bed to the gas outlet.

Since the FTS are highly exothermic, it is important to rapidly remove the heat of reaction in order to avoid overheating of the catalyst. The slurry phase reactor is high heat removal reactor and tends towards isothermal operation resulting in lower rate of deactivation due to sintering. Moreover, it gives more flexibility

towards temperature control, so its operating temperature can be higher than in TFBR without the catalyst deactivation.

Basically, the main deactivation occured in SPR are similar to those in a fixed bed reactor which is related to the concentration of sulphur in the feed and to the partial pressure of water in the reactor. Unlike the catalysts in fixed bed reactors which the top section acts as a sulphur guard, the catalysts in SPR are in continuous circulation, therefore, sulphur poisons over the whole catalysts. In addition, the continuous catalyst circulation ensures that all the catalysts are periodically in the top section of the SPR, which the partial pressure of water is the highest. Nevertheless, the suitability of SPR for periodic on-line replacement of catalysts results in nearly constant catalyst activity and selectivity with time on line.

2.4 Fischer-Tropsch Catalysts

The metal catalysts used in FTS must be able to dissociate CO (split the carbon-oxygen bond). Transition metal catalysts on the left side of the periodic table are used in FTS, whereas those on the right side are methanol synthesis catalysts as shown in Figure 2.7. However, the line is shifted further to the right at high temperatures and at these temperatures (473-573 K) CO is able to dissociate even on copper and palladium.
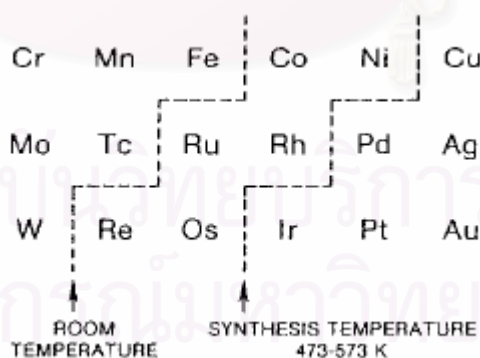
Figure 2.7 Metals that adsorb CO dissociatively and non-disociatively at ambient temperature and Fischer-Tropsch reaction temperatures (Brode′n et al., 1976 cited in Wender, 1996).

For commercial application, only the metals iron, nickel, cobalt and ruthenium have the required FT activity. On the relative price as the scrap iron as 1.0 shows that the approximate cost of nickel, cobalt, and ruthenium are 250, 1000 and 50,000, respectively (Dry, 2002). Nickel metal is unsuitable catalysts because it is a very active hydrogenation catalyst and thus under practical operating conditions too much methane is generated. Ruthenium is the most excellent FT catalyst due to high activity and over 90% C_5^+ selectivity at lower temperature operating conditions (Zhang et al., 2002). Nevertheless, ruthenium is expensive and unavailable supply for large scale application. This leaves only iron and cobalt as practical catalysts.

2.4.1 Iron-Based Catalysts

Iron-based catalysts used in the low-temperature process are prepared by precipitation technique, promoted with Cu and K_2O for high reducibility and activity and bounded with SiO_2 for higher mechanical strength. The iron catalysts used in the high-temperature application is prepared by fusing magnetite together with K_2O and structural promoters such as Al_2O_3 or MgO. The active catalyst is in the form of iron carbide phases after it is reduced in hydrogen stream. The main products in the low-temperature operation are hydrocarbons which can be converted to high quality diesel fuel via hydrocracking, whereas most of the high-temperature process products are low molecular weight olefins, which are the feedstock for petrochemical production. FT iron catalysts have good water gas shift (WGS) activity, producing hydrogen, in contrast to cobalt catalysts, so the apparent H_2/CO usage becomes smaller. Thus, CO-rich syngas, H_2/CO molar ratio: 1.0, obtained from high-temperature coal or heavy oil gasification through partial oxidation is favorable for this kind of catalysts. However, it is undesirable for FT synthesis from hydrogen-rich syngas produced from natural gas.

Anderson (Anderson ed., 1956 cited in Epinoza, 1999) proposed kinetic equations for iron and cobalt based FT catalysts. These rate expressions are shown in eq. (2.13) and (2.14).

Iron :
$$-r_{FT} = \frac{k_{FT}P_{CO}P_{H_2}}{P_{CO} + bP_{H_2O}} \tag{2.13}$$

Cobalt :
$$-r_{FT} = \frac{k_{FT}P_{CO}P_{H_2}^2}{1 + bP_{CO}P_{H_2}^2}$$
(2.14)

The equation proposed for cobalt contains only H_2 and CO terms, whereas the equation for iron catalyst is related to term of water. There is an agreement that the FT kinetics for cobalt-based catalysts is not affected by water inhibition. On the other hand, iron-based catalysts with high activity in WGS reaction to produce water and CO_2, has an inhibiting effect of water on the kinetics. Thus, the rate of reaction of iron catalysts will decrease the conversion, not only due to the consumption of the reactants but also due to the formation of reaction products, water and CO_2. Because of the iron catalyst characteristics discussed above, the recent interest in FT catalysts for diesel fuel production from natural gas has been concentrated on cobalt-based catalysts.

2.4.2 Cobalt-Based Catalysts

The use of cobalt based catalysts is an alternative way for FTS in the future because of their environmentally friendly byproducts as water. On the other hand, iron based catalysts have high activity in WGS reaction to produce water and CO_2 as a by product which causes an environmental problem, i.e. greenhouse effect. Besides, the FTS is a group of highly exothermic reactions, therefore, the slurry-phase reactors, which have high heat removal capabilities, are appropriate for this reaction in order to operate at or near isothermal conditions. With both fixed-bed and slurry reactors, the catalyst particles should be able to use without crushing. With Co-based catalyst, this may not be a serious problem because the support can be chosen to provide the physical integrity required for either operation, while an iron based-catalyst has not been supported. Unsupported iron catalysts will be crushed to become fine catalysts, which either plug the fixed-bed reactor, generating high pressure gradients, or can not be separated at a reasonable rate from the catalyst-containing slurry (Jager, 1995). All the reasons above, nowadays many researches are focus on cobalt metal as FT catalysts.

Because of the high price of Co, it is desirable to minimize the amount of used Co but to maximize the available surface area of the metal. Currently, catalyst preparation techniques focus on production of a well-dispersed cobalt phase on high

surface supports such as Al_2O_3, SiO_2 or TiO_2 (Oukaci et al., 1999). Industrial FTS catalysts are a multi-component system, and the typical catalyst formulations of the major petroleum corporations are presented in Table 2.2.

Table 2.2 Composition of the patented Co catalysts of several petroleum companies (Zhang, 2002).

Company	Component of main catalyst*			Reactor
	Oxide Promoter	Noble metal promoter	Support	
Shell	IIIB, IVB, VB	Pt, Ir, Rh, Re, Ru	SiO_2	Fixed-bed
Exxon	Th, Zr, Hf, Ce, U, Al, Si	Re, Ru	TiO_2	-
Gulf Oil	La, Mn, Th, Mg, IIIB,IVB	Ru	η,γ-Al_2O_3	Fixed-bed
Sasol	Zr, Ti, Cr	Pt	γ-Al_2O_3	Slurry-bed
IFP	Cu, Sc, Mo, K, Ti	-	SiO_2	-
Statoil	La	Re	γ-Al_2O_3	-

* Active component of the catalyst: Co.

The formation of highly dispersed cobalt catalyst requires strong interaction between support and cobalt precursor. This interaction leads to obstruct the low-temperature reduction of the precursor to cobalt metal. High reduction temperatures are required for strongly interacting support resulting in the formation of large Co metal particles. On weakly interacting supports, although cobalt precursors are easily reduced, very small precursor crystallites are not stabilized during impregnation and drying steps. Thus, the optimum cobalt dispersion is favored by the combination of support-precursor with intermediate interaction strength (Soled et al., 1995 cited in Iglesia, 1997).

2.5 Development of Co-Based Catalyst

2.5.1 Support Effect

In the absence of diffusion limitation, the rate of a catalysed reaction should be proportional to the surface area of the active phase. To maximize the active phase for a given mass of active metal, it is necessary to make the particles as small as possible, i.e. to maximize the atoms on the surface: this fraction is termed the dispersion or the fraction exposed. Such fine metal particles can be easily made by

using support. The advantages of using the metal supported catalysts include the following (Bond 1987).

1) The catalyst is easily and safely handle.

2) The catalyst is easily to be recovered by filtration.

3) Metal supported catalysts do not grow in size by sintering when heated to high temperature in high temperature treatments.

4) The support provides chances of bringing promoters into close contact with the active metal.

The research about the effects of the supports in FT catalysts are collected as follows.

The result from Reuel and Bartholomew (1984) indicated that the specific activity of cobalt significantly decreases with increasing its dispersion. Product selectivity is the best correlated with dispersion and extent of reduction; the molecular weight of hydrocarbon products is lower and the CO_2/H_2O ratio is higher for the catalysts having higher dispersion and lower extent of reduction. This effect may be due to stable oxides in the well dispersed, poorly reduced catalysts, which catalyze WGS reaction thereby increasing the H_2/CO ratio at the surface. Their results show that significant fractions of CO_2 are produced on highly-dispersed, poorly-reduced cobalt catalysts, showing behavior of a typical iron catalyst. The high selectivity to CO_2 of iron catalysts is probably due to the presence of iron oxides which catalyze the WGS reaction. Similarly, the high CO_2 selectivity of poorly reduced cobalt catalysts may be due to the abundance of stable surface oxides, e.g., cobalt spinels such as cobalt aluminate, which are inactive in CO hydrogenation but it is active in WGS reaction. WGS reaction increases the H_2/CO ratio at the catalyst surface by promoting the formation of lighter hydrocarbon products such as methane.

Rathousky et al. (1991) studied the use of complex metal oxides as support. They found that the catalytic properties of 10 wt% $Co/SiO_2-Al_2O_3$ was more similar to Co/SiO_2 than to Co/Al_2O_3, but not so different from Co/Al_2O_3 and Co/SiO_2. The $SiO_2-Al_2O_3$ multiplex could lead to the formation of more acid sites resulting in the increase of isomerization product.

Lapidus and Krylova (1992) investigated the influence of calcinations temperature on the catalytic properties of 10wt % Co/Al_2O_3 and Co/SiO_2. The total

hydrocarbon yield decreased on Co/SiO_2 catalysts but increased on Co/Al_2O_3 catalysts when the calcinations temperature increased. Moreover, they found that the oxide phases had some effects on catalytic properties. On the surface of the Co/SiO_2 catalyst, Co_3O_4 supposedly reduces the total hydrocarbon yield. The cobalt-support surface compounds on Co/Al_2O_3 catalysts cause an increase in the total hydrocarbon yield and C_5^+ fraction selectivity.

Bessell (1993) investigated the catalytic activity and product selectivity in FT reaction of cobalt catalysts supported on Kieselguhr, silica, alumina, bentonite, zeolite Y, mordenite and ZSM-5. The correlation of catalyst reducibility, adsorptive properties, as well as support acidity, surface area and structure were considered. It was found that the high surface area supports gave high cobalt dispersion, producing high FT activity as long as the reducibility of the cobalt is not hindered by metal-support interactions or ion exchange, or the pore diffusion or blocking effects are not taking place. The support acidity strongly influenced hydrocarbon products; non-zeolitic supports with low acidity promoted the classic straight chained FT product. For the zeolite-supported catalysts, the strongly acidic ZSM-5 supported catalyst produced the branched products.

Voß et al. (2002) characterized the properties of Co catalysts supported on Al_2O_3, SiO_2 and TiO_2 by temperature programmed reduction (TPR) and X-ray photoelectron spectroscopy (XPS). It was found that the dispersion of Co metal was in the sequence of $Co/Al_2O_3 > Co/TiO_2 > Co/SiO_2$. In the case of alumina- and titania-supported cobalt catalysts, there are the formations of high-temperature compounds, $CoAl_2O_3$ and $CoTiO_3$, respectively. In addition, Co/Al_2O_3 showed higher degree of dispersion than Co/SiO_2, although the metallic Co surface related to the total mass of the catalyst is smaller in the case of Co/Al_2O_3. This can be explained that only the reducible Co amount is taken into consideration, which is significantly smaller for Co/Al_2O_3 due to some Co embedded into the Al_2O_3 lattice (Coulter et al, 1995).

Saib et al. (2002) studied the effect of pore diameter over 20 wt% Co/SiO_2 catalysts and found that the supports with 10 nm pore size proved to be the most active and selective for hydrocarbon formation.

Zhang et al. (2003) found that the acidity of support shows a great influence on the interaction between metallic cobalt and support including the reducibility of cobalt. The support with low acidity leads to the higher active FTS catalysts. The higher reducibility and more bridged-type CO, which is favored by γ-alumina with low acidity, appear to be responsible for high C_5^+ hydrocarbon selectivity and low methane selectivity.

2.5.2 Preparation and Treatment

Ming and Baker (1995) investigated the effect of the impregnation solution pH value on the dispersion, reducibility and reaction performance of Co/SiO_2 catalysts. The pH value of impregnation solution first influenced the surface charge and then the physical and chemical properties of the cobalt species on the surface of the silica gel. For example, at pH < 2 the silica surface is positively charged making lower dispersion of cobalt leading to poor catalytic activity. At pH $\geq$ 5, cobalt reacts to form silicates or irreducible hydrosilicates.

Kraum and Baerns (1999) examined the influence of cobalt precursors (e.g. $Co(COO)_2$, $Co(CH_3COO)_2$ and $Co(NO_3)_2$) on the properties of Co/TiO_2 catalysts. The dispersion of Co catalysts from organic cobalt salts was higher than that of Co/TiO_2 catalysts from $Co(NO_3)_2$.

Sun et al. (2000) prepared FT catalysts with 10% Co/SiO_2 from mixed cobalt salts. The co-impregnation of cobalt acetate and cobalt nitrate could improve the catalytic activity of cobalt on silica catalyst. The supported cobalt acetate had stronger interaction with SiO_2 than cobalt nitrate and was difficult to be reduced. It was assumed that the metal cobalt readily reduced from cobalt nitrate could promote the reduction of Co^{2+} to the metallic state in cobalt acetate via the H_2 spillover mechanism during the reduction step as shown in Figure 2.9.

Tsubaki et al. (2001a) prepared bimodal silica by introducing SiO_2 sol into large pores of SiO_2 gel pellet directly. Cobalt supported on this bimodal silica support provided significantly high activity because of large surface area of this support enhancing higher cobalt dispersion and its large pore size improving the diffusion of reactants and products in liquid-phase Fischer-Tropsch synthesis.
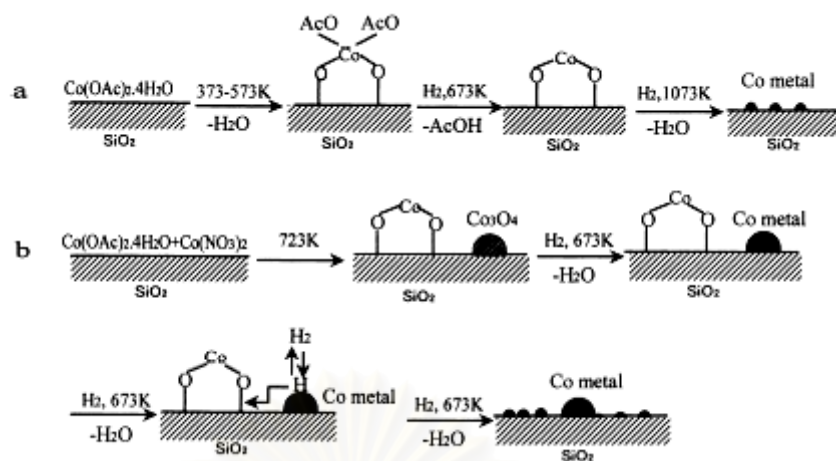
Figure 2.8 Proposal reduction procedure of Co(II)acetate, Co(II)nitrate/Co(II)acetate on silica during catalyst preparation.;a: Co(II)acetate; b: Co(II)nitrate/Co(II)acetate

Zhang et al. (2003) studied the influence of chemical treatment on Co/γ-Al$_2$O$_3$ catalysts. Cobalt catalysts supported on ammonia and ammonium nitrate treated alumina with lower acid sites number show higher reducibility and more bridge-form CO resulting in high activity and C$_5^+$ hydrocarbons selectivity. However, alumina treated by water, ethanol and acetic acid can suppress the catalytic activity of Co catalysts. The existence of acetate and high acid sites number increase the interaction between cobalt and support leading to the lower reducibility of catalyst.

2.5.3 Promoter Effect

Promoter is used to denote the action a substance which is added to enhance the catalytic performance. The functions of the promoters for Co catalysts are summed up by Zhang et al. (2002) as follows:

1) to structurally modify the metal surfaces induced by promoter
2) to improve the reducibility and dispersion of metal cobalt
3) to transfer charge between the promoters and the metal
4) to play important roles in the activation of CO and H$_2$
5) to improve the longevity of Co catalysts

Generally, promoters can be divided into structural promoters and electronic promoters (Wieckowski, 2003). The structural promoters enhance and

stabilize the dispersion of the dispersed active phase on the catalyst support, while the electronic ones enhance the catalytic properties of the active phase by modifying the chemisorption properties of the catalyst surface. This effect involves the chemisorptive bond strength of reactants and intermediates.

2.5.3.1 Rare Earth Metal Oxide Promoter

Rare earth metal (e.g. La, Ce, Gd) usually occur together in minerals as their oxides and are difficult to separate because of their chemical similarity (Columbia Encyclopedia, 2005). An investigation of La-modified 10wt%Co/Al_2O_3 catalysts by Vada et al. (1994 cited in Zhang, 2002) demonstrated that the addition of La favored the formation of heavy hydrocarbons and increased the selectivity of olefins and chain growth probability at low La loading (La/Co=0.05). However, at high La loading (La/Co=0.10) the catalytic activity, heavy hydrocarbon and olefin selectivity all decreased.

Haddad et al. (1996) studied the influence of La promotion on the reaction performance of 20wt% Co/SiO_2 catalysts in a La/Co range between 0 and 0.75. They found the similar conclusions to those for the La-promoted Co/Al_2O_3 catalysts. These authors thought that La could weaken the interaction between metal cobalt and the support, and induce more CO to become the active state.

Ernst et al. (1999) compared the function of Ce and La on the reaction performance of 25wt%Co/SiO_2. They found that both Ce and La acted as hydrogen storage agents and thus enhanced the selectivity of methane formation. The promotion with Ce and La catalysts had a low catalytic activity.

2.5.3.2 Noble Metal Promoter

Supported noble metals are excellent FT catalysts because the noble metals have H_2 spillover effect which enhance the activity of FTS. However, because of their high cost and unavailable supplies, the noble metals are preferably used as promoters. Usually, the catalysts are promoted with a small amount of noble metal such as Pt, Ru, Re which is claimed to enhance the reducibility and also keep the cobalt metal surface clean during FT reaction (Iglesia, 1992).

Tsubaki et al. (2001b) proposed the different functions of Ru, Pd and Pt added into Co/SiO_2 catalysts. The catalytic activity varied in order of RuCo >

PdCo > PtCo > Co. The addition of small amount of Ru can remarkably increase the catalytic activity and the reduction degree, whereas Pt and Pd promoted cobalt dispersion. The characterization data suggested that Ru enriched on cobalt surface promoted the reduction of Co catalysts, while Pt and Pd uniformly dispersed in the form of Pt-Co or Pd-Co alloy enhanced the dispersion and scarcely affected the reducibility of Co catalysts. Rhenium is also a promoter for supported Co catalysts.

Rygh et al. (2000) used the DRIFTS technique to investigate the influence of 1%Re promoter on the properties of 12% Co/Al_2O_3 catalysts. They found that Re promoted the reduction of metal cobalt, increased the adsorption amount of bridged-type CO and lowered the reduction temperature of cobalt catalysts.

Li et al. (2002) investigated the influence of B, Ru and Re on the performance of Co/TiO_2 catalysts and found that catalytic activity and C_5^+ hydrocarbon selectivity of Ru and Re promoted catalysts increased. They proposed that Re could suppress the aggregation of metal cobalt and favor the formation of diesel fractions, whereas Ru increased the number of active sites and promoted the selectivity of gasoline and diesel fractions.

Schanke et al. (1995) found that the activities of Pt-modified catalysts were approximately 3 to 5 times greater than those of the unmodified catalysts, but the product selectivity was hardly influenced. Their study revealed that Pt could lower the reduction temperature of Co catalysts, increase the reaction intermediates but not affect the intrinsic rate.

2.5.3.3 Metal Oxide Promoter

Although noble metals provide promotional effects on FTS, their applications are limited because of their high cost. As a result, addition of metal oxides as promoters is a preferable way to improve the performance of FTS catalyst due to their cheap prices and available supplies. Oxides such as SiO_2, Al_2O_3, MgO, ThO_2, La_2O_3 and ZnO, which are difficult to be reduced, are called structural promoters. They provide large surface areas and prevent active metal from recrystallization and sintering (Wender, 1996).

Stranick et al. (1987) studied the influence of TiO_2 on 3 wt%Co/Al_2O_3 catalysts and found that the dispersion of metal cobalt increased with TiO_2 loading

and there was an interaction between cobalt and TiO_2 in the form of $CoTiO_3$ observed by XRD. Furthermore, the addition of TiO_2 could improve the product selectivity of the FT catalysts.

Ali et al. (1995) studied the influence of Zr addition 20 wt% Co/SiO_2 on FTS using catalysts prepared in different ways. The Zr-promoted catalysts exhibited higher overall rates of FTS compared to unpromoted Co/SiO_2. The sequentially impregnated $Co/Zr/SiO_2$ catalysts showed the most active. However, the co-impregnation method of preparation increased cobalt dispersion. The active interface created in ZrO_2-Co could facilitate CO dissociation leading to high activity in FTS reaction.

Feller et al. (1999) observed that the addition of ZrO_2 in Co/SiO_2 decreased the dispersion of cobalt and weakened interaction between cobalt and SiO_2. Consequently, the reducibility of the catalysts was increased Rohr et al. (2000) examined the effect of ZrO_2 on the properties of Co/Al_2O_3 catalysts and found that ZrO_2 could improve the concentrations of reactive intermediates but hardly affect the reducibility, dispersion and intrinsic rate. Chen et al. (2001 cited in Zhang, 2002) found that a Co-ZrO_2 interface formed on the $Co/Zr/SiO_2$ catalysts that increased hydrogen and CO uptake adsorbed at low temperatures and affected the adsorption-mode of CO.

The specific activities of these catalysts still need improvement. To reach this purpose, the variation of promoters is being considered. It is interesting to study the effects of other metal oxides as promoters on the Co/SiO_2 catalysts such as Al_2O_3, TiO_2 and ZrO_2.

CHAPTER III

EXPERIMENTAL AND CHARACTERIZATION

3.1 Materials

The silica supports used in this study was Cariact Q-10 silica, which were received from Fuji Silysia Chemicals Ltd. (specific surface area: 283 m^2 g^{-1}, pore volume: 1.22 ml g^{-1}, pellet size: 75-500 μm and mean pore diameter: 10nm). Alumina supports were prepared by using NA-3 alumina from Nikki Universal Co.,Ltd. (specific surface area: 136.23 m^2 g^{-1}, pore volume: 0.59 ml g^{-1} and mean pore diameter: 17nm). Titania supports used using JRC-TIO-4 from Catalysis Society of Japan (specific surface area: 55.55 m^2 g^{-1}, pore volume: 0.17 ml g^{-1} and mean pore diameter: 12.34nm). Metal oxide precursors consisting of titanium (IV) bis (ammoniumlactato) dihydroxide 50% wt. solution in water [(($CH_3CHCO-)CO_2NH_4)_2Ti(OH)_2$], cobalt (II) nitrate hexahydrate [$Co(NO_3)_2.6H_2O$], aluminium nitrate enneahydrate [$Al(NO_3)_3.9H_2O$], zirconium nitrate oxide dihydrate [$ZrO(NO_3)_2.2H_2O$] and n-hexadecane,liquid medium in slurry-phase reaction, were purchased from Kanto Chemical. Pure gas and syngas were purchased from Takachiho Chemical Industrial.

3.2 Catalyst Preparation

The impregnation method was chosen as catalyst preparative method because the precipitation method lead to the containment of some cobalt metals inside the granules. This procedure may render cobalt inaccessible to the reagents. Moreover, the precipitated catalysts have low mechanical strength (Lapidus et al., 1992). Consequently, the impregnation is used as a preparative method to overcome the above-mentioned problem and to prepare an effective catalyst with low cobalt content.

There were two impregnation methods performed to study the effect of preparations related to the cobalt-metal oxide formation. The first method was sequential-impregnation method and the second one was co-impregnation method.

3.2.1 Sequential-Impregnation Method

The metal oxide-containing supports were prepared by incipient wetness of commercially available silica gel (Cariact Q-10) with aqueous solution of the metal nitrates. The metal oxide promoted supports were evacuated for 1 h to disperse the nitrate precursor on the supports and then dried in air at 393 K for 12 h. After that, they were calcined at 673 K for 2 h. Cobalt nitrate was dissolved in distilled water and impregnated into the obtained supports by incipient wetness method. The cobalt loading was 10 wt% on all supports. The catalysts were dried at 393 K for 12 h and calcined at 673 K for 2 h to decompose nitrate ions.

3.2.2 Co-Impregnation Method

Usually, if more than one element is impregnated on the support, the word "co-impregnation" is used. Metal oxide together with cobalt nitrate was dissolved in water to impregnate on silica support. The co-impregnated catalysts were evacuated for 1 h to remove air in the pores of supports, and dried in air at 393 K for 12 h. After that, they were calcined at 673 K for 2 h.

```
┌─────────────────┐
│  Dissolve a metal │
│ oxide precursor in │
│  deionized water  │
└─────────────────┘
         │
         ▼
┌─────────────────┐
│  Add the precursor │
│ solution on the support │
└─────────────────┘
         │
         ▼
┌─────────────────┐
│    Evacuate for   │
│  dispersion of the │
│  precursor solution │
└─────────────────┘
         │
         ▼
┌─────────────────┐
│ Dry the impregnated │
│  support for water │
│      removal      │
└─────────────────┘
         │
         ▼
┌─────────────────┐
│    Calcine to     │
│    decompose     │
│   nitrate ions    │
└─────────────────┘
```
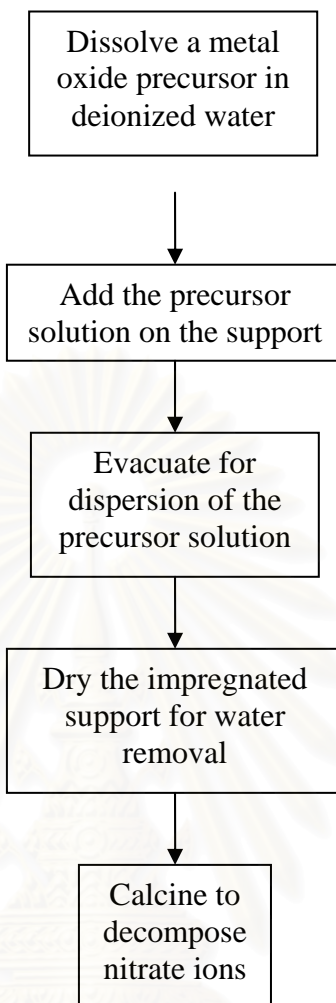
Figure 3.1 Schematic diagram showing the various steps of impregnation process.

3.3 Catalyst Activation

The reduction of catalysts was carried out in the glass tubular reactor. Before reduction, calcined catalyst (2.5 g) was initially flushed with nitrogen at 373 K for 1 h and then reduced under flowing H_2 100 % at 673 K for 10 h. After the activated catalysts were cooled down to room temperature, they were passivated by 1 % oxygen in nitrogen to prevent them form oxidation with oxygen in air. The schematic diagram was shown in Figure 3.2.
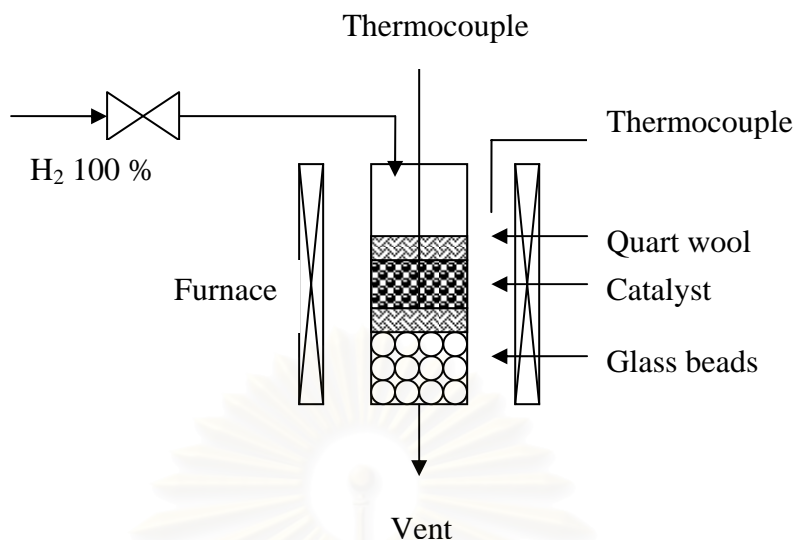
Figure 3.2 Schematic diagram of the reduction experiment

3.4 Fischer-Tropsch Synthesis in Semi-Batch Slurry-Phase Reactor.

FTS reaction was carried out in a semi-batch slurry-phase reactor with inner volume of 80 ml. The passivated catalyst 1.0 g was loaded in the reactor with 20 ml liquid medium (n-hexadecane). Before the reaction, reactant gas of 0.1 MPa was used to in situ reduce the catalyst again at 513 K for 1 h. Syngas flow rate in the reduction was 75 ml/min. During the reaction, effluent gas released from the reactor was first cooled with an ice trap, and then introduced to an online gas chromatograph. The configuration of the reactor is illustrated in Figure 3.3.
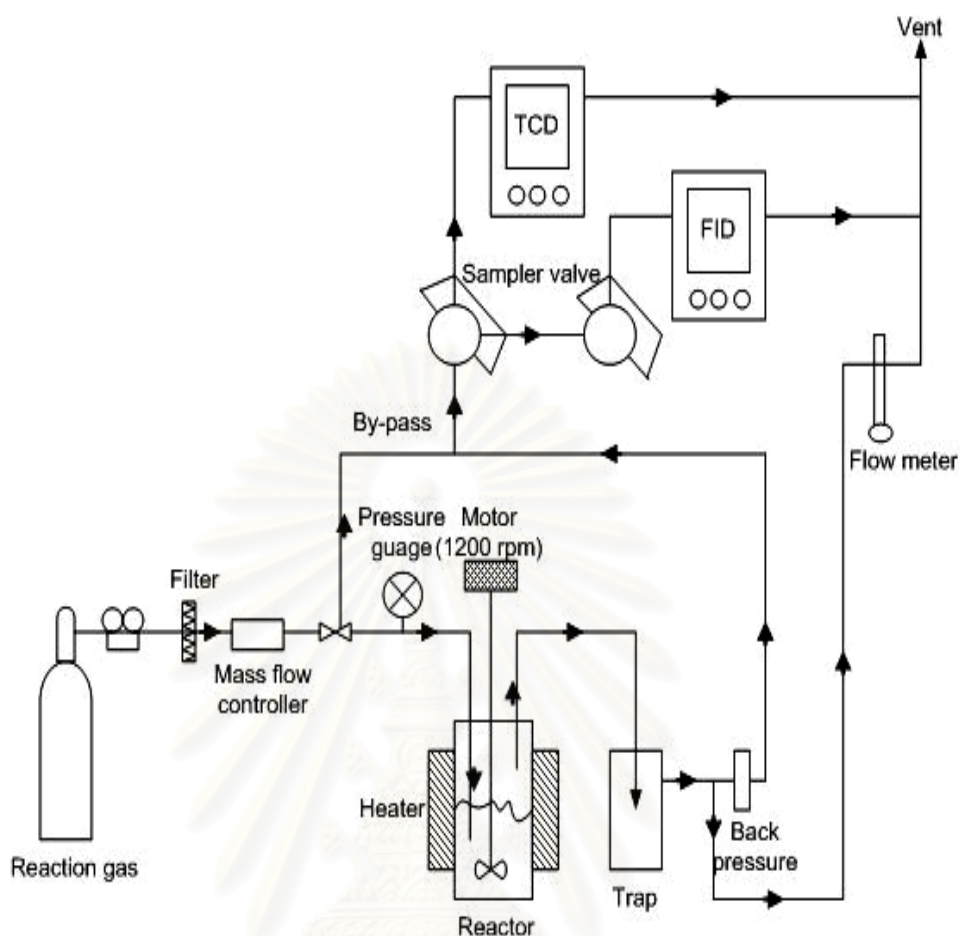
Figure 3.3 Schematic diagram of the reactor set-up

Gaseous products (CO, CO_2 and CH_4) were analyzed by using a gas chromatograph equipped with thermal conductivity detector (TCD), JC science GC 320, and active carbon column (3 mm I.D. and 2 m length). H_2 was used as a carrier gas. On-line GC with flame ionization detector (FID), Shimadzu GC 8 A, with a Porapak-Q column, 3 mm I.D. and 2 m length was used to analyze light hydrocarbons (C_1-C_5). Argon was employed as an internal standard with a concentration of 3% in the feed gas. The conditions of GC are listed as follows:

Initial temperature:	70°C
Ramping rate:	10°C/min
Final temperature:	230°C
Final time:	30 min
Carrier gas:	N_2 (99.99% purity)

The standard reaction conditions were P (total) =1.0 MPa, T=513 K, CO/H_2=1/2, W/F (CO+H_2+Ar) = 5 g-cat. h mol^{-1}. The liquid products collected in the ice trap and the products remaining in the slurry were combined and all of them were analyzed with gas chromatograph equipped with FID detector and an SE-30 column, 3 mm. I.D. and 2 m length. The conditions of GC are listed as follows:

Initial temperature:	40°C
Ramping rate:	5°C/min
Final temperature:	300°C
Final time:	40 min
Carrier gas:	N_2 (99.99% purity)

3.5 Catalyst Characterizations

3.5.1 X-Ray Diffraction (XRD)

X-ray diffraction (XRD) patterns were investigated on Rigaku X-ray diffractometer equipped with a RINT 2000 wide angle goniometry using CuK_α radiation with a generator voltage and generator current of 40 kV and 40 mA, respectively. The catalyst sample were ground and packed in a glass holder. Scan speed of 1.5° (2θ)/min with a scan step of 0.02° (2θ) was used during a continuous run in the 20° to 80° (2θ) range. The digital output of proportional x-ray diffraction and goniometry angle measurements were transferred to an online microcomputer to record data and subsequent analysis.

An X-ray diffractometer was used to investigate supported cobalt crystalline size of the passivated catalysts. The crystalline average size was calculated by $L = K\lambda / \Delta(2\theta)\cos\theta_0$, where L is the crystalline size, K is a constant (K =0.9 ~

1.1), λ is the wavelength of X-ray (CuK$_\alpha$ = 0.154 nm), and $\Delta(2\theta)$ is the width of the peak at half height.

3.5.2 Brunauer-Emmett-Teller (BET)

BET was used to study total surface area measurement, pore volume and average pore diameter of supports. BET surface area was determined by adsorption method using Autosorb-1 Gas Sorption System (Quantachrome Corporation). Nitrogen gas was used as adsorbate at the liquid nitrogen temperature (77 K). Before a measurement, the 0.03 g of calcined sample was outgased by heating at 473 K for 2 h under vacuum to eliminate moisture on the surface.

3.5.3 Chemisorption Analysis

Chemisorption was used to investigate the metal surface area, metal dispersion, average crystallite size and H$_2$ uptake of Co metal on the catalysts. The chemisorption experiments were carried out in a static volumetric glass high-vacuum system using Autosorb-1 (Quantachrome Corporation). Research grade gases (H$_2$: 99.9995%, CO: 99.99%, Takachiho Corporation) were used without further purification. Before adsorption of H$_2$, the catalysts, which were previously reduced by H$_2$ and passivated, were treated in H$_2$ at 673 K for 1 h, followed by evacuation. H$_2$ adsorption isotherms were measured at 373 K. The chemisorbed uptake (at 373 K) was measured using the double-isotherms method as described by Bartholomew et al.(cited in Zowtiak et al., 1983, Reuel et al.,1984). Bartholomew et al. pointed that H$_2$ chemisorption at 373 K was the most reliable for silica-supported cobalt catalyst. The cobalt dispersion was measured by assuming a 1:1 H:Co surface stoichiometry. The calculations of dispersion and average crystalline diameter were described by Sun et al. (2000). Dispersion percentage (D%) was calculated according to the equation (3.1) where X is the total H$_2$ uptake in micromoles per gram of catalyst, W is the weight percentage of cobalt, and f is the fraction of cobalt reduced to the metal determined from temperature-programmed reduction (TPR), so the unreduced cobalt was not included in the calculation of D%.

$$D\% = \frac{1.179X}{Wf} \qquad\qquad (3.1)$$

Average crystallite diameters were calculated from D% assuming spherical metal crystallites of uniform diameter d with a site density [SD(Co)] of 14.6 atoms/nm^2.

$$d_p(nm) = \frac{6.59 \times SD(Co)}{D\%} \qquad (3.2)$$

3.5.4 Temperature-Programmed Reduction (TPR)

Temperature-programmed reduction was used to study reduction temperatures and reduction degrees of the catalysts. The experiments were carried out in a quartz tube reactor. The reducing gas, a mixture of 5.1% H_2 diluted by argon, was fed via a mass flow controller at 50 ml min^{-1}. After the reaction, effluent gas was passed through 5A molecular sieve trap to remove the water produced. Calcined catalyst (0.2 g) was initially flushed with argon at 323 K for 40 min. Then, the reducing gas was switched on at 50 ml min^{-1}, and the temperature was raised at a rate of 8 K min^{-1} from 323 K to 1073 K. The effluent gas was determined by Shimadzu GC 8A (TCD) with active carbon column, where argon was used as carrier gas.

3.5.5 Diffuse Reflectance Infrared Fourier Transform Spectroscopy (DRIFTS)
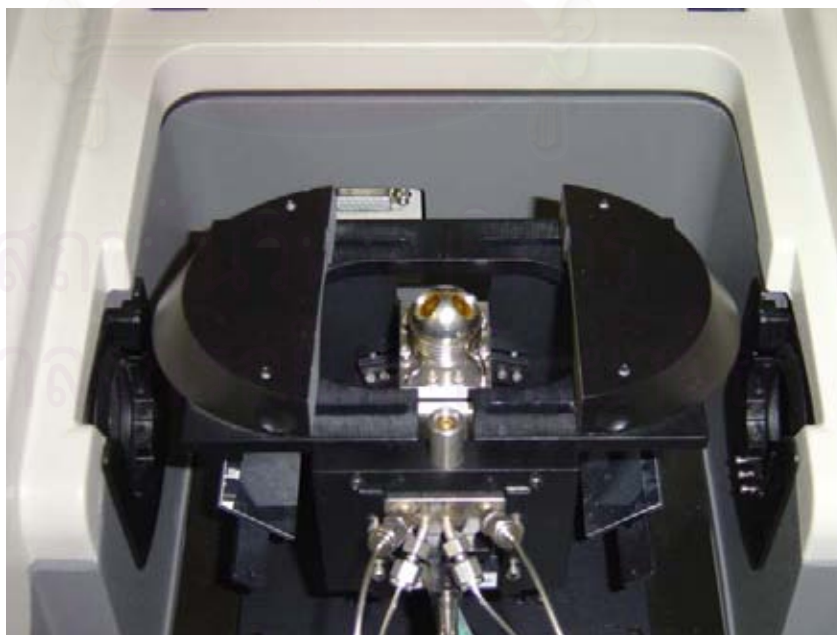
Figure 3.4 A diffuse reflectance infrared cell with a ZnSe window

In-situ diffuse reflectance infrared Fourier transform spectroscopy (DRIFTS) shown in Figure 3.4 was used to study the type bands of CO adsorption on the catalyst surface. DRIFT spectra were collected on a Nicolet Nexus 470 FT-IR spectrometer supplied with a diffuse reflectance attachment and with a MCT detector. 14 mg of catalyst powder was contained in a diffuse reflectance infrared cell with a ZnSe window which can work at high temperatures and high pressures. The absorbance spectra were obtained by collecting 32 scans at 2 cm^{-1} resolution. Before the adsorption of CO, the catalysts were treated in-situ in He flowing at 20 cm^3 min^{-1} at 298 K for 20 min, and then 473 K for 1 h. The treated catalysts were reduced in H$_2$ flowing at 50 cm^3 min^{-1} at 673 K at 0.5 MPa for 1.30 h and swept with He at 673 K for 1 h. After that the catalyst were cooled down in He to the adsorption temperature at 298 K at 0.1 MPa for 1 h and then, exposed to CO/He at the ratio of 10/10 flowing at a total rate of 20 cm^3 min^{-1} for 1 h. The spectra of CO adsorption species were collected under He flow 20 cm^3 min^{-1} in every 30 min for 2 h.

3.5.6 Transmission Electron Microscope (TEM)

Transmission electron microscope (TEM) analysis on a JEOL JEM-2010 apparatus equipped with Oxford Instruments Link Isis 300 X-ray microanalysis was used to investigate surface microstructures and surface compositions. A small amount of sample was dispersed in ethanol by sonication and dropped on a Lacey carbon film 300 mesh Cu grid. The TEM photographs were taken by using 200 kV electron beam with a magnification of 500 K with an optimal point-to-point resolution of 0.23 nm. The EDX (Energy dispersive X-ray analysis) patterns were identified with the reference database supplied with the equipment.

3.5.7 Scanning Electron Microscope (SEM)

The morphologies of the catalyst samples and their element distribution are investigated by the JEOL JSM-5800 scanning electron microscope. The energy dispersive spectrometer (EDS) is attached with the JSM-5800 for the identification, localization and quantification of the chemical components within the specimen. Before testing, a small amount of sample was dispersed on a sticky tape and covered with gold by Balzers SCD 040 ION SPUTTERING. The SEM instrument has a image resolution of 3.5 nm and can be operated at magnification of

x18 - x300,000. After the SEM micrographs were taken, EDS was performed to determine the element on the catalyst surface.

CHAPTER IV

EFFECTS OF Al$_2$O$_3$ PROMOTION ON Co/SiO$_2$ CATALYST

Alumina is regarded as a favorite support for cobalt based catalyst on Fischer-Tropsch synthesis because of its mechanical properties and adjustable surface properties. According to high reactivity with cobalt precursor, alumina support contributes the formation of a smaller supported metal cluster on the surface and highly dispersed Co, resulting in the limited reducibility (Kogelbauer et al., 1996). Chin (1982, 1984 cited in Kent et al., 1995) proposed that Co^{2+} ions can diffuse into the support lattice and form a spinel of CoAl$_2$O$_4$, which can not be reduced under H$_2$ at temperature below 800°C. In the case of silica support, it is considered as an inert support possessing low dispersion of metal cobalt and high reduction degree due to large Co particles which are readily reduced at lower temperature than alumina-supported catalysts. The comparison between alumina support and silica support is summarized in Table 4.1.

Table 4.1 Comparison between Al$_2$O$_3$ and SiO$_2$ support

Alumina Support	Silica support
Strong interaction with Co	Inert support
Stabilize a small Co cluster size	Yield a large Co cluster size
Highly dispersed metal Co	Low dispersion of metal Co
Impede the reducibility	Offer the highest reducibility

Therefore, small amount of Al$_2$O$_3$ are thought to be able to enhance the dispersion of cobalt metal without preventing the Co reducibility. In this chapter, a study of the catalytic performance of using Al$_2$O$_3$ as a promoter on cobalt catalyst supported on silica will be presented as a function of catalyst preparation and loading amount of Al$_2$O$_3$.

4.1 Results and Discussion

4.1.1 Catalytic Activity Screening

This section shows the activities of Al_2O_3-promoted catalysts. The activity performances were investigated in a semi-batch slurry phase reactor under the operating condition: P (total) =1.0 MPa, T=513 K, CO/H_2=1/2, W/F ($CO+H_2+Ar$) = 5 g-cat. h mol^{-1}. CO conversion indicated the catalytic performance of Co/SiO_2 catalysts.

Table 4.2 Reaction performance of Al_2O_3-promoted catalyst by sequential-impregnation method

Al_2O_3 loading (wt%)	CO conversion (%)	CH_4 selectivity (%)	CO_2 selectivity (%)
0	46.5	8.33	0.56
5	61.8	9.11	0.52
10	66.5	7.90	0.47
15	63.5	7.86	0.60
20	63.5	8.32	0.51
30	52.9	7.29	0.37

The influence of different Al_2O_3 loading on the activity of Co/SiO_2 catalyst was investigated. Table 4.2 and 4.3 showing the CO conversion of Al_2O_3-promoted Co/SiO_2 catalysts on FT reaction indicated that the addition of Al_2O_3 could increase the activity of Co/SiO_2 for both sequential-impregnation and co-impregnation catalysts. The optimal Al_2O_3 loading at 10 wt% could increase the CO conversion of Co/SiO_2 66.5 % on sequential-impregnation catalyst and 64.2 % on co-impregnation catalyst. The increasing amount of Al_2O_3 did not lead to higher conversion. Therefore, it was not necessary to load Al_2O_3 in higher than 10 wt% since almost the same activity in 10, 15 and 20 wt% Al_2O_3 loading was observed. The 30 wt% Al_2O_3 loaded catalyst in table 4.2 showed less activity than other loading

amounts but still higher than unpromoted catalyst. High amounts of promoter generally decrease catalytic activity due to the coverage of active sites.

Table 4.3 Reaction performance of Al_2O_3-promoted catalyst by co-impregnation method

Al_2O_3 loading (wt%)	CO conversion (%)	CH_4 selectivity (%)	CO_2 selectivity (%)
0	46.5	8.33	0.56
5	63.9	8.07	0.53
10	64.2	7.65	0.49
15	62.3	8.56	0.62
20	62.6	7.48	0.52

CH_4 is an undesirable product in FTS reaction; therefore the catalyst with low selectivity in CH_4 is needed. Since the water gas shift reaction affects the efficiency of the carbon monoxide utilization hence the water gas shift reactivity of the catalysts determines the CO_2 yield. Besides, the value of CO_2 selectivity is used to indicate the activity in Boudouard reaction ($2CO \rightarrow C + CO_2$), which is the most favorite reaction for the coke formation. This not only deactivates the catalyst by covering the surface, but also destroys the mechanical properties of the catalyst structure (Sharma et al., 2001). The results from table 4.2 and 4.3 indicate that the loading of Al_2O_3 is not significant in the CH_4 and CO_2 formation.
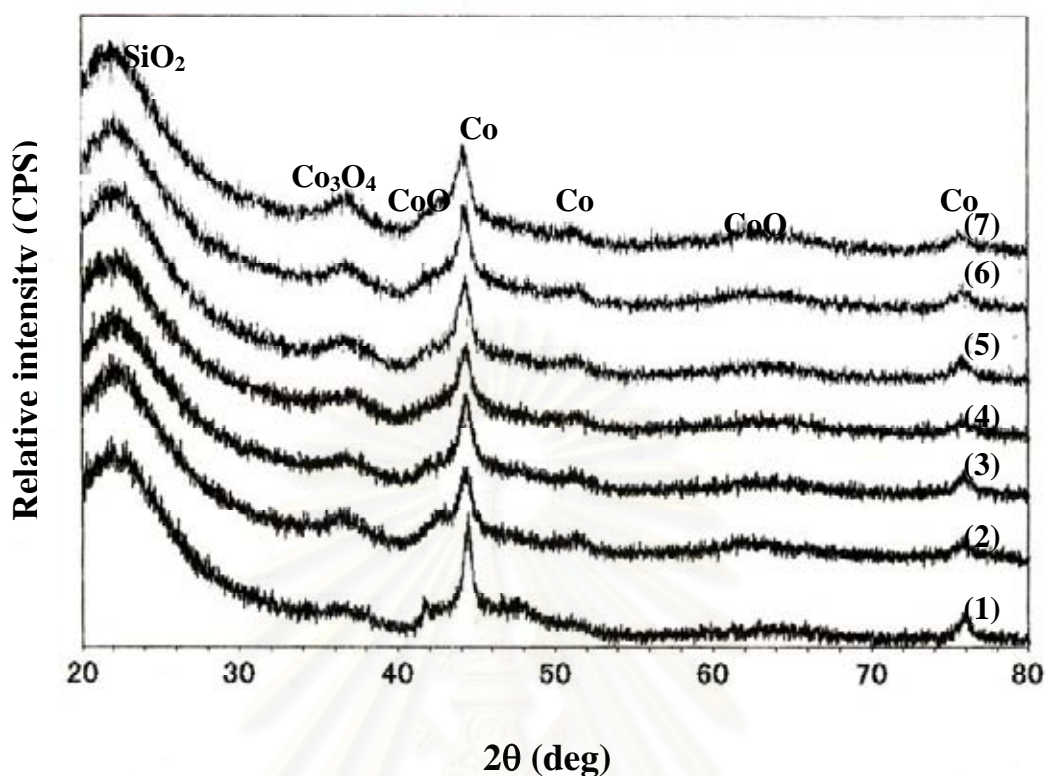
4.1.2 Catalyst Characterization

The catalysts were characterized by BET to determine the surface area of the catalysts as shown in Table 4.4. BET tests of the co-impregnation catalysts were used calcined catalysts, while those of impregnation catalysts were used alumina-added supports without cobalt component. The data suggested that the addition of alumina on the support did not significantly change the surface area of silica support, so the activity changes of modified catalysts did not due to the surface change of silica support.

XRD patterns in Figure 4.1 indicated that Al_2O_3 was highly dispersed on Co/SiO_2 and Al_2O_3 should not be present as a single element crystal cluster on the catalytic surface since no Al_2O_3 compound phases were detected. The cobalt peak of unmodified catalyst was sharper than that of additional Al_2O_3 catalysts. Metallic Co was identified at 44.33° of 2θ from the XRD pattern of Co/SiO_2 while Co_3O_4 and CoO were observed from 2θ peak at 36.75° and 41.72°, respectively. The addition of Al_2O_3 was observed to reduce the intensity of Co peaks.

Table 4.4 BET analysis of Al_2O_3-promoted catalysts

Al_2O_3 Loading (wt%)	Impregnation catalyst Surface area (m^2/g)	Co-impregnation catalyst Surface area (m^2/g)
0	283.0	283.0
5	272.8	239.4
10	270.2	240.7
15	262.3	257.9
20	257.7	254.3

Figure 4.1 XRD patterns of various 10 wt% Co/SiO_2 reduced catalysts : the sequential-impregnation catalysts with Al_2O_3 addition (1) 0 wt%, (2) 5 wt%, (3) 10 wt%, (4) 15 wt%, the co-impregnation catalysts with Al_2O_3 addition (5) 5 wt%, (6) 10 wt%, (7) 15 wt%

The activity of cobalt catalyst depends on the number of active sites on the surface of crystalline metal formed by reduction. Cobalt particle size and reduction degree determine the number of active site. The particle size of promoted catalysts was determined by XRD and H_2 chemisorption. The reduction performance of catalysts was determined by temperature-programmed reduction (TPR) as shown in Figure 4.2.

For non Al_2O_3 catalyst, the first peak located at 570.8 K and the second one was at 645.8 K. These two peaks of TPR profile are attributed to the reduction of Co_3O_4 to CoO followed by reduction at higher temperature to metallic Co^0 (Jacobs et al., 2002) as shown below.

$$H_2 + Co_3O_4 \rightarrow H_2O + 3CoO \qquad (4.1)$$

$$H_2 + CoO \rightarrow H_2O + Co^0 \qquad (4.2)$$

For all Al_2O_3-loaded catalysts, the sharp low temperature peaks located at 595 K and another broad peak distributed around 620 K to 1000 K. The broad region at high temperature indicates the existence of several species reduced at approximately the same temperature (Rosynek, 1991). Besides, the appearance of high temperature peaks implied that cobalt has strong interaction with the support. The reduction degrees of various catalysts were calculated by TPR data from 323 K to 1073 K. The reduction degrees of Al_2O_3-added catalysts are almost equivalent to that of non-Al_2O_3 catalyst as shown in Table 4.4.
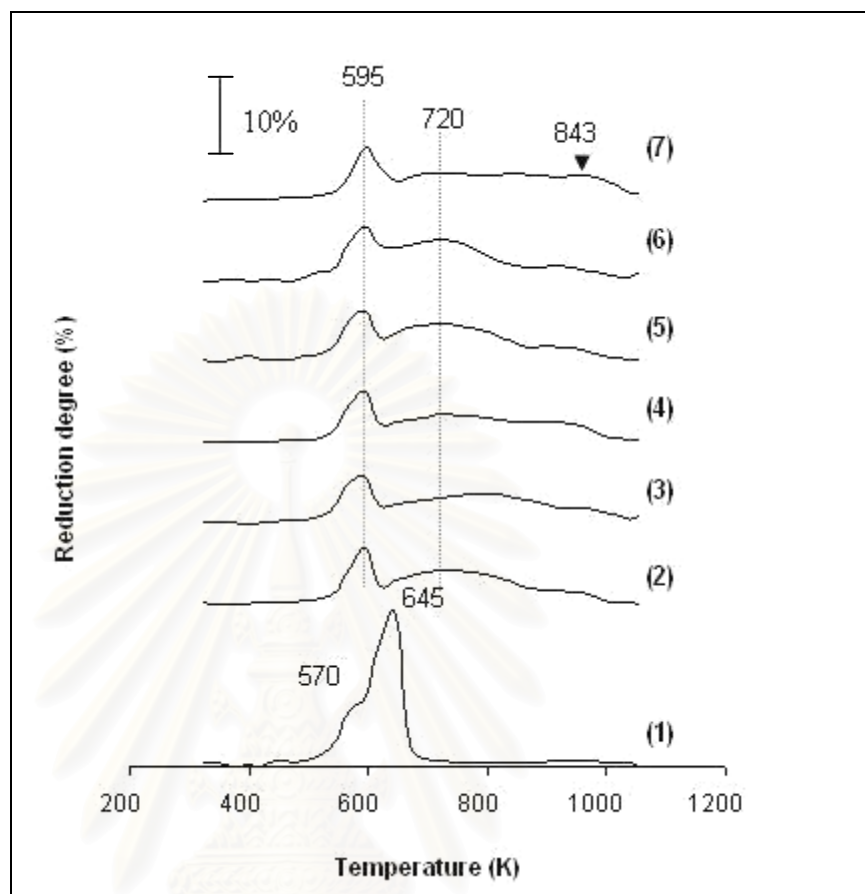
Figure 4.2 TPR profile of various 10 wt% Co/SiO_2 calcined catalysts. : the sequential-impregnation catalysts with Al_2O_3 addition (1) 0 wt%, (2) 5 wt%, (3) 10 wt%, (4) 15 wt%, the co-impregnation catalysts with Al_2O_3 addition (5) 5 wt%, (6) 10 wt%, (7) 15 wt%

Table 4.5 Properties of Co/SiO$_2$ with different Al$_2$O$_3$ loadings from XRD and H$_2$ chemisorption analyses.

Method	Al$_2$O$_3$ Loading (wt%)	XRD Size (nm)	H$_2$ chemisorption				TPR Red. (%)[d]
			Size (nm)	Co Disp.[a] (%)	S.A.[b] (m^2/g)	H$_2$[c] uptake	
Impregnation	0	13	19.09	5.217	2.366	29.66	67
Impregnation	5	10	14.22	7.000	2.863	35.88	60
Impregnation	10	9	13.41	7.426	3.085	38.67	61
Impregnation	15	10	14.47	6.883	2.757	34.55	59
Co-impregnation	5	9	13.92	7.155	3.237	40.58	67
Co-impregnation	10	9	13.91	7.160	3.238	40.59	67
Co-impregnation	15	8	13.70	7.273	3.292	41.26	67

Note: [a] cobalt dispersion calculated from H$_2$ chemisorption at 373 K

[b] active cobalt surface area calculated from H$_2$ chemisorption at 373 K

[c] H$_2$ uptake (μmol/g) calculated from H$_2$ chemisorption at 373 K

[d] Calculated from TPR from 323 K to 1073 K

The supported cobalt particle sizes of various catalysts were determined by XRD and H$_2$ chemisorption exhibited in Table 4.5. The results from H$_2$ chemisorption suggest that the average Co metal sizes for the loaded-Al$_2$O$_3$ catalysts were approximately 13 nm, which was smaller than that of unpromoted catalyst (19 nm). The Co particle sizes calculated from XRD are 13 nm for non-Al$_2$O$_3$ catalyst, while that of Al$_2$O$_3$ promoted catalysts are around 9 nm. Thus, both H$_2$ chemisorption and XRD results indicated that the addition of Al$_2$O$_3$ on Co/SiO$_2$ catalysts provide smaller cobalt particle size.

Previous reports of support and dispersion effects on cobalt FT activity suggest that high cobalt dispersions result in a reduction of easily reducible metal and cancel out the available metallic surface cobalt, thereby decreasing the FT activities (Kent et al., 1995). In our experiment for Al$_2$O$_3$-promoted catalyst, not only the dispersion of Co metal was increased from 5% in unpromoted catalyst to 7% in Al$_2$O$_3$ promoted catalysts but the active cobalt metal surface area was also increased. These results indicated that the cobalt-alumina interaction favors the distribution of Co over
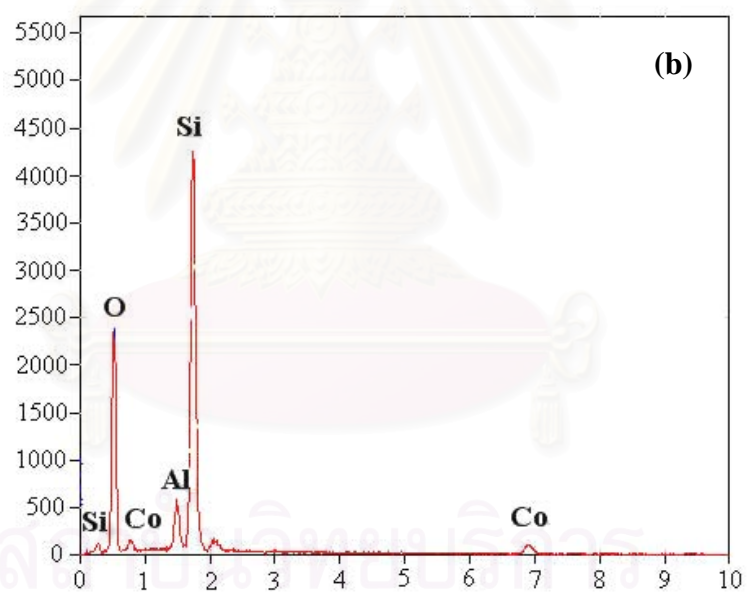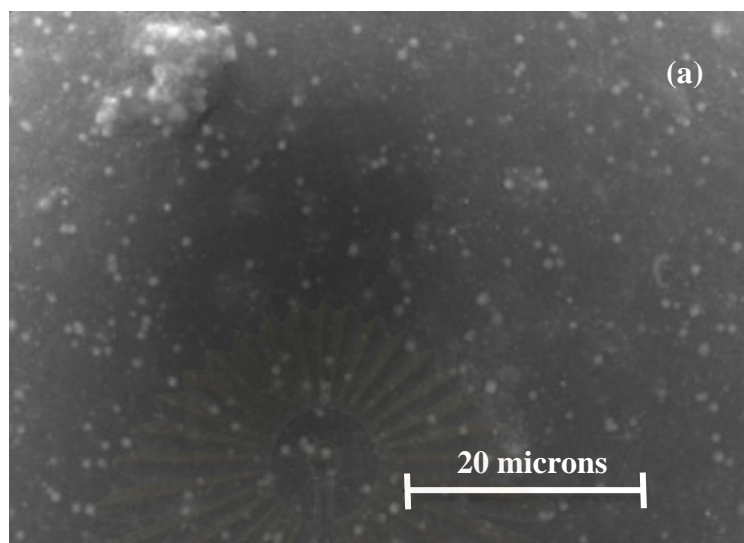
the silica support. The results suggested that the activity of the Al_2O_3-loaded catalysts increased due to the high cobalt dispersion on the silica supports. Our results were all the same to that of Bessell (1993) who proposed that high surface area supports give high cobalt dispersion and tend to produce high FT activity, as long as the reducibility of the cobalt is not hindered by metal-support interactions or ion exchange, or pore diffusion or blocking effects not taking place.

Scanning electron microscope (SEM) was used to investigate the morphologies of the catalysts samples and Energy dispersive X-ray analysis (EDX) was used to determine the element dispersed on the surface at the selected points. The SEM micrographs in Figures 4.3 and 4.4 shows the metal cluster on the SiO_2 surface. The white or light spots on the external surfaces represent high concentrations of Co and the gray areas represent the silica or Al-modified silica support with minimal Co present as evidenced by EDX in Figure 4.3. In the impregnation method, aluminium precursor was dropped on silica support and after calcinations step Al_2O_3 might partially cover the silica surface. Next, when cobalt precursor was dropped on this modified catalyst, cobalt might prefer to clamp on Al_2O_3. It might be possible that the interaction of Co-Al easily occur than that of Co-Si because silica is considered as inert material. Consequently, the addition of Al_2O_3 promoter could prevent cobalt metal from sintering effect resulting in high dispersion and cobalt surface area.

In the case of co-impregnation, the Al_2O_3 and cobalt precursor were mixed very well and form fine mixed alumina-Co phase, which could provide fine dispersion of cobalt, before loading on silica support. Thus, the co-impregnation method might provide regularly dispersive cobalt metal on the surface leading to steady cobalt dispersion in different Al_2O_3 loading. However, some cobalt might be covered with alumina due to the mixing of cobalt and alumina precursor before impregnation step. Consequently, the density of surface-cobalt on co-impregnation catalyst was less than that of sequential-impregnation catalyst as shown in Figure 4.3 and 4.4.
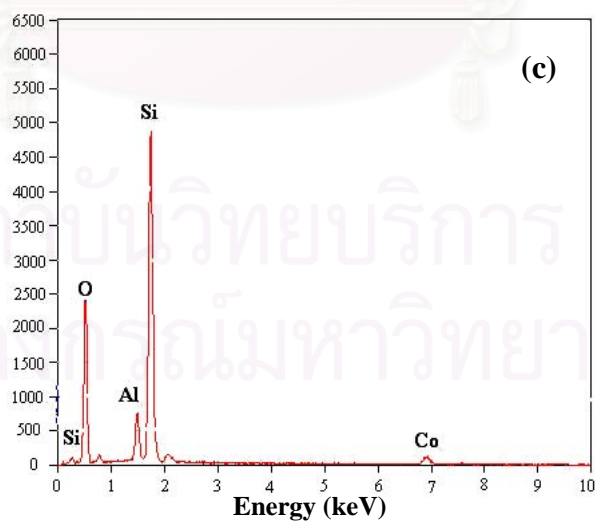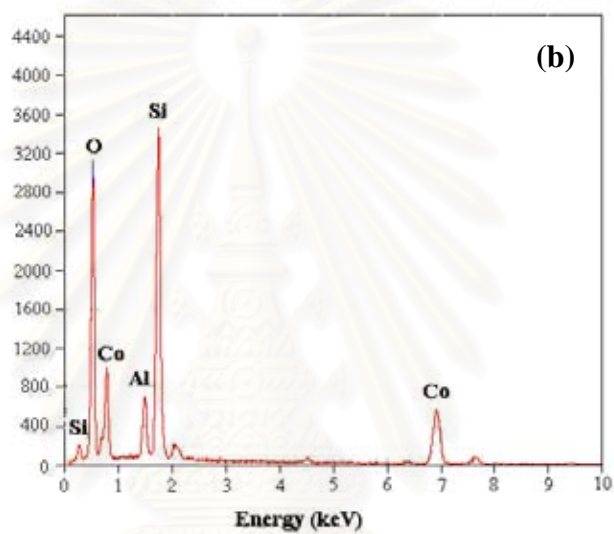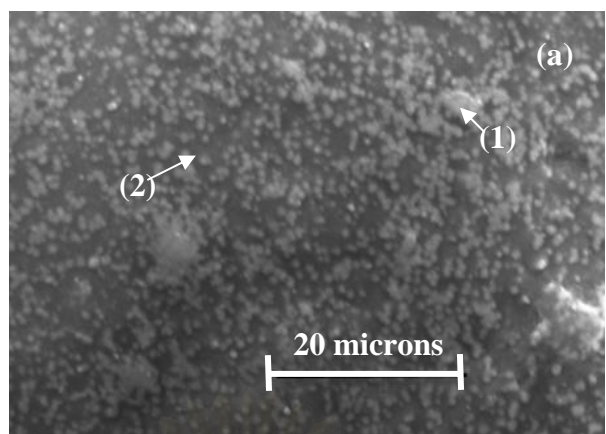
Figure 4.3 (a) SEM image of the 10wt% Al_2O_3 on SiO_2 catalyst by sequential-impregnation, (b) EDX result at point (1), (c) EDX result at point (2)

Figure 4.4 (a) SEM image of the 10wt% Al_2O_3 on SiO_2 catalyst by co-impregnation and (b) EDX results at this area

Based on the studies suggested from all characterization analysis, we proposed the surface model in Figure 4.5. Since the silica support is an inert support, which does not form the strong interaction with cobalt precursor, the sintering of cobalt metal will occur during high temperature treatments in calcination and reduction steps. The agglomeration of cobalt particle causes lower dispersion and lower metal surface area leading to decreasing in FT activity. The addition of the small amount of Al_2O_3 forms the strong interaction with cobalt, which not only prevents cobalt metal from sintering but also not decreases the reducibility, resulting in high dispersion and metal surface area.
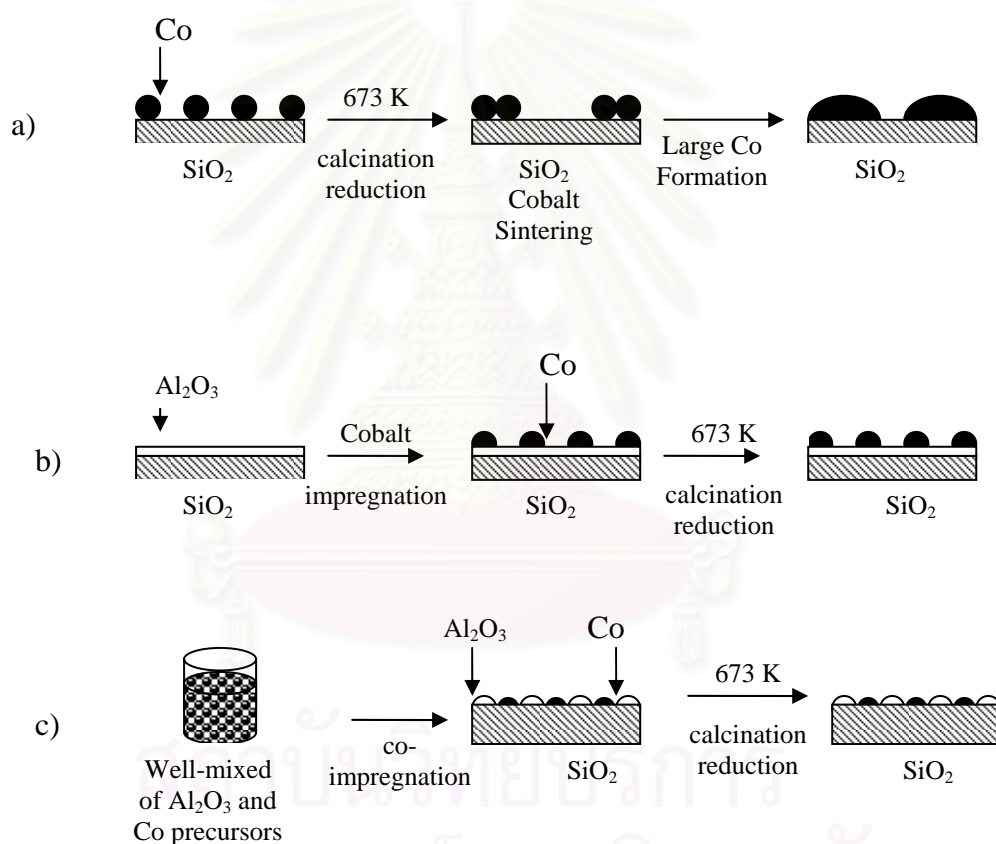
Figure 4.5 Proposed surface model of Co/SiO_2, Al_2O_3-promoted on Co/SiO_2 by sequential-impregnation and co-impregnation method; **a**: Co/SiO_2; **b**: Al_2O_3-promoted Co/SiO_2 by sequential-impregnation; **c**: Al_2O_3-promoted Co/SiO_2 by co-impregnation.

The adsorbed type of CO on cobalt based-catalyst affects the activity on FTS reaction. Figure 4.6 shows the surface CO species on FT catalyst consisting of carbonyl species, linear CO and bridge-type CO. The surface carbonyl species, which have strong C-O bond, may appear on the kink corner site or on the small cobalt metal, while the linear form and bridge-type form always happen on the large and flat cobalt metal. Usually the bridged-form CO is considered to be more active than the linear CO. Thus, the high activities seem also be associated with the increase in the bridge-type CO, which is easily dissociated to oxygen and carbon.
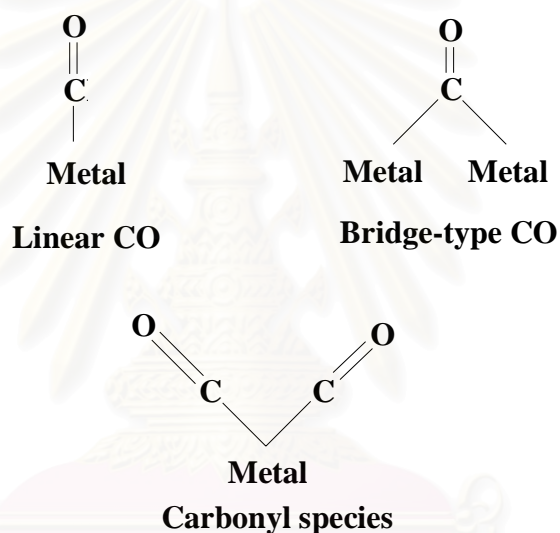
Figure 4.6 Surface CO species on metal catalyst

In-situ diffuse reflectance infrared Fourier transform spectroscopy (DRIFTS) was used to study the adsorbed CO for the reduced catalysts as compared in Figure 4.7. Many studies report that linearly bonded molecular band locates in the 2000-2050 cm^{-1} range after CO adsorption (Heal, 1978 and Mohana, 1988). In our investigation, 10wt% Al_2O_3 promoted catalysts were selected to study the adsorption mode of CO because it provided the highest activity in FTS reaction.

For non-Al_2O_3 catalyst the 2037 cm^{-1} peak was assigned to CO adsorbed on cobalt metal in linear geometry. The 2058 cm^{-1} shoulder peak could be assigned to the surface carbonyl species, $Co(CO)_x$ (where X>1), which readily happened on corner sites of the cobalt metal, and the band of 1937 cm^{-1} peak are

attribute to the bridged-type CO adsorbed on cobalt metal sites (Rohr et al., 2000). The positions of peaks of 10% Al_2O_3 loaded catalysts were equivalent to that of non-loaded Al_2O_3 catalysts. This result indicated that the addition of Al_2O_3 did not affect the adsorption mode of CO on Co/SiO_2 catalyst, and the high activity of Al_2O_3 promoted catalysts were not due to the increase in bridge-type adsorbed CO.
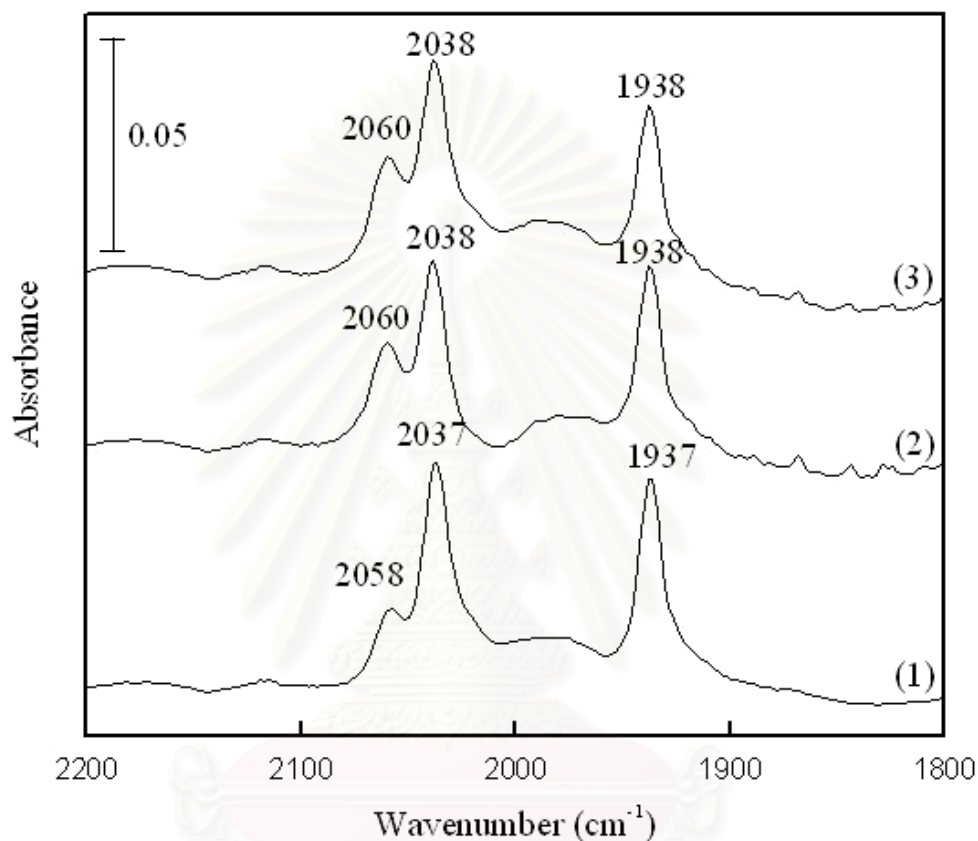
Figure 4.7 FTIR spectra of CO adsorbed on the catalysts reduced at 673 K; (1) Co/SiO_2, (2) 10 wt% Al_2O_3-added catalyst by sequential-impregnation, (3) 10 wt% Al_2O_3-added catalyst by co-impregnation

4.1.3 Product Distribution of Al_2O_3-Promoted Co/SiO_2 Catalyst

The chain growth probability α for Co/SiO_2 was calculated by Anderson-Schulz-Flory equation as shown in Table 4.6. Usually, the large cobalt particle has high chain growth probability due to a strong tendency for readsorption and incorporation of reactive compound into growing chain. Compared to the unmodified catalyst, Al_2O_3-added catalysts had lower chain growth probability due to small cobalt crystalline size as evidenced by XRD and H_2 chemisorption in Table 4.5.

The intrinsic activity of cobalt atom is determined by turnover frequency (TOF) value based on H_2 chemisorption. The addition of Al_2O_3 did not significantly affect on TOF of Co/SiO_2 catalysts. This result implied that the addition of Al_2O_3 did not increase the site activity of Co/SiO_2 catalyst. Therefore, in this study the increase in metallic cobalt site was the main reason in higher activity on FTS reaction.

Table 4.6 Product distribution of Co/SiO_2 with different Al_2O_3 loading

Method	Sequential-impregnation catalyst				Co-impregnation catalyst		
Al_2O_3 Loading (%)	0	5	10	15	5	10	15
Chain growth probability	0.86	0.83	0.84	0.84	0.83	0.83	0.82
Turn over frequency (s^{-1}) [a]	0.15	0.16	0.16	0.17	0.14	0.15	0.14
Product distribution (%) [b]							
C_1	6.85	4.79	6.73	6.81	7.55	6.41	7.06
C_2	1.18	1.65	1.07	1.08	1.15	0.96	1.09
C_3	3.16	3.55	3.28	2.61	3.65	2.34	3.62
C_4	4.15	7.53	4.93	5.71	4.64	4.19	6.39
C_5^+	84.67	82.49	83.99	83.8	83.01	86.11	81.84

Note:[a] Based on total H_2 uptake calculated from H_2 chemisorption

[b] The calculation was based on the number of carbon atom for each product.

4.2 Conclusions

Addition of Al_2O_3 onto Co/SiO_2 significantly improved the catalytic activity of FTS by increasing the dispersion of Co metal on SiO_2 support without significantly obstructing the reducibility of Co. The optimal Al_2O_3 loading was 10 wt%. The Al_2O_3-loaded on Co/SiO_2 catalyst was an excellent FT catalyst because it possessed high cobalt dispersion while the reducibility of the cobalt was not hindered by metal-support interactions. However, the small supported Co particles on promoted catalysts slightly lowered the chain growth probability. The TOF of promoted catalysts was equivalent to that of unpromoted catalyst. These results implied that the addition of Al_2O_3 did not affect the site activity of Co/SiO_2 catalysts. The increase in active metal surface was the main reason for higher reactivity of the Al_2O_3-promoted Co/SiO_2 catalysts.

CHAPTER V

EFFECTS OF TiO$_2$ PROMOTION ON Co/SiO$_2$ CATALYST

It is well know that support plays an important role in determining the structure and activity of supported metal catalysts. Various supports have been studied the effects of FTS reaction and titania is one of the investigated supports.

Titania exists in two tetragonal crystallographic forms, a metastable form, anatasse, and a stable form, rutile. The volume free energy of the rutile phase is always lower than that of anatase. Therefore, on heat treatment the anatase phase transforms to the stable rutile form. Two major causes of reductions in surface area and porosity were identified: (1) the crystallite growth of the anantase phase before the phase transformation; (2) the enhanced sintering and grain growth of the rutile phase as a result of phase transformation (Kumar, K.N.P., et al., 1993). Thus at elevated temperatures, the structure of titania is not stable due to the solid-state sintering, which leads to grain growth, and eventually complete collapse of the structure (Varghese et al., 2003).

Titanium oxide exhibits the so-called Strong Metal-Support Interaction (SMSI) effect. This phenomenon is characterized by suppression of the capacity of the metal to chemisorb hydrogen after high-temperature reduction. Ho et al.(1992) found that CoTiO$_3$-like phase was the main species after calcinations at 400 °C. The reduced TiO$_x$ phase resulted in a decrease in the fraction of exposed surface cobalt and a decline in activity due to the suppression of H$_2$ chemisorption.

Riva et al. (2000) studied the interaction of cobalt with two different kinds of support: silica and titania. According to the formation of a surface compound, CoTiO$_3$, the interaction is much stronger in the case of titania. The low reactivity of cobalt with silica favors sintering effects after reduction and reoxidation treatment. Conversely, due to the high reactivity of cobalt with titania, the coverage of TiO$_2$ by cobalt tends to increase after the same treatment.

The silica support is an inert support which does not provide the SMSI effect with supported cobalt (Tauster and Fung, 1978). The small amount of doped-

titanium oxide on Co/SiO$_2$ catalysts might promote the preferable result in higher cobalt dispersion by preventing sintering effect. Therefore in our study, we investigate the effects of using titanium oxide as the promoter in Co/SiO$_2$ catalyst.

5.1 Results and Discussion

5.1.1 Catalytic Activity Screening

This part exhibits the activities of TiO_2-doped catalysts. The activity performances were investigated in a semi-batch slurry phase reactor under the operating condition: P (total) =1.0 MPa, T=513 K, CO/H_2=1/2, W/F $(CO+H_2+Ar)$ = 5 g-cat. h mol^{-1}. CO conversion indicated the catalytic performance of Co/SiO_2 catalysts.

Table 5.1 Reaction performance of TiO_2-promoted catalyst by sequential-impregnation method

TiO_2 loading (wt%)	CO conversion (%)	CH_4 selectivity (%)	CO_2 selectivity (%)
0	53.4	5.66	0.92
2	68.7	8.44	1.65
5	64.9	7.18	1.33
10	63.5	8.31	1.26
15	61.9	8.07	1.18

For sequential-impregnation catalysts, the introduction of titania oxide to Co/SiO_2 results in the increase in FT activity represented in CO conversion in Table 5.1. The optimal TiO_2 loading was 2 wt% which could increase the CO conversion to 68.7 %. High amounts of promoter generally decrease catalytic activity due to the coverage of active sites; therefore the addition of TiO_2 more than 2 wt% caused lower activity in FTS reaction. As compared with unmodified catalyst, the methane and CO_2 selectivity of TiO_2-added catalysts was not significantly changed. The activity of Co-impregnation catalysts was almost the same trend as in sequential-impregnation catalysts, but the CO conversion of 10 wt% TiO_2-added catalyst drastically decreased as illustrated in Table 5.2.

Table 5.2 Reaction performance of TiO_2-promoted catalyst by co-impregnation method

| TiO_2 loading (wt%)	CO conversion (%)	CH_4 selectivity (%)	CO_2 selectivity (%)
0	53.4	5.66	0.92
2	63.6	9.17	0.81
5	58.8	7.39	1.28
10	10.80	12.27	0.00

5.1.2 Catalyst Characterization

Results of surface area measurements by physisorption of nitrogen are reported in Table 5.3. Results show that the addition of TiO_2 by both impregnation and co-impregnation methods decreased the surface area SiO_2 supports. Therefore, the increase in activity and dispersion of TiO_2-promoted catalysts was not due to the increase in the surface area of silica support.

Table 5.3 BET analysis of TiO_2-promoted catalysts

TiO_2 Loading (wt%)	Impregnation catalyst Surface area (m^2/g)	Co-impregnation catalyst Surface area (m^2/g)
0	283.0	283.0
2	257.4	225.8
5	258.6	226.3
10	233.3	228.0

Figure 5.1 shows the X-ray diffraction patterns of TiO_2-promoted catalysts. TiO_2 compound phase was not detected in low TiO_2 loading and in impregnation catalysts. In contrast, a diffraction peak of cobalt titanate ($CoTiO_3$) can be observed in 10% added-TiO_2 co-impregnation catalyst at 35.72° from 2θ peak. This compound must have been formed from TiO_2 and divalent CoO during the calcinations process (Voß et al., 2002).
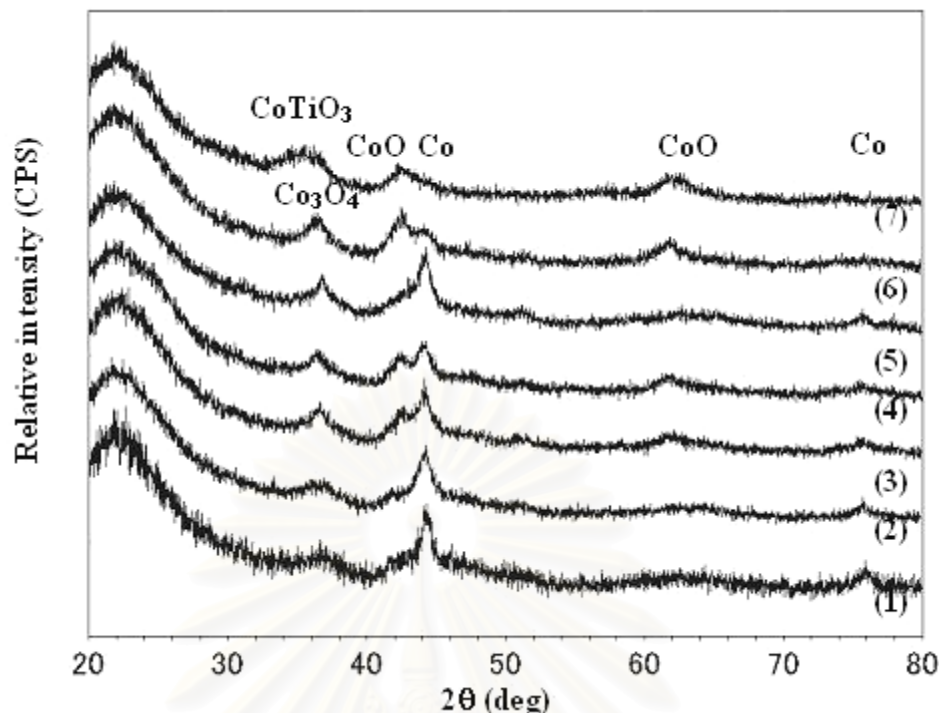
Figure 5.1 XRD patterns of various 10 wt% Co/SiO$_2$ reduced catalysts: the
sequential-impregnation catalysts with TiO$_2$ addition (1) 0 wt%, (2) 2
wt%, (3) 5 wt%, (4) 10 wt%, the co-impregnation catalysts with TiO$_2$
addition (5) 2 wt%, (6) 5 wt%, (7) 10 wt%

Figure 5.2 illustrates the TPR profiles for unpromoted and promoted
Co/SiO$_2$ catalysts. For unpromoted catalyst, two peaks were observed at 571 and 646
K, respectively. The TiO$_2$-added catalysts had the first peaks at the same position as
unpromoted catalyst. The second peaks of modified catalysts shifted to higher
temperature around 750 K. The third peaks, which generally agree to be a cobalt
oxide surface species interacting strongly with the support, were found in 5%, 10%
TiO$_2$ co-impregnated, and 10% TiO$_2$ impregnated catalysts at around 910 K. A
quantitative analysis of the peak area from 323 to 1073 K indicated that the reduction
degrees of TiO$_2$ added catalysts were almost equivalent to that of non TiO$_2$ catalyst.
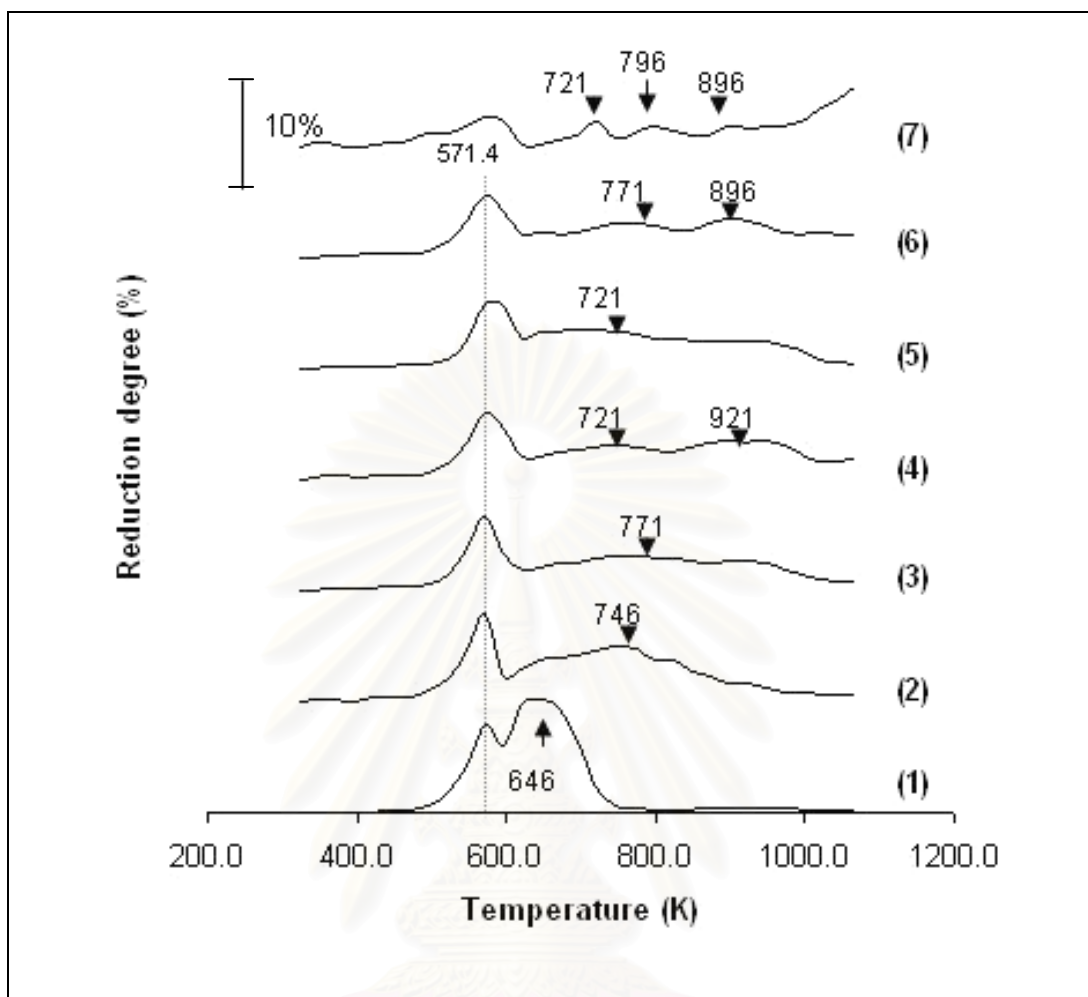
Figure 5.2 TPR profile of various 10 wt% Co/SiO_2 calcined catalysts. : the sequential-impregnation catalysts with TiO_2 addition (1) 0 wt%, (2) 2 wt%, (3) 5 wt%, (4) 10 wt%, the co-impregnation catalysts with Al_2O_3 addition (5) 2 wt%, (6) 5 wt%, (7) 10 wt%

Only the 10% TiO_2 co-impregnated catalyst had very low reduction degree at 46 % because large amount of TiO_2 addition might resulted in high formation of strong metal-support interaction (SMSI) compound, $CoTiO_3$, which hardly reduced at this study temperature range. Our result is similar to those of Riva et al. (2000). They suggested that cobalt titanate was more resistant to reduction than Co_3O_4. Consequently, the CO conversion of 10%loaded-TiO_2 was very low due to low active cobalt surface.

Table 5.4 Properties of Co/SiO_2 with different TiO_2 loadings from XRD and H_2 chemisorption analyses.

Method	TiO_2 Loading (wt%)	TEM Size (nm)	XRD Size (nm)	H_2 chemisorption			TPR Red. (%)[d]
				Size (nm)	Co Disp.[a] (%)	S.A.[b] (m^2/g)	H_2[c] uptake	
Impregnation	0	15-20	10.33	15.31	6.508	2.809	35.21	64
Impregnation	2	12-15	9.09	13.59	7.329	3.449	43.23	70
Impregnation	5	-	9.90	14.15	7.041	2.878	36.07	60
Impregnation	10	-	11.24	16.52	6.028	2.804	35.15	69
Co-impregnation	2	12-15	9.92	13.80	7.217	3.093	38.76	63
Co-impregnation	5	-	-[e]	20.13	4.947	2.224	27.87	66
Co-impregnation	10	-	-	34.77	2.865	0.887	11.12	46

Note: [a] cobalt dispersion calculated from H_2 chemisorption at 373 K

[b] active cobalt surface area calculated from H_2 chemisorption at 373 K

[c] H_2 uptake (μmol/g) calculated from H_2 chemisorption at 373 K

[d] Calculated from TPR from 323 K to 1073 K

[e] No cobalt peak could be detectable

The XRD and chemisorption results are shown in Table 5.4. For impregnation catalysts, the cobalt particles were gradually increasing size in the order 9.09, 9.90 and 11.24 nm of 2%, 5% and 10% of TiO_2 loading, respectively. The reason might be the decreasing support surface area after loading TiO_2 leading to low dispersion of cobalt in high TiO_2 addition catalysts. The results suggested that the small amount of TiO_2, in the range of 2-5 wt%, could facilitate well-dispersed cobalt phases and stabilize the active cobalt phase against high temperature sintering as

evidenced by higher cobalt dispersion than unpromoted catalyst, while the large amount of TiO_2 decreased the surface area of supports resulting in the decrease of metal dispersion and the increasing sizes of cobalt particles.

For TiO_2 promoted catalyst with co-impregnation, the metal particle size calculated from XRD data is inconformity with that from H_2 chemisorption. XRD was unable to detect cobalt signals of 5% and 10% added TiO_2 co-impregnation catalysts, whereas the results from chemisorption analysis showed very large cobalt particles. An explanation of this observation might be that the effect of the formation of $CoTiO_3$ compound is increased with increasing the loading of TiO_2. In the case of Co/TiO_2 system, the determination of crystallite size from H_2 adsorption was poor (more than 200% high) because of an SMSI effect which suppressed H_2 adsorption (Reuel et al., 1984). Thus, in most cases its accuracy is comparable with that of transmission electron microscope (TEM). Not only the adsorption of H_2 is reduced by SMSI effect, but the adsorption of CO is also decreased. Consequently, Boudouard reaction hardly occurs on the co-impregnated 10wt% TiO_2 catalyst which has $CoTiO_3$ compound. Thus, its CO_2 formation is too small to be detected by GC.

For a TEM image of the Co/SiO_2 catalyst with TiO_2 promoter, dark crystalline spots was observed on bright amorphous region. Due to the strong mass differences between Si and Co it can be assumed that the dark spots indicate Co oxide crystallites, which are embedded into amorphous SiO_2. The atomic masses of Co and Ti do not differ considerably from one another, so it is no possible to distinguish which items are Co component and which are Ti component. Thus, using the EDX technique can determine the composition of the surface at the selected points, the results indicates all deposited elements exist on the metal cluster. TEM analysis in Table 5.4 is comparable to that evaluated by XRD and H_2 chemisorption. Nevertheless, it is so difficult to get an accurate measurement of cobalt crystallite size with high titania loading. As can be seen in Figure 5.3 (c), the high TiO_2 loading caused the increase in the spreading of the cobalt particle on the support. Thus, we can not separate each cobalt particle.
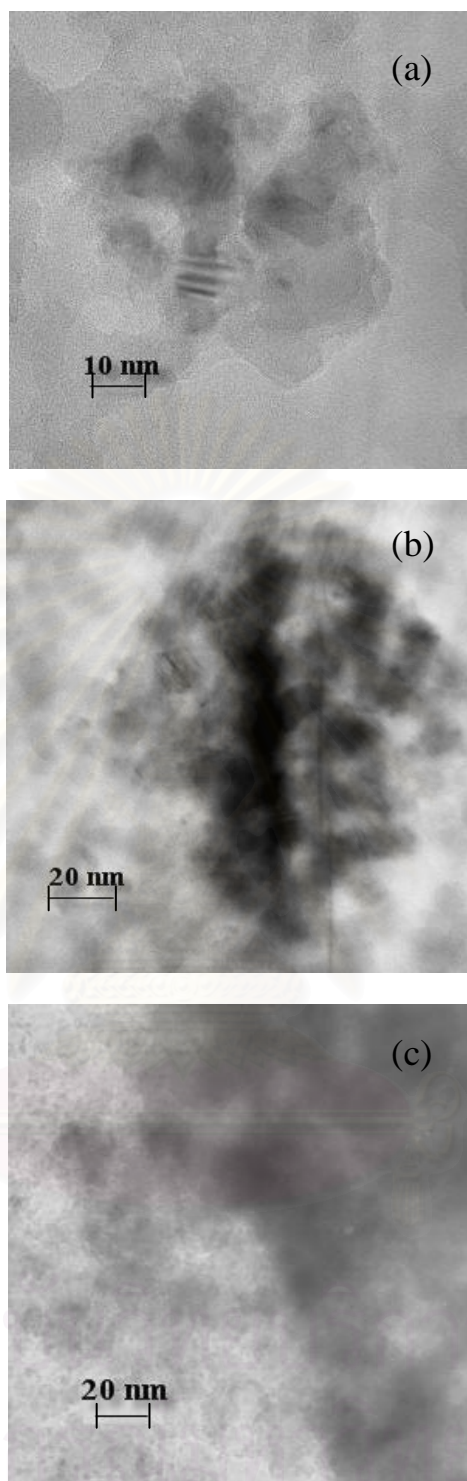
Figure 5.3 TEM images of the 2 wt%TiO$_2$ on SiO$_2$ catalyst (a) sequential-impregnation (b) co-impregnation catalyst (c) 10wt% TiO$_2$ on SiO$_2$ catalyst by co-impregnation

When large amount of TiO_2 was loaded on Co/SiO_2, the partial amount of titania, which did not react with cobalt to form $CoTiO_3$, could migrate on the surface metal particle and block some of cobalt active sites. Figure 5.4 shows the migration and sintering of TiO_x species onto the silica support by TEM and EDX analysis. The particle size of TiO_x is very large around 80-230 nm. Therefore, our results in Table 5.4 show that the active metal surface and cobalt dispersion decrease with increasing the loading amount of titania resulting in low activity.
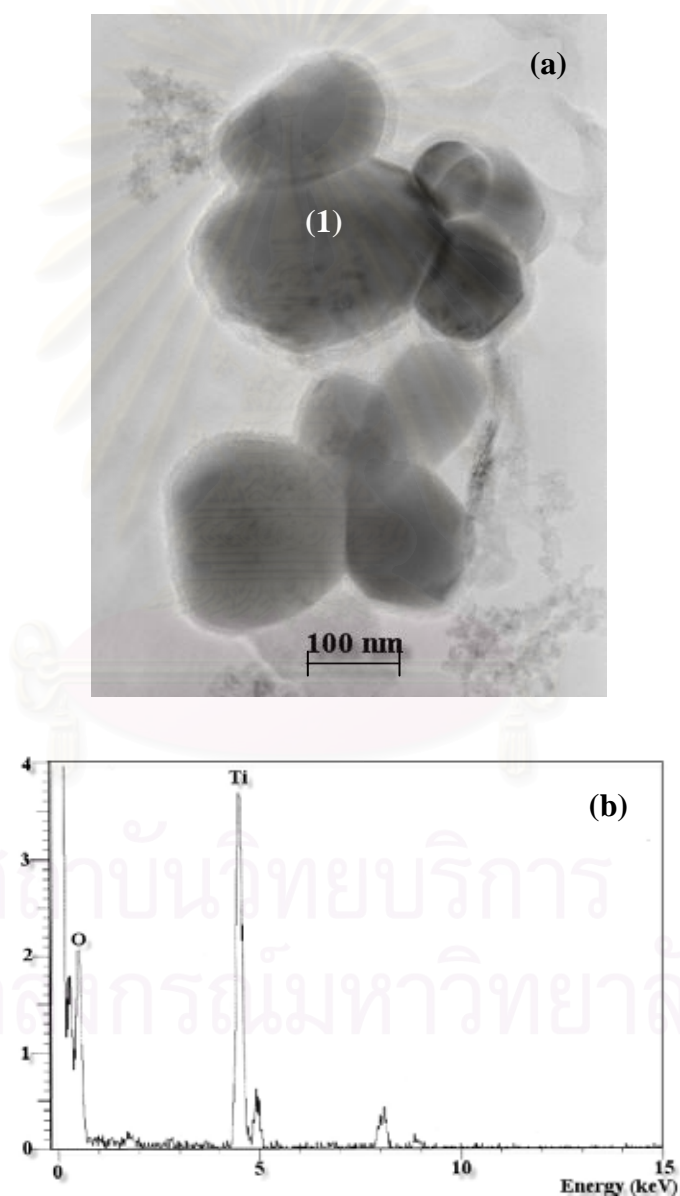
Figure 5.4 (a) TEM image of the 10wt% TiO_2 on SiO_2 catalyst by co-impregnation and (b) EDX result at point (1) on the image

TiO_2-promoted catalyst prepared by impregnation method exhibited high dispersion than unpromoted catalysts and SMSI did not drastically affected the decrease in cobalt metal surface area as illustrated in Table 5.4. The titania precursors was impregnated on silica support and then calcined before cobalt impregnation. The silica support was covered by titanium oxide; therefore the cobalt might spread on titania leading to higher dispersion than non-TiO_2 added catalyst. The titanium oxide might not strongly interact with cobalt, because its reactivity lost in TiO_2-$SiO_2$ interaction. This could prevent cobalt metal from agglomeration during high temperature reduction without reducibility obstruction because the reduction degree in Table 5.4 was unchanged.

The performance of TiO_2-promoted catalysts by co-impregnation catalysts was sensitive to loading amount of TiO_2 due to the formation of $CoTiO_3$. It might be explained that the formation of Co-TiO_2 in co-impregnation method is easier than that in sequential-impregnation method. Since the cobalt precursor and titania precursor were mixed before loading on silica support, the titanium might form the strong interaction with cobalt and more easily produce $CoTiO_3$ compound than sequential-impregnation catalyst at high temperature during calcination and reduction steps. Thus, $CoTiO_3$ phase of 10% TiO_2 loading by co-impregnation catalyst could be detected by XRD, while the cobalt metal peak disappeared. TEM image shows the metal cluster on the silica support, which was discovered to contain highly dispered phase of cobalt and titania as shown in Figures 5.5, 5.6 for sequential-impregnation and co-impregnation catalysts respectively. The results from EDX indicate that all deposited elements exist on the metal cluster. Ti possibly located in the thin layer partially covering the cobalt cluster.
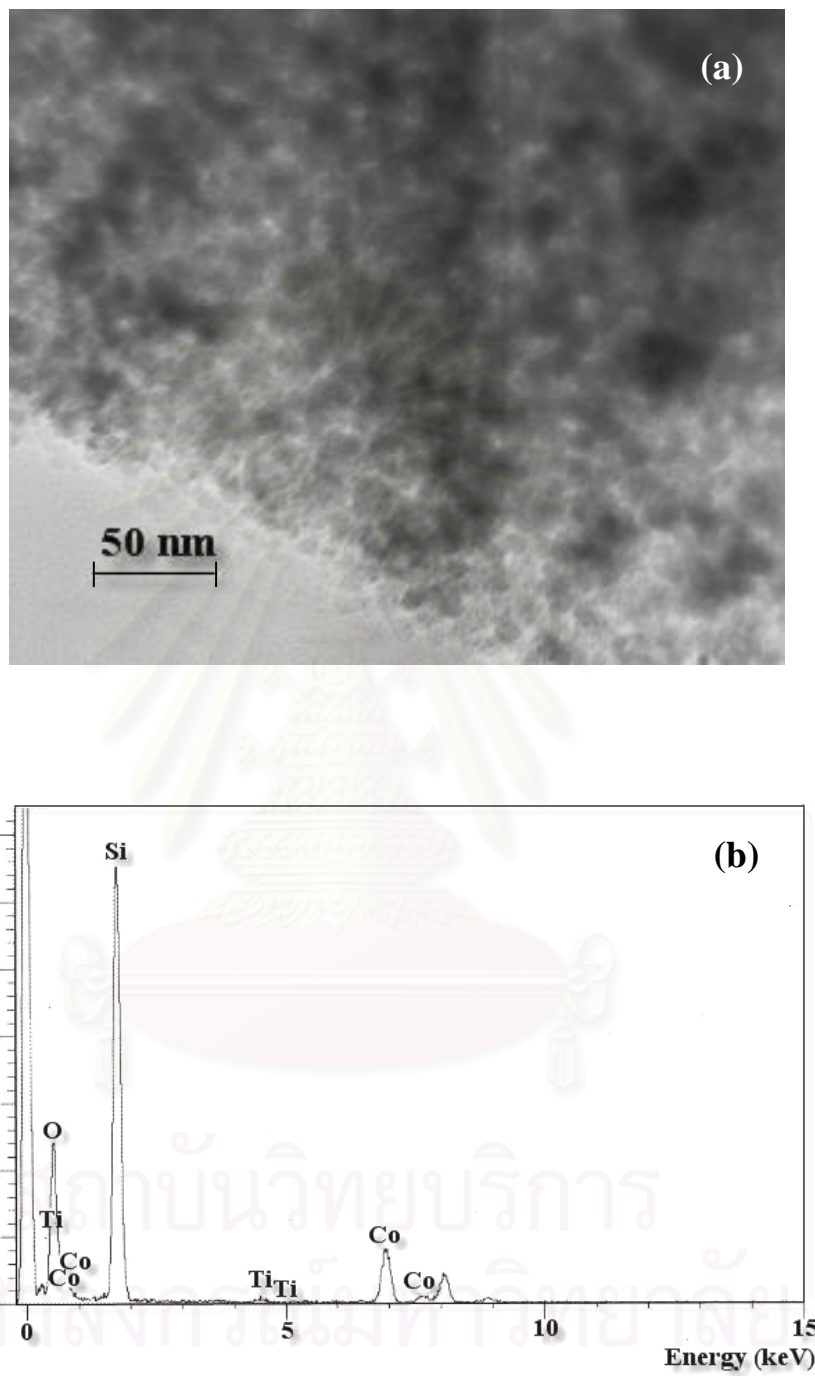
Figure 5.5 (a) TEM image of the 2wt% TiO_2 on SiO_2 catalyst by sequential-impregnation and (b) EDX results on this image
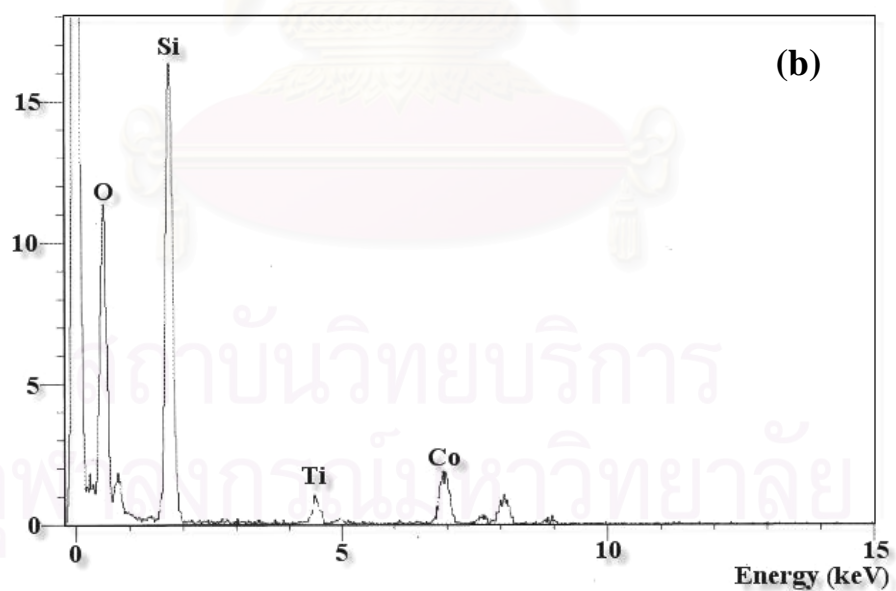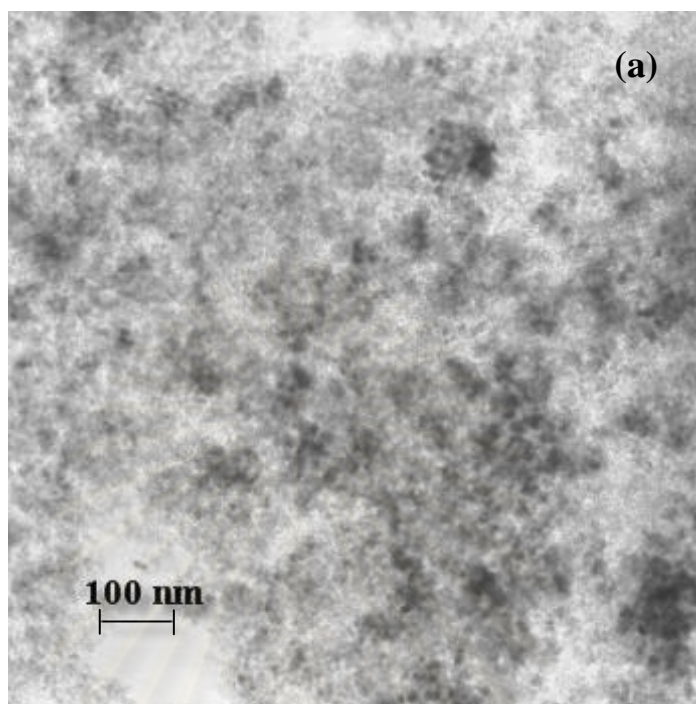
Figure 5.6 (a) TEM image of the 2wt% TiO_2 on SiO_2 catalyst by co-impregnation and
(b) EDX results on this image

According to the previous studies, we propose the surface model of TiO_2-promoted catalysts in Figure 5.7. The introduction of TiO_2 enhanced the spread of cobalt on silica support leading to high dispersion and metal surface area.
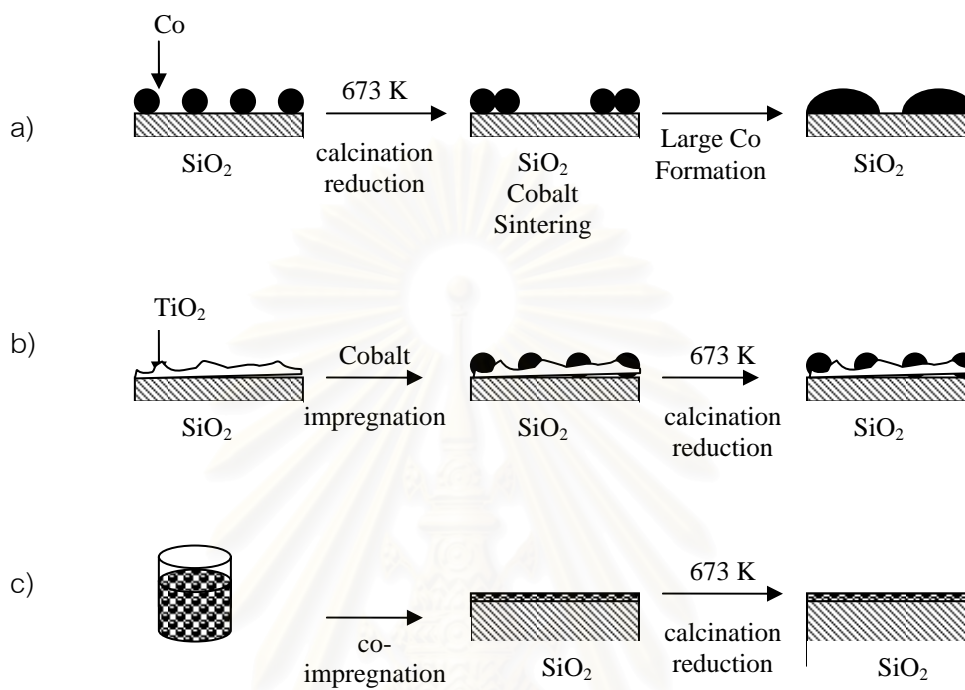
Figure 5.7 Proposed surface model of Co/SiO_2, TiO_2-promoted on Co/SiO_2 by sequential-impregnation and co-impregnation method; **a**: Co/SiO_2; **b**: TiO_2-promoted Co/SiO_2 by sequential-impregnation; **c**: TiO_2-promoted Co/SiO_2 by co-impregnation.
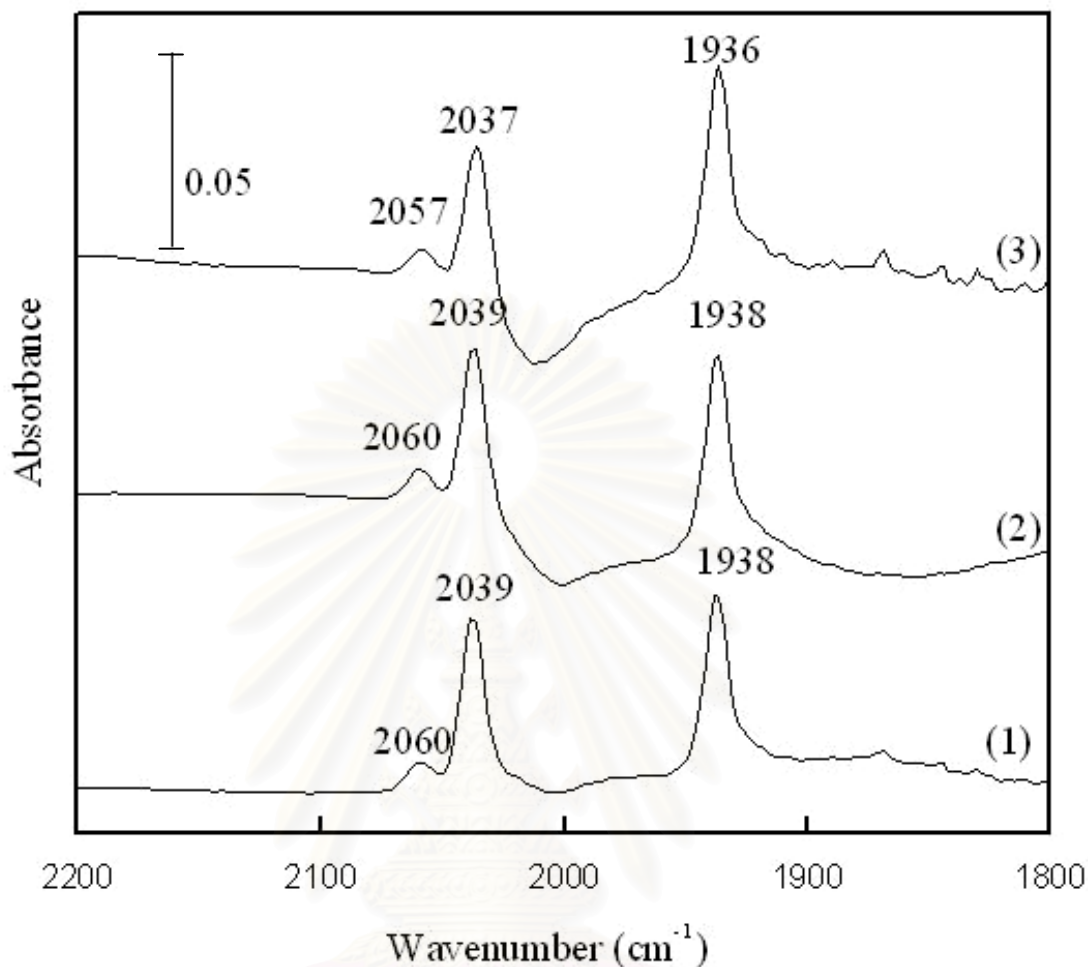
Figure 5.8 FTIR spectra of CO adsorbed on the catalysts reduced at 673 K; (1)
Co/SiO$_2$, (2) 2 wt% TiO$_2$-added catalyst by sequential-impregnation, (3)
2 wt% TiO$_2$-added catalyst by co-impregnation

In-situ diffuse reflectance infrared Fourier transform spectroscopy
(DRIFTS) was used to study the adsorbed CO for the reduced catalysts as compared
in Fig 5.8. For non-TiO$_2$ catalyst, the 2039 cm^{-1} peak was assigned to CO adsorbed on
cobalt metal in linear geometry. The 2060 cm^{-1} shoulder peak could be assigned to the
surface carbonyl species, Co(CO)$_x$ (where X>1), and the 1938 cm^{-1} peak was due to
the bridged CO on Co sites (Rohr et al., 2000). The positions of peaks of 2% TiO$_2$
loaded catalysts were equivalent to that of non-loaded TiO$_2$ catalysts. This result
indicated that the addition of TiO$_2$ did not influence the adsorption mode of CO.

5.1.3 Product Distribution of TiO_2-Promoted Co/SiO_2 Catalyst

Table 5.5 shows the product distribution on the supported cobalt catalysts with different loading amounts of TiO_2. The observed increase in the methane formation with titania loading is similar to the results reported by Vannice (1976, cited in Iglesia, 1997) for TiO_2 support catalyst. They reported that TiO_2 supports appear to lead to higher methanation turnover rates because of TiO_x overlayers influence CO and H_2 adsorption thermodynamics. Haller and Resasco (1989, cited in Dulub et al, 2000) reported that special Ti^{3+} sites at the modified Pt catalyst, or Pt sites next to the reduced TiO_x layer are thought to be responsible for the dramatic enhancement in hydrogenation activity. From Table 5.5, the 10wt% TiO_2-added catalysts had the highest C1 formation. This might be due to the TiO_x phase around the cobalt active surface; therefore the methylene ($-CH_2-$) readsorbing ability for growing chain was declined resulting in high methane formation and low chain growth probability.

The TOF were calculated from the activities and H_2 uptakes measured by chemisorption. TiO_2 did not significantly affect the TOF of Co/SiO_2 catalysts. The decrease in TOF of 10wt% TiO_2-loaded catalyst correlates with the suppression in capacity of cobalt to adsorb hydrogen due to the formation of $CoTiO_3$ phase.

Table 5.5 Product distribution of Co/SiO_2 with different TiO_2 loading

Method	Sequential-impregnation catalyst				Co-impregnation catalyst		
TiO_2 Loading (%)	0	2	5	10	2	5	10
Chain growth probability	0.84	0.82	0.82	0.81	0.83	0.82	0.82
Turn over frequency (s^{-1}) [a]	0.14	0.15	0.17	0.17	0.15	0.20	0.09
Product distribution (%) [b]							
C_1	15.68	19.14	19.00	20.8	19.76	16.50	24.24
C_2	2.28	2.92	2.84	2.78	2.63	1.84	2.82
C_3	5.24	6.60	6.47	6.63	5.81	4.78	6.96
C_4	5.66	6.82	6.39	6.99	6.37	5.47	7.32
C_5^+	71.15	64.52	65.31	62.8	65.43	71.41	58.65

Note:[a] Based on H_2 total uptake calculated from H_2 chemisorption

[b] The calculation was based on the number of carbon atom for each product.

5.2 Conclusions

    The small amount of titania could prevent cobalt metal from sintering effect at high temperature steps in catalyst preparation. Consequently, the metal active sites were increased resulting in higher activity than non-TiO_2 catalyst. High loading TiO_2 induced the formation of $CoTiO_3$, which was hardly reduced than Co_3O_4, causing the decrease in cobalt reducibility. It might be thought that the present of TiO_x phase around cobalt phase declined the methylene (-CH_2-) readsorbing ability for growing chain resulting in high methane production and low chain growth probability.

CHAPTER VI

EFFECTS OF ZrO$_2$ PROMOTION ON Co/SiO$_2$ CATALYST

Metallic cobalt is an excellent catalyst for CO hydrogenation yielding higher hydrocarbons (Fischer-Tropsch synthesis). The activity of supported catalysts depends on the surface area of the exposed metallic cobalt surface. Therefore, the high dispersion of the cobalt metal is required for highly active cobalt catalyst. However, the activity and selectivity of such catalysts still need improvement. Thus, various promoters have been used to reach this goal. The zirconium has been claimed that it can enhance the activity of Co/SiO$_2$ catalysts. Ali et al. (1995) investigated Zr promotion of Co/SiO$_2$ catalysts for FTS and found that Zr is a rate promoter. Feller et al. (1999) proposed that the addition of zirconium on Co/SiO$_2$ catalysts increase the cobalt reducibility resulting in an increased activity. Increasing zirconium content enhanced the C$_5^+$-selectivity. Rohr et al. (2000) investigated the effect of adding Zr to alumina support for Co FTS catalysts. They investigated the intrinsic activity of Co/Al$_2$O$_3$ by steady-state isotropic transient kinetic analysis (SSITKA) and found that zirconium modification had no effect.

However, the promotional effects of zirconium promoter interest us to more understand how it enhances the activity the Co/SiO$_2$ in FTS reaction. This work was to study the effects of different loading ratios of zirconium and to investigate the effect of zirconium on the physical properties of Co/SiO$_2$ by using XRD, TPR, H2 chemisorption and DRIFTS.

6.1 Results and Discussion

6.1.1 Catalytic Activity Screening

. The activity performances were investigated in a semi-batch slurry phase reactor under the operating condition: P (total) =1.0 MPa, T=513 K, $CO/H_2=1/2$, W/F $(CO+H_2+Ar)$ = 5 g-cat. h mol^{-1}. The catalytic performance of Co/SiO_2 catalysts was indicated by CO conversion.

Table 6.1 Reaction performance of ZrO_2-promoted catalyst by sequential-impregnation method

ZrO_2 loading (wt%)	CO conversion (%)	CH_4 selectivity (%)	CO_2 selectivity (%)
0	46.5	8.33	0.56
5	53.3	8.94	0.23
10	68.2	6.24	0.58
15	68.0	7.57	0.67
20	70.3	5.11	0.51
30	69.7	6.06	0.86

Tables 6.1 and 6.2 presented the performance of Co/SiO_2 catalyst with introduction of ZrO_2 by sequential-impregnation method and co-impregnation method. ZrO_2 could enhance the FTS activity of Co/SiO_2 catalysts increasing from 46 % to 70 % CO conversion. Since the results show almost the same CO conversion of 10, 15, 20, and 30 % ZrO_2- loaded catalysts, it is no need to load high amount of ZrO_2 on Co/SiO_2 catalysts. Thus, the optimal ZrO_2-loaded amount was around 10 wt% in both preparation methods. High loading of ZrO_2 might partially blocked active cobalt sites. The addition of ZrO_2 did not make much influence on the CH_4 and CO_2 selectivity.

Table 6.2 Reaction performance of ZrO_2-promoted catalyst by co-impregnation catalysts

ZrO_2 loading (wt%)	CO conversion (%)	CH_4 selectivity (%)	CO_2 selectivity (%)
0	46.5	8.33	0.56
5	63.2	6.44	0.53
10	72.8	6.31	1.10
15	69.4	5.32	0.77
20	66.5	6.13	0.73

The BET analysis is shown in Table 6.3. The surface areas of ZrO_2-added catalysts were similar to that of non-ZrO_2 catalysts; therefore, the activity change in Co/SiO_2 might not result from the changes in surface area of silica support. However, high load (20 wt%) of ZrO_2 could block the silica pore leading to lower surface area of support.

6.1.2 Catalyst Characterization

Table 6.3 BET analysis of ZrO_2-promoted catalysts

ZrO_2 Loading (wt%)	Impregnation catalyst Surface area (m^2/g)	Co-impregnation catalyst Surface area (m^2/g)
0	283.0	283.0
5	276.5	244.1
10	267.3	245.2
15	270.1	242.2
20	245.0	227.7
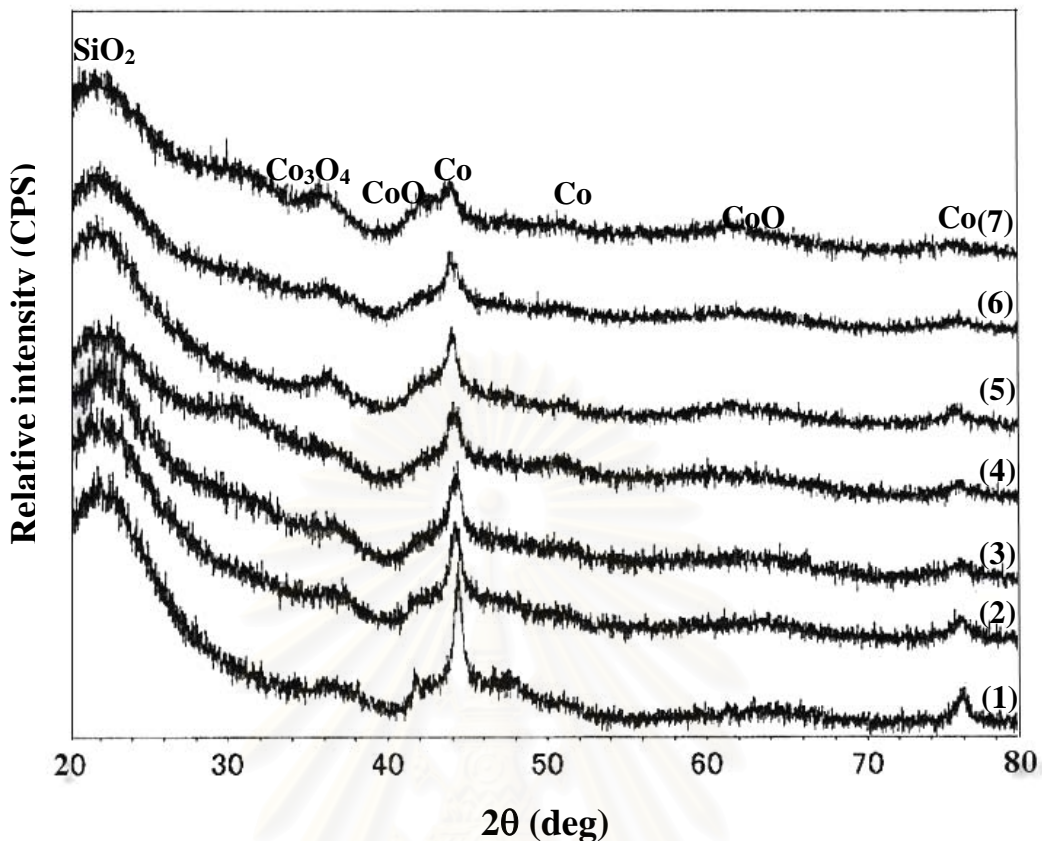
Figure 6.1 XRD patterns of various 10 wt% Co/SiO$_2$ reduced catalysts : the sequential-impregnation catalysts with ZrO$_2$ addition (1) 0 wt%, (2) 5 wt%, (3) 10 wt%, (4) 15 wt%, the co-impregnation catalysts with ZrO$_2$ addition (5) 5 wt%, (6) 10 wt%, (7) 15 wt%.

The reduced catalysts were examined by XRD to determine the existing phase as presented in Figure 6.1. No zirconium phase was detected by XRD of the ZrO$_2$ promoted Co/SiO$_2$ catalysts. This indicates that ZrO$_2$ was highly dispersed on the silica support. Metallic cobalt was located at 44.33° of 2θ from the XRD pattern of Co/SiO$_2$, while Co$_3$O$_4$ and CoO were observed from 2θ peak at 36.75° and 41.72°, respectively. The more ZrO$_2$ was added, the more intensity of XRD peak of cobalt metal was decreased.
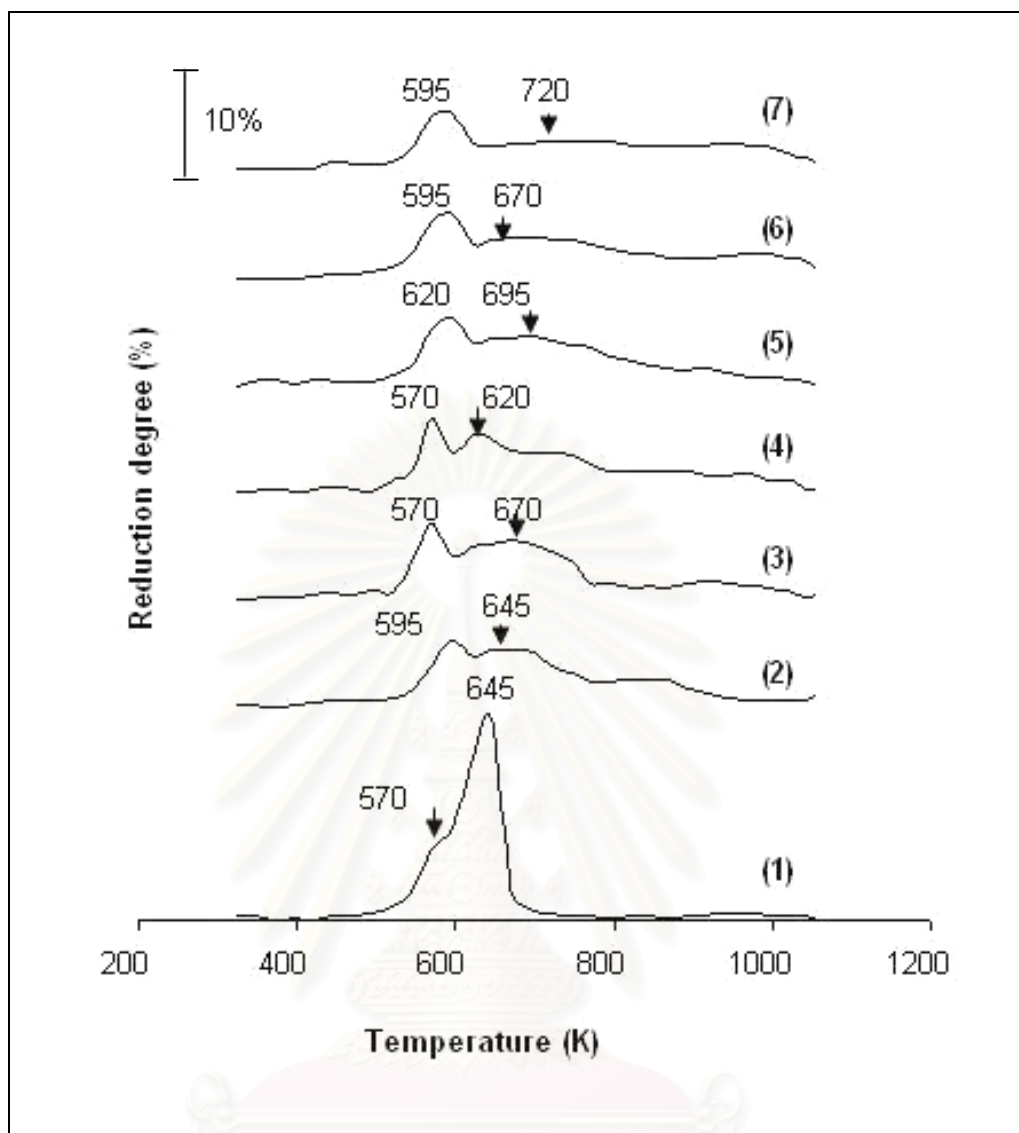
Figure 6.2 TPR profile of various 10 wt% Co/SiO$_2$ calcined catalysts. : the sequential-impregnation t catalysts with ZrO$_2$ addition (1) 0 wt%, (2) 5 wt%, (3) 10 wt%, (4) 15 wt%, the co-impregnation catalysts with ZrO$_2$ addition (5) 5 wt%, (6) 10 wt%, (7) 15 wt%.

The reduction performance of catalysts was determined by temperature-programmed reduction (TPR). The TPR diagram of ZrO$_2$-promoted catalysts is shown in Figure 6.2. Two reduction peaks of an unpromoted catalyst located at 570 and 645 K which can be attributed to the two steps of reduction Co$_3$O$_4$→CoO→Co°. The first peaks of promoted catalysts occurred at the same position of unpromoted catalyst around 570-600 K, while the second peaks were broad peaks around 620-720 K. These broad peaks were generally agreed to be a

cobalt oxide surface species interacting strongly with the support. The degree of reduction was nearly independent of promotion with zirconia as can be seen from table 6.4. As a result, the activity enhancing effect of zirconia was not due to an increase in the cobalt reducibility. Our results are in agreement with that of zirconia-modified alumina (Rohr et al., 2000).

Table 6.4 Properties of Co/SiO_2 with different ZrO_2 loading from XRD and H_2 chemisorption analyses.

Method	ZrO_2 Loading (wt%)	TEM Size (nm)	XRD Size (nm)	H_2 chemisorption				TPR Red. (%)[d]
				Size (nm)	Co Disp.[a] (%)	S.A.[b] (m^2/g)	H_2[c] uptake	
Impregnation	0	15-20	13	19.09	5.217	2.366	29.66	67
Impregnation	5	-	11	12.73	7.822	3.358	42.09	63
Impregnation	10	11-14	11	9.18	10.85	4.716	59.11	64
Impregnation	15	-	9	9.89	10.07	4.350	54.53	64
Co-impregnation	5	-	12	12.11	8.224	3.577	44.84	64
Co-impregnation	10	10-13	9	9.97	9.990	4.630	58.09	68
Co-impregnation	15	-	9	11.62	8.573	3.771	47.26	65

Note: [a] cobalt dispersion calculated from H_2 chemisorption at 373 K

[b] active cobalt surface area calculated from H_2 chemisorption at 373 K

[c] H_2 uptake (μmol/g) calculated from H_2 chemisorption at 373 K

[d] Calculated from TPR from 323 K to 1073 K

The supported cobalt particle sizes of various catalysts were determined by XRD and H_2 chemisorption exhibited in Table 6.4. The average crystallite sizes of cobalt metal, determined by line width broadening in XRD-pattern, indicate that the size of ZrO_2-added catalysts was smaller than that of normal catalyst. The H_2 chemisorption results showed that the cobalt particle size became smaller than that of unpromoted catalyst. Ali et al. (1995) proposed that it was possible that Zr

promotion cause the H_2 spillover which caused an underestimation of the average Co crystallite size. Therefore, TEM image was used to measure the particle size of ZrO_2-added cobalt catalysts as shown in Figure 6.3 and 6.4. The measurement from TEM image in Table 6.4 indicated that the average size of the cobalt metal was similar to that of H_2 chemisorption. Thus, the estimation of H_2 chemisorption was not inhibited by H_2 spillover effect.

The dispersion of cobalt metal was increased from 5.22 % to the optimal value of 10.85 %. Furthermore, the cobalt metal surface areas of modified catalyst were increased. Therefore, the zirconia could enhance the activity on FTS reaction by growing the dispersion of cobalt metal with no inhibiting the cobalt reducibility. 10wt % of ZrO_2 loading is the best loading amount which provided the highest cobalt dispersion and surface area both in sequential and co-impregnation methods.
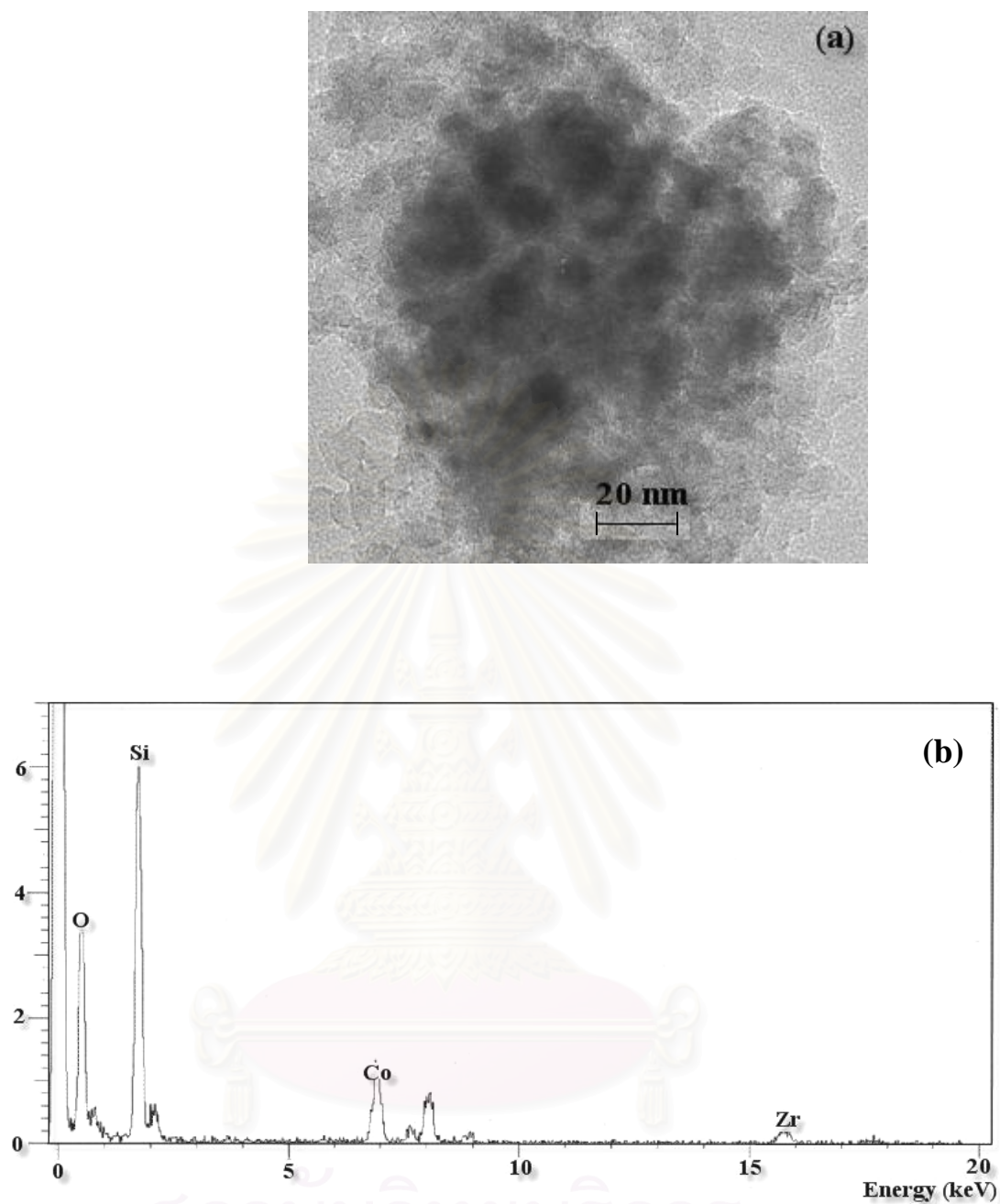
Figure 6.3 (a) TEM image of the 10wt% ZrO_2 on SiO_2 catalyst by sequential-impregnation and (b) EDX result on this image
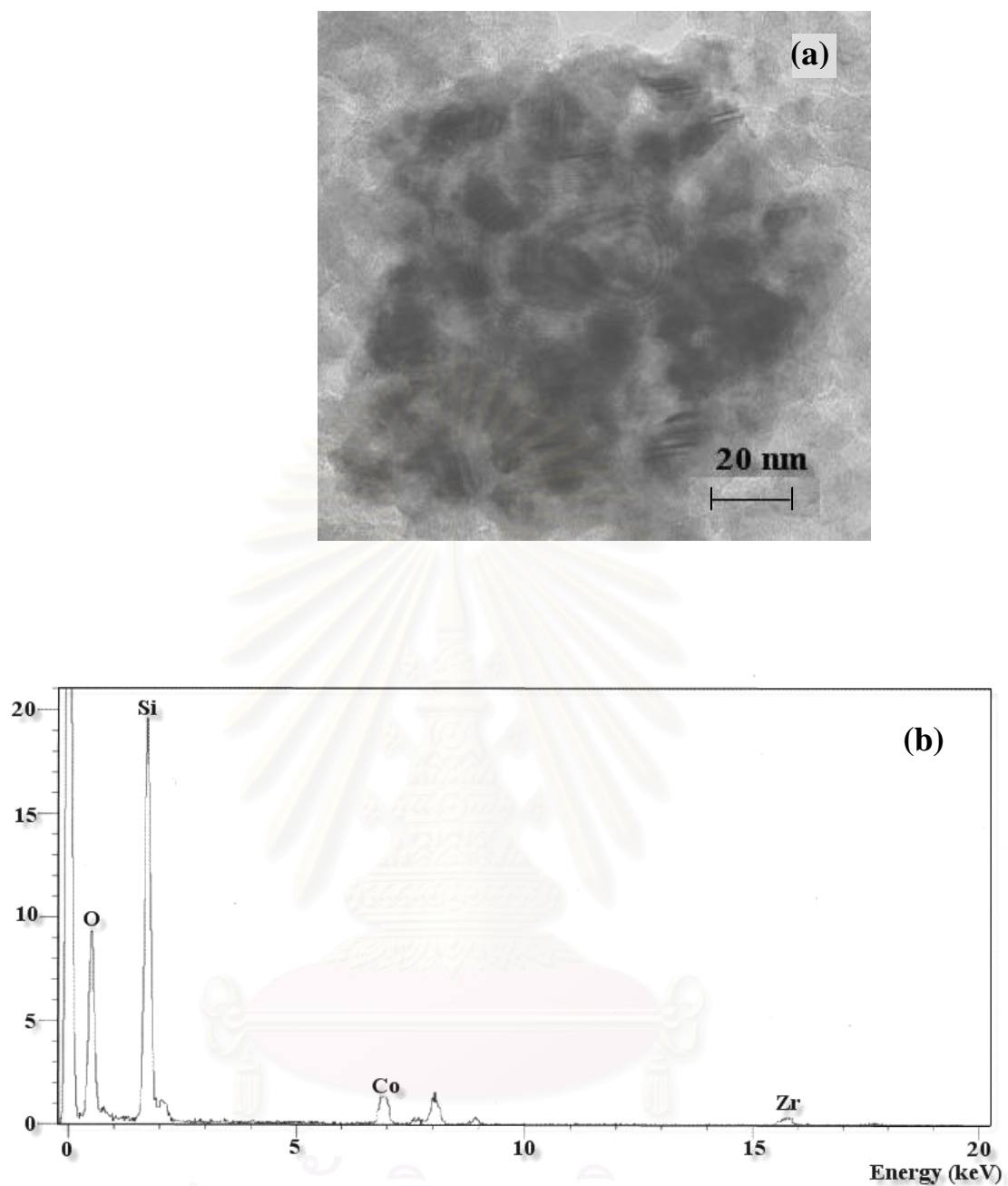
Figure 6.4 (a) TEM image of the 10wt% ZrO_2 on SiO_2 catalyst by co-impregnation and (b) EDX result on this image

The compositions of metal cluster were investigated by TEM and EDX as shown in Figure 6.4. The results indicated that cobalt and zirconium element existed on the silica support. This might be explained that cobalt-zirconium interaction was formed during impregnation step. Feller et al. (1999) and Jongsomjit et al (2003) found that zirconium modification could significantly increase the reducibility of supported cobalt metal as cobalt-zirconium species can be easily reduced at low temperature. Ali et al.,(1995) and Enache et al. (2004) proposed that the use of ZrO_2 could improve the H_2 adsorption via a spillover mechanism. In our case, Zr modification increased the amount of H_2 uptake as can be seen in Table 6.4. However, the reduction degrees of modified catalyst were still the same. It might be possible that the addition of ZrO_2 led to the formation of Zr-Co phase around high dispersed metallic cobalt. Maybe this phase not only prevented cobalt metal from sintering at high temperature, but also enhanced the capability of chemisorbing hydrogen via a spillover mechanism. Thus, the small cobalt particle could be reduced resulting in highly dispersed cobalt metal on this catalyst without low reducibility caused by strong metal-support interaction.
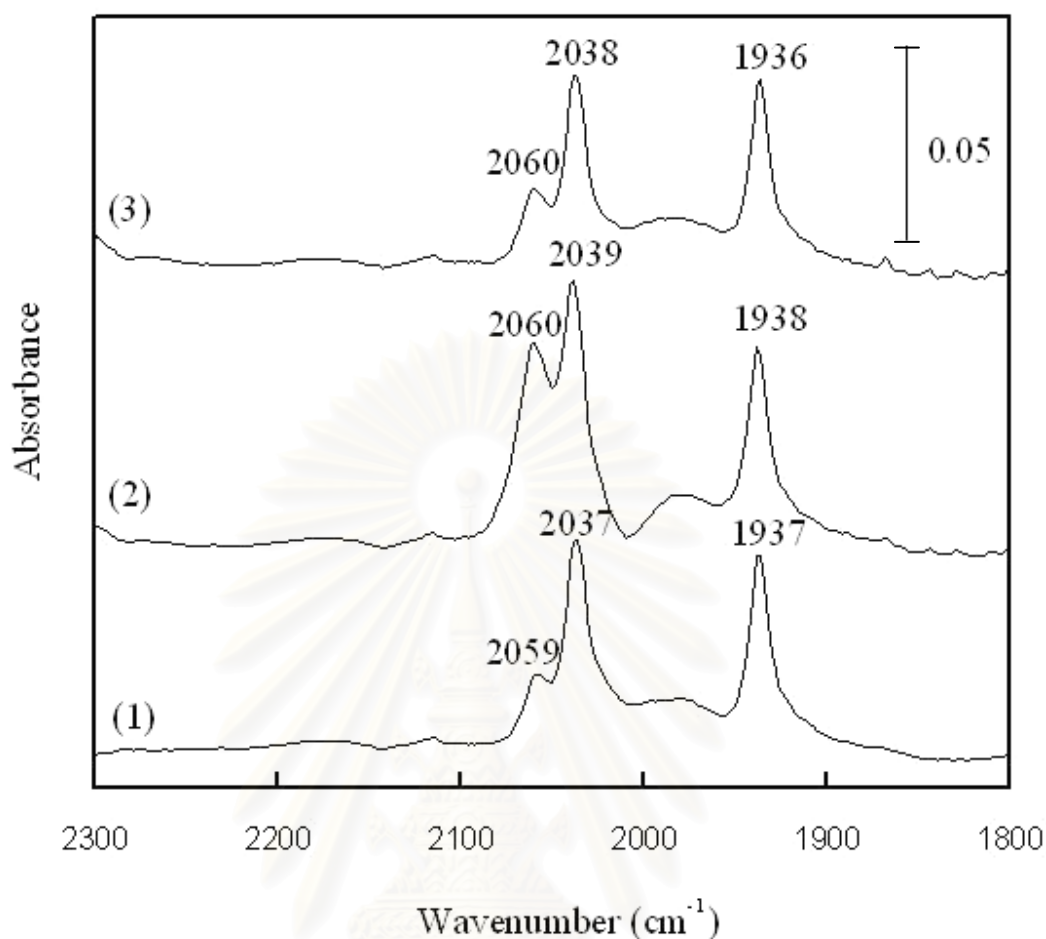
Figure 6.5 FTIR spectra of CO adsorbed on the catalysts reduced at 673 K; (1) Co/SiO$_2$, (2) 10 wt% ZrO$_2$-added catalyst by sequential-impregnation, (3) 10 wt% ZrO$_2$-added catalyst by co-impregnation

Ali et al. (1995) suggested that high activity in ZrO$_2$-promoted catalyst might be due to the Zr-Co active interface, which facilitates CO dissociation. Thus, this experiment used DRIFTS to investigate the adsorbed CO type on ZrO$_2$-added catalysts. The linear adsorbed CO on unmodified cobalt catalyst located at 2037 cm^{-1} peak as illustrated in Figure 6.5. The shoulder peak at 2059 cm^{-1} was assigned to the surface carbonyl species and 1937 cm^{-1} peak band were attributed to the bridged-type CO adsorbed on cobalt metal sites. 10% ZrO$_2$ added catalysts provided the adsorbed CO peak at the same position as in non-ZrO$_2$ loaded catalyst. According to high dispersion of cobalt metal, the co-impregnation catalyst with ZrO$_2$ promoter had the strong shoulder peak of surface carbonyl species at 2060 cm^{-1}, which is always found

on the corner site of cobalt metal or on the small cobalt metal. The DRIFTS results suggested that ZrO_2 modification did not increase bridge-type adsorbed CO. Therefore, the enhancement in Co activity did not cause from a facilitation of CO dissociation.

6.1.3 Product Distribution of ZrO_2-Promoted Co/SiO_2 Catalyst

Table 6.5 expresses the catalytic performance and product distribution of ZrO_2-promoted catalysts. The Zr promotion did not significantly affect the chain growth probability and product distribution of Co/SiO_2 catalyst. No significant effect of Zr addition on the TOF, based on H_2 chemisorption results, was compared with simple cobalt catalyst. These results mean that the increase in activity of ZrO_2-promoted catalysts was not from the increase in site activity of Co/SiO_2.

Table 6.5 Product distribution of Co/SiO_2 with different ZrO_2 loadings.

Method	Sequential-impregnation catalyst				Co-impregnation catalyst		
ZrO_2 Loading (%)	0	5	10	15	5	10	15
Chain growth probability	0.86	0.86	0.85	0.85	0.86	0.89	0.86
Turn over frequency (s^{-1}) [a]	0.15	0.12	0.11	0.12	0.13	0.12	0.14
Product distribution (%) [b]							
C_1	6.85	7.21	4.59	4.74	6.24	4.18	4.64
C_2	1.18	0.99	0.73	1.56	0.96	0.68	0.72
C_3	3.16	3.24	2.68	3.85	3.37	2.54	3.17
C_4	4.15	4.47	4.33	7.23	5.00	3.98	4.68
C_5^+	84.67	84.09	87.67	82.60	84.42	88.63	86.80

Note:[a] Based on H_2 total uptake calculated from H_2 chemisorption

[b] The calculation was based on the number of carbon atom for each product.

6.2 Conclusions

The zirconium promotion increased the catalytic activity of FTS by growing the cobalt metal dispersion. The formation of Zr-Co phase might enhance the reducibility of small cobalt particle by H_2 spillover evidenced by high amount of H_2 uptake from H_2 chemisorption analysis. The chain growth probability and product distribution were not affected from zirconium addition. Zr promoter did not improve the TOF of promoted catalyst; therefore the increase in FT activity was resulted from the increase in active metal sites.

CHAPTER VII

CONCLUSIONS AND RECOMMENDATIONS

7.1 Catalytic Performance

All metals oxide promoters can enhance the performance of Co/SiO_2 catalyst on FTS reaction as illustrated in Figure 7.1. The CO conversion of Co/SiO_2 could be increased approximately 40% with Al_2O_3 promoter, 50% with ZrO_2 promoter and 24% with TiO_2 promoter. The CO conversion obtained from the sequential-impregnation and the co-impregnation methods in the presence metal oxide promoters was slightly different. However, the dramatic decrease in CO conversion was found in 10wt%TiO_2-loaded catalyst by co-impregnation method due to the formation of $CoTiO_3$ as described in Chapter 5.
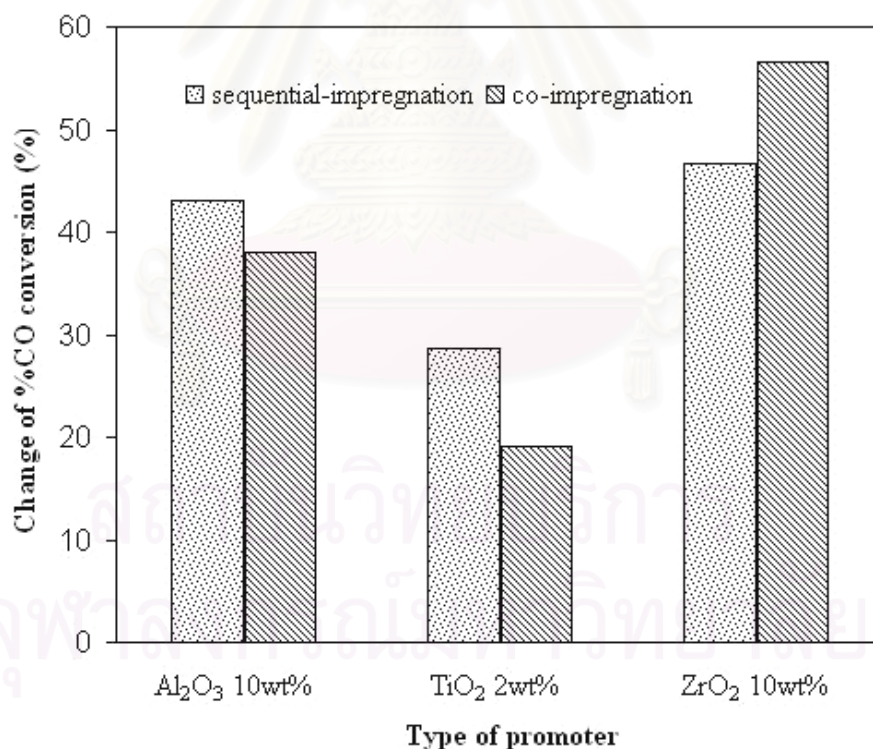
Figure 7.1 Percentage change of % CO conversion of Co/SiO_2 catalysts with metal oxide promoters compared with unpromoted catalyst

7.2 Catalyst Characterization

The addition of metal oxide promoter could prevent the sintering of cobalt metal during high temperature treatments in calcination and reduction steps. The decrease in cobalt sintering causes higher cobalt dispersion and higher cobalt active site leading to the increase in FT activity of metal oxide promoted catalysts as can be seen in Table 7.1. Among three kinds of metal oxide promoters, ZrO_2-added catalysts provided the smallest cobalt particle size and the highest cobalt active surface. It might be possible that the Zr-Co phase has the additional function that is not only prevention of cobalt sintering effect but also enhancement in the capability of hydrogen chemisorption via a spillover mechanism. Thus, the small cobalt particle could be reduced resulting in highly dispersed cobalt metal on this catalyst without low reducibility causing by strong metal-support interaction as shown in Table 7.2.

Table 7.1 Properties of 10 wt% Co/SiO_2 with different metal oxide promoters

Metal Oxide Type	Metal oxide Loading (wt%)	Preparation method	H_2 chemisorption			
			Size (nm)	Co Disp.[a] (%)	S.A.[b] (m^2/g)	H_2[c] uptake
None		impregnation	19.09	5.217	2.366	29.66
Al_2O_3	10	impregnation	13.41	7.426	3.085	38.67
	10	Co-impregnation	13.91	7.160	3.238	40.59
TiO_2	2	impregnation	13.59	7.329	3.449	43.23
	2	Co-impregnation	13.80	7.217	3.093	38.76
ZrO_2	10	impregnation	9.18	10.85	4.716	59.11
	10	Co-impregnation	9.97	9.990	4.630	58.09

Note: [a] cobalt dispersion calculated from H_2 chemisorption at 373 K

[b] active cobalt surface area calculated from H_2 chemisorption at 373 K

[c] H_2 uptake (μmol/g) calculated from H_2 chemisorption at 373 K

The intrinsic activity of cobalt atom is determined by turnover frequency (TOF) value based on H_2 chemisorption. The results from Table 7.2 indicated that the addition of metal oxide promoters did not impact on TOF of Co/SiO_2 catalysts. These results implied that the main reason in higher activity on FTS reaction of promoted catalysts is the increment of metallic cobalt site.

Table 7.2 Effects of promoters on the catalytic properties of 10 wt%Co/SiO$_2$

Metal Oxide Type	Metal oxide Loading (wt%)	Preparation method	Reduction Degree (%)	TOF	$\propto$
None		impregnation	67	0.15	0.86
Al$_2$O$_3$	10	impregnation	61	0.16	0.84
	10	Co-impregnation	67	0.15	0.83
TiO$_2$	2	impregnation	70	0.15	0.82
	2	Co-impregnation	63	0.15	0.83
ZrO$_2$	10	impregnation	64	0.11	0.85
	10	Co-impregnation	68	0.12	0.89

7.3 Product Distribution

Chain growth probability ($\propto$) is represented the product distribution of FT reaction (Anderson et al., 1984). The high value of chain growth probability gives higher molecular weight product. Usually, the adsorption of CO molecules is influenced by the size of metallic cluster. The light hydrocarbon production is favored by increasing the metal dispersion, and vice versa, an increase of molar weight of reaction product is obtained by a decrease in dispersion.

Our investigation suggested that the addition of promoter resulted in higher dispersion and smaller particle of cobalt metal on silica support as described in Table 7.1. However, the value of chain growth probability was not significantly changed as shown in Table 7.2. TiO$_2$-promoted catalyst had the lowest chain growth probability because TiO$_x$ phase are though to be responsible for the dramatic enhancement in hydrogenation activity (Haller and Resasco 1989, cited in Dulub et al, 2000). Consequently, the production of light hydrocarbon was found in TiO$_2$-added catalyst more than in Al$_2$O$_3$ and ZrO$_2$-promoted catalysts as presented in Figure 7.2.
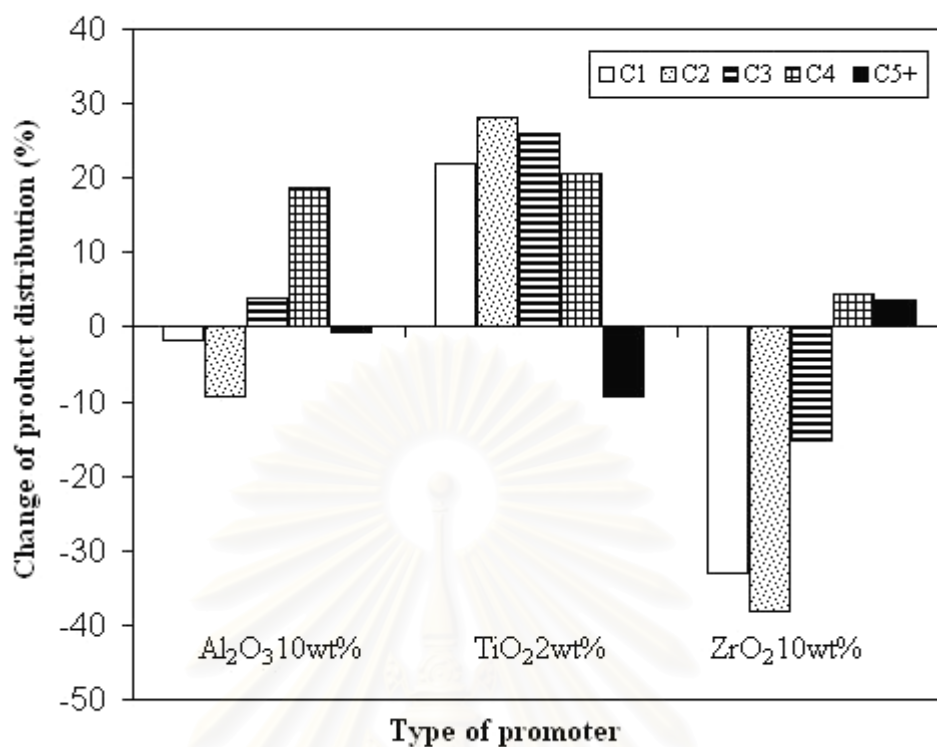
Figure 7.2 Effect of promoter types on the change of product distribution

7.4 Conclusions

The results of metal oxide addition such as Al_2O_3, TiO_2 and ZrO_2 onto the silica support indicated the improvement on the catalytic activity of cobalt in FTS reaction by increasing the cobalt dispersion without obstructing the reducibility. The method of preparation of Al_2O_3 and ZrO_2 loaded onto Co/SiO_2 catalyst did not affect the catalytic activity, unlike the results from the preparation of TiO_2-promoted catalyst. The formation of hardly reducible $CoTiO_3$ from the co-impregnation method was easier than that from the sequential-impregnation method. Hydrogen spillover might be the reason for the enhancement of activity in ZrO_2-promoted catalyst. However, the small supported cobalt particles on promoted catalysts slightly lowered the chain growth probability. In addition, the result showed that the turn over frequency (TOF) of promoted catalysts was unchanged. It implied that the promoter did not influence the site activity of Co/SiO_2 catalysts. Consequently, it might be concluded that the increase in the active site was the main reason for higher reactivity of metal-oxide promoted catalyst.

7.5 Recommendation

A further study of the cobalt-based catalyst with metal oxide for Fischer-Tropsch catalyst should be concerned with the following aspect:

1. The increase in heavy hydrocarbon product

Although cobalt catalyst with metal oxide promoter had higher CO conversion compared with non-promoter catalyst, it could not increase the selectivity of the heavy hydrocarbons as evidenced by low chain growth probability. One reason for the high methane selectivity of our catalyst was the small pore structure. Large-pore catalyst would provide the selectivity of the heavy hydrocarbons due to the high diffusion efficiency of hydrocarbon product. For further research work, large-pore silica supports with metal oxide promoter should be investigated the FTS activity.

2. Improvement of support for FTS reaction

According to metal oxide such as Al_2O_3, TiO_2 and ZrO_2 could improve the activity of silica-support catalyst; the SiO_2 is thought to be promoter for other support in further research work. The supports like Al_2O_3 and TiO_2 have strong interaction to active metal, leading to formation of small supported cobalt with limited reducibility. The addition of SiO_2 on these supports should decrease the strong metal-support interaction, resulting in easily reducible metal formation and the increase in FT activity.

3. The addition of noble metal on cobalt catalyst with metal oxide promoter

The addition of metal oxide could increase the dispersion of cobalt on silica support leading the increase in active site of cobalt. However, the reducibility of cobalt was not improved. Other research works suggest that the addition of small amount of noble metal could increase the reducibility of cobalt under low temperature. Thus, the addition of both metal oxide promoter and noble metal promoter on cobalt catalyst should be carried out.

REFFERENCES

Ali, S.; Chen, B.; and Goodwin, J.G. Zr promotion of Co/SiO₂ for Fischer-Tropsch synthesis. <u>Journal of Catalysis</u> 157 (1995): 35-41.

Anderson, R.B. <u>The Fischer-Tropsch Synthesis</u>. Orlando: Academic Press, 1984.

Bessell, S. Support effects in cobalt-based Fischer-Tropsch catalysis. <u>Applied Catalysis A: General</u> 96 (1993): 253-268.

Bond, G.C. <u>Heterogeneous catalysis: principles and applications</u>. Oxford: Clarendon Press, 1987.

Columbia Encyclopedial. <u>Rare-earth metals</u> [online]. Available from: http://www.encyclopedia.com [2005, May 19]

Coulter, K.E.; and Sault, A.G. Effects of activation on the surface properties of silica-supported cobalt catalysts. <u>Journal of Catalysis</u> 154 (1995): 56-64.

Dry, M.E. Practical and theoretical aspects of the catalytic Fischer-Tropsch process. <u>Applied Catalysis A: General</u> 138 (1996): 319-344.

Dry, M.E. The Fischer-Tropsch process: 1950-2000. <u>Catalysis Today</u> 71 (2002): 227-241.

Dulub, O.; Hebenstreit, W.; and Diebold, U. Imaging cluster surfaces with atomic resolution: the strong metal-support interaction state of Pt supported on TiO₂ (110). <u>Physical Review Letters</u> 84 (2000): 3646-3649.

Enache, D.I.; Auberger, M.R.; and Revel, R. Differences in the characteristics and catalytic properties of cobalt-based Fischer-Tropsch catalysts supported on zirconia and alumina. <u>Applied Catalysis A: General</u> (2004): 51-60.

Energy research centre of the Nethalands. Fischer-Tropsch [online]. Available from: http://www.enc.nl/biomassa/research/poly/fischertropsch.en.html [2005, May 19]

Epinoza, R.L.; Steynberg, A.P.; Jager, B.; and Vosloo, A.C. Low temperature Fischer-Tropsch synthesis from a Sasol perspective. Applied Catalysis A: General 186 (1999): 13-26.

Ernst, B.; Hilaire, L.; and Kiennemann, A. Effects of highly dispersed ceria addition on reducibility, activity and hydrocarbon chain growth of a Co/SiO_2 Fischer-Tropsch catalyst. Catalysis Today 50 (1999): 413-427.

Feller, A.; Claeys, M.; and Steen, E.V. Cobalt cluster effects in zirconium promoted Co/SiO_2 Fischer-Tropsch catalysts. Journal of Catalysis 185 (1999): 120-130.

Haddad, G.J.; Chen, B.; and Goodwin, J.G. Effect of La^{3+} promotion of Co/SiO_2 on CO hydrogenation. Journal of Catalysis 161 (1996): 274-281.

Heal, M.J.; Leisegang, E.C.; and Torington, R.G. Infrared studies of carbon monoxide and hydrogen adsorbed on silica-supported iron and cobalt catalysts. Journal of Catalysis 51 (1978): 314-325.

Ho, S.W.; Cruz, J.M.; Houalla, M.; and Hercules, D.M. The structure and activity of titania supported cobalt catalysts. Journal of Catalysis 135 (1992): 173-185.

Iglesia, E. Design, synthesis, and use of cobalt-based Fischer-Tropsch synthesis catalysts. Applied Catalysis A: General 161 (1997): 59-78.

Iglesia, E.; Soled, S.L.; and Fiato, R.A. Fischer-Tropsch synthesis on cobalt and ruthenium, metal dispersion and support effects on reaction rate and selectivity. Journal of Catalysis 137 (1992): 212-224.

Jacobs, G., et al. Fischer-Tropsch synthesis: support, loading, and promoter effects on the reducibility of cobalt catalysts. Applied Catalysis A: General 233 (2002): 263-281.

Jager, B.; and Espinoza, R. Advances in low temperature Fischer-Tropsch synthesis. Catalysis Today 23 (1995): 17-28.

Kent, E.C.; and Allen, G.S. Effects of activation on the surface properties of silica-supported cobalt catalysts. Journal of Catalysis 154 (1995): 56-64.

Kogelbauer, A.; Oukaci, R.; and Goodwin, J.G. Ruthenium promotion of Co/Al_2O_3 Fischer-Tropsch catalysts. Journal of Catalysis 160 (1996): 125-133.

Kraum, M.; and Baerns, M. Fischer-Tropsch synthesis : the influences of various cobalt compounds applied in the preparation of supported cobalt catalysts on their performance. Applied Catalysis A: General 186 (1999): 189-200.

Kumar, K.N.P.; Keizer, K.; Burggraaf, A.J.; Okubo, T.; and Nagamoto, H. Synthesis and textural properties of unsuppoted and supported rutile (TiO_2) membranes. Journal of Materials Chemistry 3 (1993): 923-929.

Lapidus, A.; and Krylova, A. Hydrocarbon synthesis from carbon monoxide and hydrogen on impregnated cobalt catalysts: II. activity of 10% Co/Al_2O_3 and 10% Co/SiO_2 catalysts in Fischer-Tropsch synthesis. Applied Catalysis A: General 80 (1992): 1-11.

Li, J.L.; Jacobs, G.; and Zhang, Y.Q. Fischer-Tropsch synthesis: effect of small amounts of boron, ruthenium and rhenium on Co/TiO_2 catalysts. Applied Catalysis A: General 223 (2002): 195-203.

Ming, H.; and Baker, B.G. Characterization of cobalt Fischer-Tropsch catalysts I. Unpromoted cobalt-silica gel catalysts. Applied Catalysis A: General 123 (1995): 23-36.

Mohana Rao, K.; Scarano, D.; Spoto, G.; and Zecchina, A. CO adsorption on cobalt particles supported on MgO: An IR investigation. Surface Science 204 (1988): 319-330.

Oukaci, R.; Singleton, A.H. ; and Goodwin, J.G. Comparison of patented Co F-T catalysts using fixed-bed and slurry bubble column reactors. Applied Catalysis A: General 186 (1999): 129-144.

Rathousky, J.; Zukal, A.; Lapidus, A.; and Krylova, A. Hydrocarbon synthesis from carbon monoxide + hydrogen on impregnated cobalt catalysts : Part III. cobalt (10%)/silica-alumina catalysts. Applied Catalysis A: General 79 (1991): 167-180.

Reuel, R.C.; and Bartholomew, C.H. The stoichiometries of H_2 and CO adsorptions on cobalt: effects of support and preparation. Journal of Catalysis 85 (1984): 63-77.

Riva, R.; Miessner, H.; Vitali, R.; and Piero, G.D. Metal-support interaction in Co/SiO_2 and Co/TiO_2. Applied Catalysis A: General 196 (2000): 111-123.

Rohr, F.; Lindrag, O.A.; Holmen, A.; and Blekkan, E.A. Fischer-Tropsch synthesis over cobalt catalysts supported on zirconia-modified alumina. Catalysis Today 58 (2000): 247-254.

Rosynek, M.P.; and Polansky, C.A. Effect of cobalt source on the reduction properties of silica-supported cobalt catalysts. Applied Catalysis 73 (1991): 97-112.

Rygh, L.E.S.; and Nielson, C.J. Infrared study of CO adsorbed on a $Co/Re/\gamma-Al_2O_3$ - based Fischer-Tropsch catalyst. Journal of Catalysis 194 (2000): 401-409.

Schanke, D., et al. Study of Pt-promoted cobalt CO hydrogenation catalysts. Journal of Catalysis 156 (1995): 85-95.

Schulz, H. Short history and present trends of Fischer-Tropsch synthesis. <u>Applied Catalysis A: General</u> 186 (1999): 3-12.

Sharma, B.K., et al. Studies on cobalt-based Fischer-Tropsch catalyst and characterization using SEM and XPS techniques. <u>Applied Catalysis A: General</u> 211 (2001): 203-211.

Siab, A.M.; Claeys, M.; and Steen, E.V. Silica supported cobalt Fischer-Tropsch catalysts : effect of pore diameter of support. <u>Catalysis Today</u> 71 (2002): 395-402.

Stranick, M.A.; Houalla, M.; and Hercules, D.M. Spectroscopic characterization of TiO_2/Al_2O_3 and Co/Al_2O_3---TiO_2 catalysts. <u>Journal of Catalysis</u> 106 (1987): 362-368.

Sun, S.; Tsubaki, N.; and Fujimoto, K. The reaction performances and characterization of Fischer-Tropsch synthesis Co/SiO_2 catalysts prepared from mixed cobalt salts. <u>Applied Catalysis A: General</u> 202 (2000): 121-131.

Tauster, S.T.; and Fung, S.C. Strong metal - support interactions: occurrence among the binary oxides of groups IIA - VB. <u>Journal of Catalysis</u> 55 (1978): 29-35.

Tsubaki, N.; Sun, S.; and Fujimoto, K. Different functions of the noble metals added to cobalt catalysts for Fischer-Tropsch synthesis. <u>Journal of Catalysis</u> 199 (2001): 236-246.

Tsubaki, N.; Zhang, Y.; Sun, S.; Mori, H.; Yoneyama, Y.; Li, X.; Fujimoto, K. A new method of bimodal support preparation and its application in Fischer-Tropsch synthesis. <u>Catalysis communications</u> 2 (2001): 311-315.

Varghese, O.K.; Gong, D.; Paulose, M.; Grimes, C.A.; and Dickey, E.C. Crystallization and high - temperature structural stability of titanium oxide nanotube arrays. Journal of Materials Research 18 (2003): 156-165.

Voß, M.; Borgmann, D.; and Wedler, G. Characterization of alumina, silica, and titania supported cobalt catalysts. Journal of Catalysis 212 (2002): 10-21.

Wender, I. Reaction of synthesis gas. Fuel Processing Technology 48 (1996): 189-297.

Wieckowski, A.; Savinova, E.R.; and Vayenas, C.G. Catalysis and electrocatalysis a nanoparticle surfaces. Basel: Marcel Dekker, 2003.

Zhang, J.; Chen, J.; Ren, J.; and Sun, Y. Chemical treatment of γ-Al$_2$O$_3$ and its influence on the properties of Co-based catalysts for Fischer-Tropsch synthesis. Applied Catalysis A: General 243 (2003): 121-133.

Zhang, J.; Chen, J.; Ren, Y.; Li, Y.; and Sun, Y. Support effect of Co/Al$_2$O$_3$ catalysts for Fischer-Tropsch synthesis. Fuel 82 (2003): 581-586.

Zhang, J.; Chen, J.; and Sun, Y. Recent technological developments in cobalt catalysts for Fischer-Tropsch synthesis. Journal of Natural Gas Chemistry 11 (2002): 99-108.
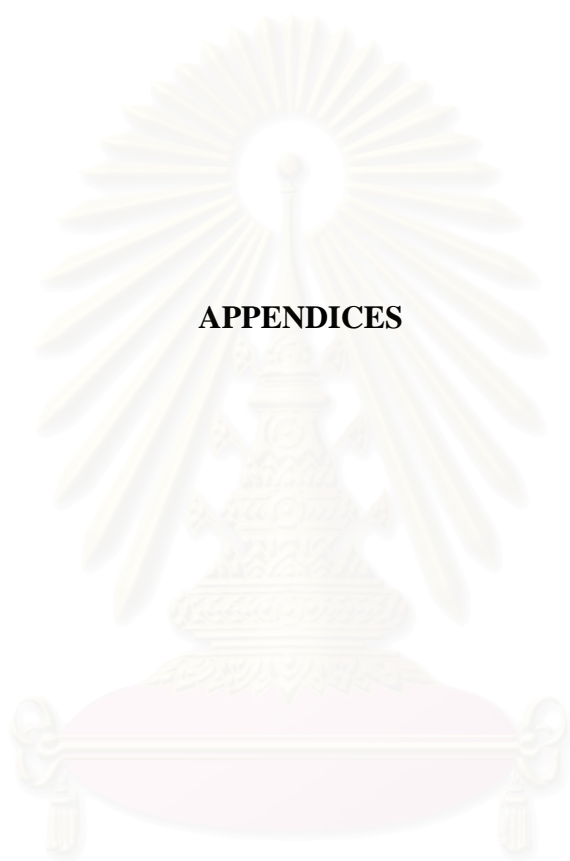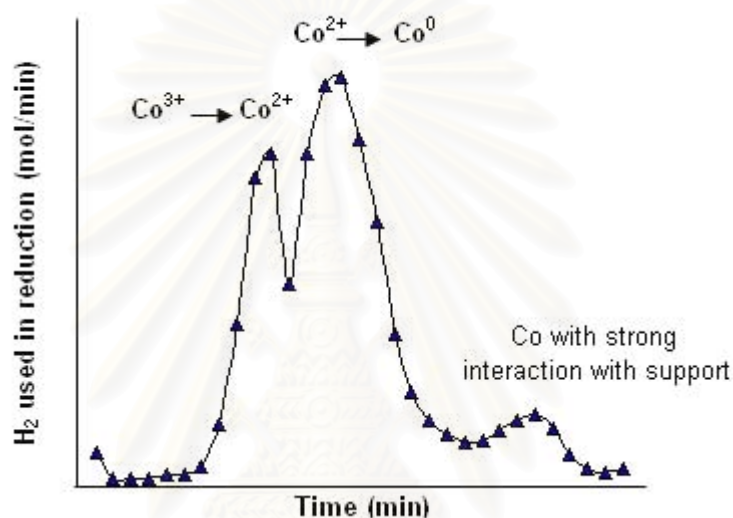
APPENDICES

Appendix A

Calculation of Reduction Degree from Temperature Programmed Reduction (TPR)

There are two steps of reduction. The first step is the reduction of Co_3O_4 to CoO followed by the reduction at high temperature to Co^0 as shown in this figure.

Figure A-1   Reduction profile of Co/SiO_2 catalyst

The total equation of H_2 used in two step reduction is shown in equation below

$$H_2 + Co_3O_4 \rightarrow H_2O + 3CoO$$

$$H_2 + CoO \rightarrow H_2O + Co^0$$

$$\overline{Co_3O_4 + 4H_2 \rightarrow 3Co + 4H_2O}$$
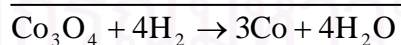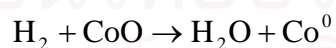
A = Weight% of Co loading

B = Weight of catalyst used in TPR analysis (g)

C = Molecular weight of Co (58.933 g)

D = Using amount of H_2 for 100% reduction degree (mol)

E = Peak area of reduction profile (mol)

F = Reduction degree (%)

$$D = \frac{4}{3} \times \frac{AB}{C}$$

$$F = \frac{E}{D} \times 100$$

Appendix B

Calculation of Crystalline Size from X-Ray Diffractometer (XRD)

The crystalline average size is calculated by :

$$L = K\lambda / \Delta(2\theta)\cos\theta_0$$

L is the crystalline size (nm)

K is a constant (K =1)

λ is the wavelength of X-ray (CuK_α = 0.154 nm)

$2\theta_2$-$2\theta_1$= $\Delta(2\theta)$ is the width of the peak at half height (in radian unit)

Example 10wt%Co/SiO₂
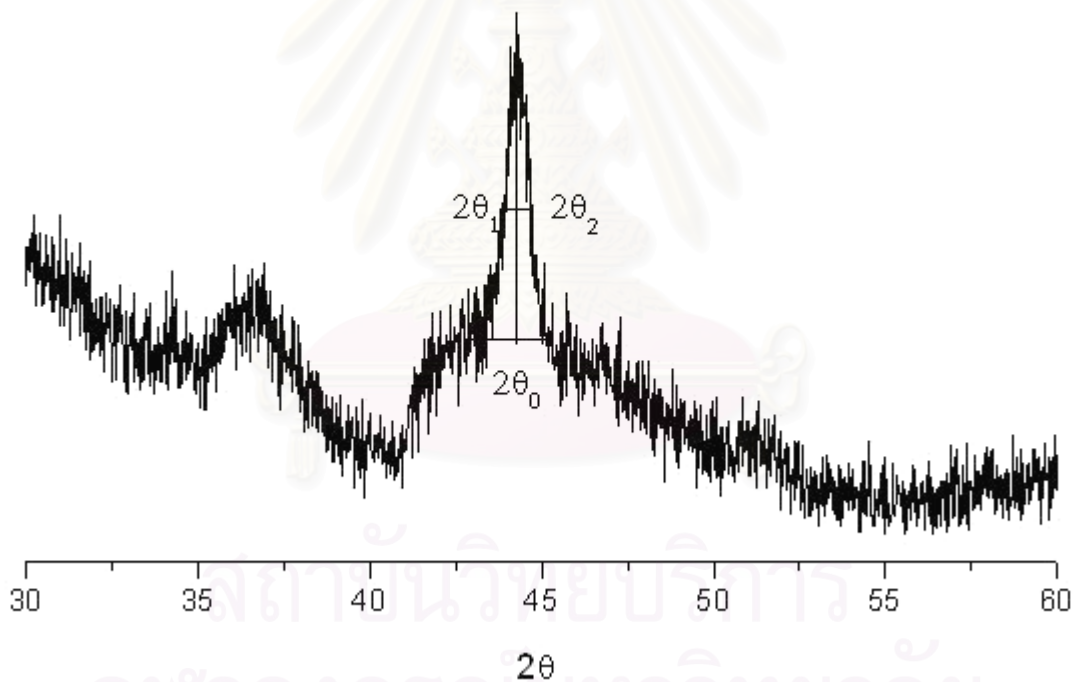
Figure B-1 XRD pattern of Co/SiO₂ catalyst

$2\theta_1 = 44.02°$, $2\theta_2 = 44.57°$, $\Delta(2\theta) = 0.55° = \dfrac{\pi(0.55°)}{180°} = 0.0096$ radian

$2\theta_0 = 44.36° = \dfrac{\pi(44.36°)}{180°} = 0.387$ radian

$L = \dfrac{(1)(0.154)}{(0.0096)\cos(0.387)} = 17.32$ nm

Appendix C

Calculation of Turn Over Frequency (TOF)

$$\text{Turn Over Frequency (TOF)} \quad = \quad \frac{CO \text{ molecule}}{(\text{Active Cobalt atom})(\text{time})}$$

Assumption: The amount of hydrogen atoms adsorbed is equal to active cobalt atoms

$$\text{H atom} = \text{Co atom}$$

A = Monolayer of H_2 uptake (μmol/gram of catalyst)

B = Cobalt atom (μmol/gram of catalyst)

Then; $\qquad\qquad\qquad\qquad\qquad B = 2A$

C = Flow rate of reaction gas (mol/h)

D = CO fraction in reaction gas

E = Flow rate of carbon monoxide (mol/h)

$$E = CD$$

F = CO adsorbed on catalyst site (mol/h)

$$F = E(\text{CO conversion})$$

G = TOF (s^{-1})

$$G = \frac{F}{B}$$

Example 10wt%Co/SiO$_2$

A = 29.66 μmol

B = 2x29.66 = 59.32 μmol

C = 0.2 mol/h

The ratio of CO/H_2 in reaction gas is ½, thus CO fraction (D) is 1/3.

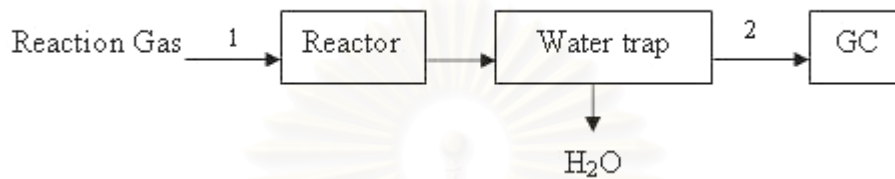$$E = (0.2)\left(\frac{1}{3}\right) = 0.067 \text{ mol/h}$$

$$F = (0.067)\frac{(46.5)}{(100)} = 0.0312 \text{ mol/h}$$

$$G = \frac{(0.0312)}{(59.32 \times 10^{-6})(3600)} = 0.15 \text{ s}^{-1}$$

Appendix D

Calculation of Selectivity

System schematic:

Streams details:

Sream#1: Volumetric flow rate: F_1 cm^3/min

    Compositions: - Carbon monoxide fraction: $y_{CO,1}$

                   - Hydrogen fraction: $y_{H2,1}$

                   - Argon fraction: $y_{Ar,1}$

Stream#2: Volumetric flow rate: F_2 cm^3/min

    Compositions: - Carbon monoxide fraction: $y_{CO,2}$

                   - Methane fraction: $y_{CH4,2}$

                   - Carbon dioxide fraction: $y_{CO2,2}$

Assumption

- the analyzed compositions received from GC are the compositions of the stream#2

Conversion:

$$= \frac{\text{Initial CO fed} - \text{Residual CO}}{\text{Initial CO fed}} \times 100\%$$

$$= \frac{\dfrac{P_1 F_1}{RT_1} \cdot y_{CO,1} - \dfrac{P_2 F_2}{RT_2} \cdot y_{CO,2}}{\dfrac{P_1 F_1}{RT_1} \cdot y_{CO,1}} \times 100\%$$

Methane selectivity:

Due to CO_2 is not specified as hydrocarbon product, then a term of divider in the selectivity equation is added CO_2 generation term.

$$= \frac{\text{Mole of } CH_4 \text{ generated}}{\text{Mole of CO consumed} - \text{Mole } CO_2 \text{ generated}} \times 100\%$$

$$= \frac{\dfrac{P_2 F_2}{RT_2} \cdot y_{CH4,2}}{(\text{CO conversion}) F_1 y_{co,1} - \dfrac{P_2 F_2}{RT_2} \cdot y_{CO2,2}} \times 100\%$$

Carbon dioxide selectivity:

$$= \frac{\text{Mole of } CO_2 \text{ generated}}{\text{Mole of CO consumed}} \times 100\%$$

$$= \frac{\dfrac{P_2 F_2}{RT_2} \cdot y_{CO2,2}}{(\text{CO conversion}) F_1 y_{co,1}} \times 100\%$$

Because the CO_2 can be generated from various side reactions such as Boudouard and water gas shift reaction (WGS), the divider in CO_2 selectivity equation is the term of CO consumed.

VITA

Miss Sukamon Hinchiranan was born on September 4, 1980 in Bangkok, Thailand. She graduated with a Bachelor's degree of Science from Department of Chemical Technology, Faculty of Science, Chulalongkorn University in 2002. She has continued her study in Ph.D. program at Department of Chemical Technology, Faculty of Science, Chulalongkorn University since 2002 and finished her study in 2005.